Numerical Methods and Approximations for the Calculation of Solar Neutrino Fluxes in Three Flavours Focused on Results for the Sudbury Neutrino Observatory

by

Ryan Martin

A thesis submitted to the Department of Physics in conformity with the requirements for the degree of Master of Science

Queen's University

Kingston, Ontario, Canada

January 2006

Abstract

In this thesis, we present an overview of numerical methods and approximations for calculating solar neutrino fluxes at the Sudbury Neutrino Observatory in three flavours. We find that the daytime flux is well approximated by a three flavour adiabatic propagation with a two-flavour jump probability. We also introduce variable step size algorithms for the numerical propagation of neutrinos through the Sun. A formula for the survival probability of solar neutrinos that have traversed the Earth is presented in three flavours and the dependence on θ_{13} is demonstrated. It is then shown that an experiment for low energy solar neutrinos would provide the best constraints on θ_{13} and that there is a theoretical dependence of the day-night asymmetry on θ_{13} but that the effect is too small to be measured with current experiments. Finally, we show the effect of matter above an underground detector, such as the Sudbury Neutrino Observatory, on a measurement of the day-night asymmetry and conclude that the night bin should be longer than is implied in the literature.

Acknowledgments

I would like to start by thanking my supervisors, Dr. Mark Chen and Dr. Ian Towner, without whom this work would have been impossible. Their cordiality and willingness to always help me are much appreciated. I am grateful for the opportunity they gave me to do theoretical research amongst the Sudbury Neutrino Observatory group. I would like to thank Dr Chen for the insight that he has given me when trying to understand the results of my calculations. I would like to thank Dr. Towner for all the help in deriving and understanding theory as well as teaching me an overall frame of mind for doing theoretical research.

It was a pleasure to work with the SNO group at Queen's as they have provided a very amicable and professional environment in which to do my work. In particular, I would like to thank Dr. Aksel Hallin and Dr. Peter Skensved for the different perspectives that they provided, from which I learned how to defend my work. It is with great pleasure that I prepare myself to start a doctorate with the SNO group.

I would also like to thank my fellow graduate students and colleagues for everything they have taught me and for creating a positive work atmosphere. In particular, I would like to thank Ryan MacLellan, Mark Kos and Jose Maneira for all the computer related help, as well as discussing my work with me. I would also like to acknowledge Alex Wright for the many insightful theoretical discussions we have had together.

Finally, I would like to thank my parents, Claudia and Reginald, as well as my sister, Cristina, for all the support they have given me over the years and for always believing in me. This work is dedicated to them.

Contents

List of Tables

List of Figures

List of Symbols

$\mathcal{A}_{\mathcal{N}-\mathcal{D}}$	Day-Night Asymmetry
ΔM_{21}	Difference in Matter energy eigenvalues
Δm_{21}	Mass squared difference between vacuum eigenstates, $m_2^2 - m_1^2$
Δm_{31}	Mass squared difference between vacuum eigenstates, $m_3^2 - m_1^2$
δ	CP violating phase
γ	Adiabaticity parameter
θ	Two flavour mixing angle (solar and reactor neutrinos)
θ_{12}	Three flavour mixing angle (solar and reactor neutrinos)
θ_{13}	Three flavour mixing angle (all neutrinos)
θ_{23}	Three flavour mixing angle (atmospheric and long baseline neutrinos)
c	Speed of light
G_f	Fermi's constant
N_e	Electron number density
N_e^c	Critical electron number density
N_e^r	Resonant electron number density
$P^{\odot}$	Probability averaged over the Sun and Sun-Earth distance
$P^{\oplus}$	Probability averaged over Earth trajectories and phase between energy eigenstates
P_{ee}	Electron neutrino survival probability
P_{SE}	Electron neutrino survival probability averaged over the Sun and the Earth
$R_{\odot}$	Radius of the Sun
$R_{\oplus}$	Radius of the Earth
T	Mixing matrix from matter basis to flavour basis
U	PMNS mixing matrix from vacuum basis to flavour basis

1 Introduction

In this thesis, we seek to examine various methods for calculating solar neutrino fluxes in the context of the Sudbury Neutrino Observatory (SNO) [2]. Throughout the thesis, we will present an overview of most of the methods and approximations available in the literature for calculating these fluxes as well as introduce our own, new, methods. We will examine the accuracy of these calculations with the goal of providing the best tools for calculating solar neutrino fluxes in three flavours, using neutrino oscillations. There is thus not much need for a distinct literature review, as this process will be carried out in the body of the thesis.

1.1 Neutrino Oscillations

The possibility that neutrinos oscillate was first suggested by Bruno Pontecorvo in [3], in analogy to oscillations in the $K_o - \bar{K_o}$ system of the quark sector [4], which then implied that neutrinos must have mass. It was not until 1998 that the SuperKamiokande experiment [5] conclusively showed that neutrinos oscillate. Neutrino flavour transformations (a strong argument for neutrino oscillations) were then shown by the Sudbury Neutrino Observatory [6] to be the conclusive solution to the longstanding solar neutrino problem. There had been an inconsistency dating from Ray Davis' experiment in 1968 [7] between the measured solar neutrino flux and that predicted by the solar models.

Neutrino oscillations occur because neutrinos are produced in weak eigenstates that are quantum admixtures of the eigenstates of the Hamiltonian. The amount of mixing is governed by the mixing matrix, which can be parametrized in terms of three angles and a complex phase, in exact analogy to the CKM matrix in the quark sector. The three mixing angles, usually labeled θ_{12}, θ_{23} and θ_{13}, govern the amplitude of the oscillations. The complex phase allows for the possibility of CP-violation. Finally, the differences in masses squared between the energy eigenstates determine the wavelengths of the oscillations. As there are three known flavours of neutrinos, only two of these mass squared differences are independent, and we have chosen to label them $\Delta m_{21} \equiv m_2^2 - m_1^2$ and $\Delta m_{31} \equiv m_3^2 - m_1^2$. Neutrino oscillations are then governed by six different parameters.

The first generation of neutrino oscillation experiments were designed to conclusively demonstrate the effect, but it has turned out that they have been able to measure the mixing angles to an acceptable degree of accuracy. In fact θ_{12} and Δm_{21} have been well constrained by solar and reactor neutrino experiments ([8], [9]), whereas θ_{23} and Δm_{31} have been constrained by atmospheric neutrinos [10]. The current focus for future experiments will then be to measure the last remaining

mixing angle θ_{13} on the one hand, and verify the possible existence of a non-zero complex phase on the other. The current accepted values are $\tan^2(\theta_{12}) = 0.45$ and $\Delta m_{21} = 8 \times 10^{-5} eV^2$ from [8]. We have used slightly obsolete values throughout the thesis, $\tan^2(\theta_{12}) = 0.42$ and $\Delta m_{21} = 7 \times 10^{-5} eV^2$ from [6] when we refer to best-fit values. Similarly, one finds $\Delta m_{31} = 2.8 \times 10^{-3} eV^2$ and $\sin^2(\theta_{23}) = 0.52$ from [11] although we have used slightly different values in this thesis, $\Delta m_{31} = 1 \times 10^{-3} eV^2$ and $\sin^2(\theta_{23}) = 0.5$, as the best fit values.

Neutrino oscillation experiments have thus progressed from showing that oscillations occur to measuring the parameters involved. The main focus of this thesis is then to examine and provide theoretical tools to model solar neutrino oscillation accurately so that the mixing angles can be constrained further with the next generation of experiments. Our work was started by considering the possibility of measuring θ_{13} with solar neutrinos, in particular by using the day-night asymmetry, and evolved into an overview of numerical methods.

We will thus examine various approximations and numerical procedures for the calculation of neutrino oscillations. In particular, we will examine the adiabatic approximation [12] and the correction due to the Jump Probability ([13], [14]), and how it can be applied in a three-flavour framework. We will also consider the effect that the Earth has on solar neutrinos and the resulting day-night asymmetry that is expected in solar neutrino experiments. Our work on this subject is close to that of [15] and [16], and we present an improved formalism for these types of calculations as compared to [16].

1.2 Outline

We will start by introducing the theoretical framework of neutrino oscillations in section (2.1). The formalism for treating neutrino oscillations in matter will then be presented and discussed thoroughly in the two-flavour framework.

Section (2.2) will then provide an overview of neutrino oscillation calculations through arbitrary media done numerically followed by various approximations presented in the literature. In particular, the case of adiabatic propagation will be examined thoroughly as well as the extension using the Jump probability. Section (2.2) will not contain any new material, but we believe that the material is presented in a way to provide the reader with a good intuition about neutrino oscillations.

In section (2.3) we will take a very detailed look at the propagation of neutrinos in the Sun. Relevant aspects of the solar model will be introduced followed by an examination of the numerical propagation of neutrinos in the Sun, and the effect of the different parameters that influence the

oscillations. We will then present numerical algorithms that we have derived in order to speed up these numerical calculations while still preserving accuracy. Section (2.3) will then conclude by examining the various approximations presented in section (2.2) when applied to solar neutrinos and recommend the most computationally efficient and precise method for propagating solar neutrinos in three flavours.

Section (2.4) will take a brief look into the propagation of neutrinos in the Earth. The effect of the Earth's density will be examined and it will be shown that the Earth can reintroduce coherence into an incoherent beam of neutrinos.

Our original work is presented in section (2.5), where we examine solar neutrinos that also traverse the Earth, and hence the day-night asymmetry. We will derive a formula that allows one to calculate neutrinos fluxes accurately in three flavours as well as significantly decrease the computational load in this type of calculation. The main aim of this formula is to model the day-night asymmetry in SNO and look at the dependence on θ_{13}.

We will conclude this thesis with two brief sections in which we apply our theoretical findings. Section (3.1) will consider more precisely the dependence of solar neutrino fluxes on θ_{13} and suggests two different methods that can be used to measure this mixing angle with solar neutrino experiments. Section (3.2) will consider the effect of modeling an underground solar neutrino detector compared to the approximation that the detector is on the Earth's surface. We will show that the matter above the detector has a small influence on the neutrino flux that is measured and should be included in a rigorous calculation.

The bulk of our work consists in an overview of existing numerical methods for the propagation of solar neutrinos. Throughout the thesis, we present tests of existing methods as well as our own, new, methods for doing these calculations. In particular, in section (2.3), we introduce new variable step size algorithms for the propagation through the Sun. The possibility of using a two-flavour jump probability in the context of the three-flavour adiabatic approximation is also, to our knowledge, a novel idea. Finally, although the formalism presented in section (2.5) is not new, we are the first to fully develop the calculation for solar neutrinos traversing the Earth in three flavours.

Section (4) will provide a summary and conclusions of the thesis.

2 Theory

2.1 Framework

In this section, the formalism that will be used to model neutrino oscillations is presented. Neutrino oscillations were first proposed in 1957 by Bruno Pontecorvo [3] where he considered the possibility of neutrino-anti-neutrino mixing, in analogy to the $\bar{K^0} - K^0$ system [4]. At the time, this was only a speculation, but after the initial results from the Ray Davis experiment in 1968 [7], the possibility of flavour non-conservation and mixing was developed further([17], [18], [19], [20]) for the case of neutrinos, in an attempt to describe Davis' results.

From the Standard Model, we know of three different types of neutrinos that couple through the Weak Charged Current (W) to the electron, the muon and the tau particle, respectively. From the decay width of the Z_o boson, it is likely that the number of low energy leptonic flavours is restricted to be three [21]. We hence infer the existence of exactly three types of neutrinos, which we label $\nu_\alpha|^{\alpha=e,\mu,\tau}$, as the three flavours of neutrinos coupling to their corresponding charged leptons. We model a neutrino as a quantum mechanical state that is, in general, a superposition of the three flavour eigenstates:

$$|\nu >= A_e|\nu_e > +A_\mu|\nu_\mu > +A_\tau|\nu_\tau > \tag{1}$$

that follows the Schrödinger equation:

$$i\frac{d}{dt}|\nu(t) >= H|\nu(t) > \tag{2}$$

where H is the Hamiltonian. In the most general case, the eigenstates of the Hamiltonian, $|\nu_i >_{i=1,2,3}$, are not the same as the flavour eigenstates, $|\nu_\alpha >_{\alpha=e,\mu,\tau}$. We thus infer the existence of a linear transformation, U, that relates the two orthonormal bases to each other, and can be expressed in terms of a 3×3 unitary matrix:

$$|\nu_\alpha >_{\alpha=e,\mu,\tau}= U|\nu_i >_{i=1,2,3} \tag{3}$$

The evolution of the neutrino can then be expressed in either basis:

$$|\nu(t) > \quad = \quad A_e(t)|\nu_e > +A_\mu(t)|\nu_\mu > +A_\tau(t)|\nu_\tau >$$

$$= \quad A_1(t)|\nu_1> + A_2(t)|\nu_2> + A_3(t)|\nu_3> \tag{4}$$

The complex amplitudes $A_\alpha(t)$ ($A_i(t)$) are time-dependent functions that represent the different flavour (energy) eigenstate contents. The probability that a neutrino created as an electron type neutrino ($A_e(t=0)=1$) and is detected later as an electron-type neutrino is thus given by $|A_e(t)|^2$, and we will call this the 'Survival Probability', which we also abbreviate as P_{ee}. In the next subsections we derive the formula for P_{ee} for neutrinos travelling in vacuum in two and three flavours, respectively and then we will show the case for neutrinos propagating in matter.

2.1.1 Two-Flavour Vacuum Oscillations

For the present section, we will go through the derivation assuming only two flavours of neutrinos. This turns out to be a very accurate approximation for considering solar neutrinos, and the SNO results are indeed analyzed in a two-flavour framework ([22]).

We label the eigenvalues of the Hamiltonian E_1 and E_2 that correspond to the two energy eigenstates $|\nu_1>$ and $|\nu_2>$, which we will also call the vacuum mass eigenstates. In two dimensions, the most general unitary transformation between the mass and flavour bases can be parametrized with a rotation through an angle, θ, which we will call the mixing angle. We also note that the most general transformation matrix can be real, as any complex phase that is allowed would disappear when a quantum mechanical probability is calculated. We can thus write the transformation as:

$$|\nu_\alpha>_{\alpha=e,\mu} \quad = \quad U|\nu_i>_{i=1,2} \tag{5}$$

$$\begin{pmatrix} |\nu_e> \\ |\nu_\mu> \end{pmatrix} \quad = \quad \begin{pmatrix} \cos\theta & \sin\theta \\ -\sin\theta & \cos\theta \end{pmatrix} \begin{pmatrix} |\nu_1> \\ |\nu_2> \end{pmatrix} \tag{6}$$

We then write the time-dependent state vector for a neutrino in the form:

$$|\nu(x,t)> = A_1(x,t)|\nu_1> + A_2(x,t)|\nu_2> \tag{7}$$

and impose the mass eigenstates to be one-dimensional plane waves that diagonalize the Hamiltonian:

$$\begin{aligned} H &= \begin{pmatrix} E_1 & 0 \\ 0 & E_2 \end{pmatrix} \\ A_i(t) &= k_i e^{ip_i t} e^{-i\frac{E_i}{\hbar}t} \end{aligned} \tag{8}$$

where $k_i = A_i(0)$ are the initial mass eigenstate contents of the neutrino. We have also taken the ultra-relativistic limit $x \to t$, where the neutrino travels essentially at the speed of light with units where $c = 1$. The neutrino wavefunction is thus completely described by:

$$|\nu(t)>= k_1 e^{ip_1 t} e^{-i\frac{E_1}{\hbar}t}|\nu_1> + k_2 e^{ip_2 t} e^{-i\frac{E_2}{\hbar}t}|\nu_2> \tag{9}$$

One now assumes that both eigenstates were created with the same momentum ($p_1 = p_2 = p$) so that one can then factor out the overall, unmeasurable, phase factor $e^{ipt}e^{-i\frac{E_1}{\hbar}t}$, which we will drop for the rest of the derivation:

$$|\nu(t)>= e^{ipt} e^{-i\frac{E_1}{\hbar}t}(k_1|\nu_1> + e^{-i\frac{E_2-E_1}{\hbar}t} k_2|\nu_2>) \tag{10}$$

At this point we make a slight deviation from the ultra-relativistic limit and allow for a small neutrino mass. We thus use the relativistic energy-momentum relation to express the energy in terms of the neutrino mass.

$$\begin{aligned} E^2 &= p^2 + m^2 \\ E &= p\sqrt{1 + \frac{m^2}{p^2}} \end{aligned} \tag{11}$$

We then assume that the neutrino mass is much smaller than its momentum, which is consistent with the limits on neutrino mass set by Tritium decay experiments [23] (of order a few eV) compared to the energy of solar neutrinos (a few MeV). This allows us to consider only the first term in a Taylor expansion, and we obtain:

$$E \approx p + \frac{m^2}{2p} \tag{12}$$

We can now express the difference in energies between the two neutrino mass eigenstates:

$$E_2 - E_1 = \frac{m_2^2 - m_1^2}{2p} = \frac{\Delta m_{21}}{2E} \tag{13}$$

where we have defined the "mass squared difference" $\Delta m_{21} \equiv m_2^2 - m_1^2$ and made the further approximation that the momentum is equal to the energy (since the masses are so small).

One should note that conservation of energy does not appear to be violated, since the amount of each mass eigenstate in the neutrino is a constant. That is, if one could measure the probability of having a $|\nu_1>$, $|<\nu_1|\nu(t)>|^2$, one finds that it is a constant ($=|k_1|^2$). Hence if the neutrino is "prepared" in a mix of energy (mass) eigenstates, that mix will stay the same in time. One often hears confusing statements about neutrinos of different mass changing into each other, which intuitively violates conservation of energy. One should not really interpret the electron and muon neutrinos as having mass but rather as eigenstates of flavour.

We can now express the neutrino wavefunction in the mass eigenstate basis as:

$$|\nu(t)>= k_1|\nu_1> + e^{-i\frac{\Delta m_{21}}{2E\hbar}t} k_2|\nu_2> \tag{14}$$

For a neutrino that started out as an electron type neutrino we then have:

$$\begin{aligned} |\nu(0)> &= |\nu_e>= \cos\theta|\nu_1> + \sin\theta|\nu_2> \\ k_1 &= \cos\theta \\ k_2 &= \sin\theta \end{aligned} \tag{15}$$

Finally, we use the mixing matrix to express the mass eigenstates in term of the flavour ones and obtain:

$$\begin{aligned} |\nu(t)> &= \cos\theta|\nu_1> + \sin\theta e^{-i\frac{\Delta m_{21}}{2E\hbar}t}|\nu_2> \\ &= \cos\theta(\cos\theta|\nu_e> - \sin\theta|\nu_\mu>) + \sin\theta e^{-i\frac{\Delta m_{21}}{2E\hbar}t}(\sin\theta|\nu_e> + \cos\theta|\nu_\mu>) \\ &= (\cos^2\theta + \sin^2\theta e^{-i\frac{\Delta m_{21}}{2E\hbar}t})|\nu_e> + \cos\theta\sin\theta(e^{-i\frac{\Delta m_{21}}{2E\hbar}t} - 1)|\nu_\mu> \end{aligned} \tag{16}$$

We now have a form where P_{ee} can be easily expressed in terms of the mixing angle and the mass squared difference:

$$\begin{aligned} P_{ee} &= |A_e(t)|^2 \\ &= |(\cos^2\theta + \sin^2\theta e^{-i\frac{\Delta m_{21}}{2E\hbar}t})|^2 \\ &= \cos^4\theta + \sin^4\theta + \cos^2\theta\sin^2\theta(e^{-i\frac{\Delta m_{21}}{2E\hbar}t} + e^{i\frac{\Delta m_{21}}{2E\hbar}t}) \\ &= \cos^2\theta(1-\sin^2\theta) + \sin^2\theta(1-\cos^2\theta) + \frac{1}{2}\sin^2(2\theta)\cos\left(\frac{\Delta m_{21}}{2E\hbar}t\right) \\ &= 1 - \frac{1}{2}\sin^2(2\theta)\left(1-\cos\left(\frac{\Delta m_{21}}{2E\hbar}t\right)\right) \end{aligned} \tag{17}$$

One can thus see that the electron content of the neutrino oscillates sinusoidally in time, even though the energy (mass) content stays fixed. This process is called neutrino oscillation. It is now widely accepted that neutrino oscillations occur in nature thus proving that neutrinos have mass. One should note that oscillation experiments can only measure mass (squared) differences between the neutrinos and not the actual scale of the masses. We can also see that we have had to introduce two new parameters into the Standard Model, namely the mixing angle and mass squared difference.

One often expresses the survival probability as a function of distance by assuming that the neutrino travels at the speed of light, and hence setting $x = ct$. One can thus extract a wavelength for the oscillations $\lambda = \frac{4\pi E\hbar c}{\Delta m_{21}}$. In some cases such as the Sun (see, for example, Figure(18)), the neutrinos are produced over a range of locations and the oscillating term is effectively averaged out. It is thus worth noting that in these cases, the survival probability is simply a constant, which we shall call the classical survival probability, given by:

$$P_{ee} = 1 - \frac{1}{2}\sin^2(2\theta) \tag{18}$$

2.1.2 Three-Flavour Vacuum Oscillations

In this section, the analogous formula for P_{ee} is derived for the case of three flavours of neutrinos traveling through vacuum. The procedure is the same as in the case of two flavours, however the algebra is more tedious.

The key difference in three flavours is that the most general unitary matrix (in 3-dimensions) can be complex. There are several ways of parameterizing this matrix and we will use the same parametrization as the Cabibbo-Maskawa-Kobayashi (CKM) matrix in the quark sector, which is defined in terms of three mixing angles and a complex phase. In the lepton sector, the mixing matrix is usually referred to as the PMNS matrix, in honour of B. Pontecorvo, Z. Maki, M. Nakagawa, and

S. Sakata ([24]), to distinguish it from the CKM matrix, since the mixing angles are different.

Again, we have:

$$|\nu_\alpha >_{\alpha=e,\mu,\tau} = U|\nu_i >_{i=1,2,3} \tag{19}$$

where:

$$U = \begin{pmatrix} U_{e1} & U_{e2} & U_{e3} \\ U_{\mu 1} & U_{\mu 2} & U_{\mu 3} \\ U_{\tau 1} & U_{\tau 2} & U_{\tau 3} \end{pmatrix} \tag{20}$$

$$= R_{23} \times R_{13} \times R_{12} \tag{21}$$

$$= \begin{pmatrix} 1 & 0 & 0 \\ 0 & c_{23} & s_{23} \\ 0 & -s_{23} & c_{23} \end{pmatrix} \times \begin{pmatrix} c_{13} & 0 & s_{13}e^{-i\delta} \\ 0 & 1 & 0 \\ -s_{13}e^{i\delta} & 0 & c_{13} \end{pmatrix} \times \begin{pmatrix} c_{12} & s_{12} & 0 \\ -s_{12} & c_{12} & 0 \\ 0 & 0 & 1 \end{pmatrix} \tag{22}$$

$$= \begin{pmatrix} c_{12}c_{13} & s_{12}c_{13} & s_{13}e^{-i\delta} \\ -s_{12}c_{23} - c_{12}s_{23}s_{13}e^{i\delta} & c_{12}c_{23} - s_{12}s_{23}s_{13}e^{i\delta} & s_{23}c_{13} \\ s_{12}s_{23} - c_{12}c_{23}s_{13}e^{i\delta} & -c_{12}s_{23} - s_{12}c_{23}s_{13}e^{i\delta} & c_{23}c_{13} \end{pmatrix} \tag{23}$$

We have thus introduced three mixing angles θ_{ij} with the notation $c_{ij} = \cos\theta_{ij}$ and $s_{ij} = \sin\theta_{ij}$ that correspond to the three rotation matrices R_{12}, R_{23} and R_{13}. The complex phase is denoted δ. One notes that θ_{12} is the mixing angle between the first two mass eigenstates, which is the same angle that appears in the two-flavour oscillation formula. The two-flavour oscillation model will thus be recovered when $\theta_{23} = \theta_{13} = 0$. In order to shorten the equations we have introduced the notation $U_{ij} = U_{\alpha j}|^{j=1,2,3}_{\alpha=e,\mu,\tau}$ and we will thus avoid plugging in the actual angle dependence until the desired formula is obtained. One also notes that, from unitarity, the inverse transformation is given by $U^{-1}_{ij} = U^*_{ji}$.

For a neutrino that originates as an electron type neutrino, we have:

$$|\nu(0) > = |\nu_e > = U_{e1}|\nu_1 > + U_{e2}|\nu_2 > + U_{e3}|\nu_3 >$$

$$k_1 = U_{e1}$$

$$\begin{aligned} k_2 &= U_{e2} \\ k_3 &= U_{e3} \end{aligned} \tag{24}$$

As before, the time dependence in the mass eigenstate basis is trivial, and we again choose to factor out the phase $e^{-i\frac{E_1}{\hbar}t}$. Having factored out the phase from the first eigenstate and expressing the energies in term of the mass squared differences, we can write the Hamiltonian as:

$$H = \frac{1}{2E}\begin{pmatrix} 0 & 0 & 0 \\ 0 & \Delta m_{21} & 0 \\ 0 & 0 & \Delta m_{31} \end{pmatrix} \tag{25}$$

And the time dependence of the neutrino is thus:

$$|\nu(t)>= k_1|\nu_1> + e^{-i\frac{\Delta m_{21}}{2E\hbar}t}k_2|\nu_2> + e^{-i\frac{\Delta m_{31}}{2E\hbar}t}k_3|\nu_3> \tag{26}$$

where we now have two mass squared differences. Hence the three-flavour neutrino oscillations now involve six parameters (three mixing angles, a complex phase and two mass squared differences) compared to only two parameters for the two-flavour oscillations.

In order to derive the formula for P_{ee}, we proceed in the same manner as for two flavours, by re-expressing the mass eigenstates in terms of the flavour ones. To make the formulas shorter, we also use the Einstein summation convention (summing over repeated indices). In order to use the convention consistently, we need to index the time dependence; we will use $f_i(t) = e^{-i\frac{\Delta m_{i1}}{2E\hbar}t}$, with $f_1(t) = 1$. In addition, indices with roman letters will run from 1 to 3 and Greek letters will stand for e, μ and τ.

$$\begin{aligned} |\nu(t)> &= f_i(t)k_i|\nu_i> \\ &= f_i(t)U_{ei}|\nu_i> \\ &= f_i(t)U_{ei}U^*_{i\alpha}|\nu_\alpha> \end{aligned} \tag{27}$$

We can now obtain the survival probability (by considering the term where $\alpha = e$):

$$P_{ee} = |f_i(t)U_{ei}U^*_{ie}|^2$$

$$
\begin{aligned}
&= \left| f_i(t)|U_{ei}|^2 \right|^2 \\
&= \left| |U_{e1}|^2 + |U_{e2}|^2 e^{-i\frac{\Delta m_{21}}{2E\hbar}t} + |U_{e3}|^2 e^{-i\frac{\Delta m_{31}}{2E\hbar}t} \right|^2 \\
&= \left(|U_{e1}|^4 + |U_{e2}|^4 + |U_{e3}|^4\right) + 2|U_{e1}|^2|U_{e2}|^2 \cos\left(\frac{\Delta m_{21}}{2E\hbar}t\right) \\
&+ 2|U_{e1}|^2|U_{e3}|^2 \cos\left(\frac{\Delta m_{31}}{2E\hbar}t\right) + 2|U_{e2}|^2|U_{e3}|^2 \cos\left(\frac{\Delta m_{21} + \Delta m_{31}}{2E\hbar}t\right)
\end{aligned} \tag{28}
$$

Plugging in the actual angle dependence, one finds:

$$
\begin{aligned}
P_{ee} &= 1 - \frac{1}{2}c_{13}^4 \sin^2(2\theta_{12}) \left(1 - \cos\left(\frac{\Delta^2 m_{21}}{2E\hbar}t\right)\right) \\
&- \frac{1}{2}\sin^2(2\theta_{13}) \left(1 - \cos\left(\frac{\Delta^2 m_{31}}{2E\hbar}t\right)\right) \\
&- \frac{1}{2}s_{12}^2 \sin^2(2\theta_{13}) \left(\cos\left(\frac{\Delta^2 m_{31}}{2E\hbar}t\right) - \cos\left(\frac{\Delta^2 m_{21} + \Delta^2 m_{31}}{2E\hbar}t\right)\right)
\end{aligned} \tag{29}
$$

We note that this formula does not depend on the mixing angle θ_{23} or on the complex phase δ. This means that experiments looking for electron-type neutrinos in a beam of neutrinos that started in the electron flavour are not sensitive to θ_{23} or the complex phase. If the two mass squared differences are not equal to each other, one will obtain two superimposed oscillation patterns, with wavelengths $\lambda_1 = \frac{4\pi E\hbar c}{\Delta m_{21}}$ and $\lambda_2 = \frac{4\pi E\hbar c}{\Delta m_{31}}$. If the oscillating terms can be averaged out, then the three-flavour classical survival probability is given by:

$$
P_{ee} = 1 - \frac{1}{2}c_{13}^4 \sin^2(2\theta_{12}) - \frac{1}{2}\sin^2(2\theta_{13}) \tag{30}
$$

The general oscillation formula between a flavour α and β is given by:

$$
P_{\alpha\beta} = |f_i(t) U_{\alpha i} U_{i\beta}^*|^2 \tag{31}
$$

and typically depends on all of the angles.

2.1.3 Matter Oscillations

So far, we have only considered oscillations in vacuum. These arise from the fact that the eigenbasis for the Hamiltonian is different from the flavour eigenbasis. In matter, the neutrinos can interact

through the charged and neutral Weak currents. Intuitively, this changes their (potential) energy, and hence their Hamiltonian, which will now be diagonal in a new basis, which we will call the matter mass eigenbasis.

In this section, we present the standard formalism for modeling neutrino propagation through matter. The idea that matter can influence the propagation of neutrinos was first suggested by Wolfenstein [25], and then developed by Mikheyev and Smirnov [26], and is called the MSW effect, in their honour. Because normal matter (such as the sun) is composed of electrons (but not muons and taus), the electron flavour neutrinos can scatter through the charged current with these electrons. This is the basic idea that leads to the electron type neutrinos seeing a different potential in normal matter than the other neutrinos. The neutral current scattering is the same for all flavours of neutrinos and is thus equivalent to an overall potential term added to the energy, which has the final effect of adding an unmeasurable phase factor to all neutrino states.

Following the work from ([27], [28]), the interaction part of the Hamiltonian for the charged current between the electron-type neutrinos and the electrons can be written as a potential energy:

$$V \equiv \sqrt{2} G_f N_e \tag{32}$$

where G_f is Fermi's constant and N_e is the number density of electrons. We can then define an interaction Hamiltonian, H_2^f, to account for the charged current interaction between electron flavour neutrinos and electrons. Because the interaction affects only the electron flavour neutrinos, this part of the Hamiltonian must be expressed in the flavour basis:

$$H_2^f = \frac{1}{2E} \begin{pmatrix} A & 0 & 0 \\ 0 & 0 & 0 \\ 0 & 0 & 0 \end{pmatrix} \tag{33}$$

where we have introduced the variable $A = 2\sqrt{2} G_f N_e E$ for later convenience.

The total Hamiltonian is thus the sum of a vacuum part, H_1^v, and a flavour part, H_2^f, both of which are expressed in different bases. We can hence express the total Hamiltonian in the flavour basis as:

$$H_{tot}^f = U H_1^v U^\dagger + H_2^f$$

$$
\begin{aligned}
&= \frac{1}{2E}\begin{pmatrix} U_{e1} & U_{e2} & U_{e3} \\ U_{\mu 1} & U_{\mu 2} & U_{\mu 3} \\ U_{\tau 1} & U_{\tau 2} & U_{\tau 3} \end{pmatrix}\begin{pmatrix} 0 & 0 & 0 \\ 0 & \Delta m_{21} & 0 \\ 0 & 0 & \Delta m_{31} \end{pmatrix}\begin{pmatrix} U^*_{e1} & U^*_{\mu 1} & U^*_{\tau 1} \\ U^*_{e2} & U^*_{\mu 2} & U^*_{\tau 2} \\ U^*_{e3} & U^*_{\mu 3} & U^*_{\tau 3} \end{pmatrix} \\
&+ \frac{1}{2E}\begin{pmatrix} A & 0 & 0 \\ 0 & 0 & 0 \\ 0 & 0 & 0 \end{pmatrix}
\end{aligned}
\tag{34}
$$

where we have used the mixing matrix U to perform a similarity transformation to convert the vacuum Hamiltonian into the flavour basis.

There now exists a new basis, $\{|\nu_i^m>\}_{i=1,2,3}$, the matter eigenstate basis, where the Hamiltonian is diagonal. In this new basis the time evolution of the eigenstates is just $e^{-i\frac{E_i}{\hbar}t}$, where E_i are the eigenvalues of the total Hamiltonian. It is a simple matter of linear algebra to diagonalize the Hamiltonian to solve for this basis and find the similarity transformation, T, back to the flavour basis:

$$
\begin{aligned}
T^\dagger H^f_{tot} T|\nu_i^m> &= E_i|\nu_i^m> \\
|\nu_f>_{f=e,\mu,\tau} &= T|\nu_i^m>_{i=1,2,3}
\end{aligned}
\tag{35}
$$

In the two flavour case, this procedure just results in a new mixing angle, usually referred to as the matter mixing angle. The total flavour Hamiltonian in two flavours is given by:

$$
H^f_{tot} = \frac{1}{4E}\begin{pmatrix} \Delta m_{21} - \Delta m_{21}\cos(2\theta) + 2A & \Delta m_{21}\sin(2\theta) \\ \Delta m_{21}\sin(2\theta) & \Delta m_{21} + \Delta m_{21}\cos(2\theta) \end{pmatrix}
\tag{36}
$$

The eigenvalues are then:

$$
\begin{aligned}
E_{1,2} &= \frac{1}{4E}\left(\Delta m_{21} + A \mp \Delta M_{21}\right) \\
\Delta M_{21} &\equiv \sqrt{\Delta^2 m_{21} + A^2 - 2A\Delta m_{21}\cos(2\theta)}
\end{aligned}
\tag{37}
$$

where we have chosen the second mass eigenstate to be the heaviest. Note that we have defined the 'matter mass squared difference', ΔM_{21} , as $E_2 - E_1$, in analogy to the vacuum case so that the

phase between energy eigenstates is equal to $\frac{\Delta M_{21}}{2E}$ (see equation (13)). By solving for the normalized eigenvectors, one can then express the similarity transformation T in terms of a mixing angle, θ_m, which can be expressed as:

$$\begin{aligned} \tan(2\theta_m) &= \frac{\Delta m_{21}\sin(2\theta)}{\Delta m_{21}\cos(2\theta) - A} \\ \sin(2\theta_m) &= \frac{\Delta m_{21}\sin(2\theta)}{\Delta M_{21}} \end{aligned} \tag{38}$$

One notes that the mixing angle depends on the density in the medium and can reach $\frac{\pi}{4}$ when $A = \Delta m_{21}\cos(2\theta)$. This point is known as the MSW resonance, where the neutrinos undergo strong flavour conversion, as the amplitude of the oscillations becomes the largest. In three flavours, one typically solves only for the eigenvalues and eigenvectors that diagonalize the Hamiltonian, without deriving the analogous matter mixing angles. One also notes that matter oscillations effectively change the masses of the Hamiltonian eigenstates and thus result in a new mass squared difference, ΔM_{21}, which now drive the oscillations, with a new matter oscillation length, $\lambda_m = \frac{4\pi E\hbar c}{\Delta M_{21}}$. The MSW resonance then takes place where ΔM_{21} is a minimum. In two flavours, the formula for P_{ee} in matter of constant density is simply given by replacing θ and Δm_{21} by their matter counterparts:

$$P_{ee} = 1 - \frac{1}{2}\sin^2(2\theta_m)(1 - cos\left(\frac{2\pi x}{\lambda_m}\right)) \tag{39}$$

2.2 Numerical Methods and Approximations Through Matter

The numerical methods for propagating neutrinos through matter as well as various common approximations are presented and discussed in this section. We first investigate the effects of propagating neutrinos through matter of varying density. This is of interest in order to better understand the accuracy of numerical calculations as well as various approximations. We then introduce the flux calculations for solar neutrinos at SNO.

In order to model the solar neutrino flux at SNO, one needs to understand how media with different density profiles influence the behavior of P_{ee}. In a basic numerical calculation, one just divides the medium into slabs of constant density and successively determines the mass eigenstates according to equation (35). The numerical calculation thus involves diagonalizing the Hamiltonian in each slab, which can easily be programmed.

It is also of interest to consider what happens at the boundary between two layers of constant density to understand better the numerical accuracy of such calculations. In one limit, consistent with propagation through parts of the sun, the density does not change very much between slabs. At the other extreme, the boundary between vacuum and the earth has a strong discontinuity in density. Furthermore, the earth density is also discontinuous at the boundary between different layers (for example, the mantle-core interface).

2.2.1 Propagation Through Matter

From considering the Hamiltonian in equation (34), one notes that matter effects should become important when the flavour part of the Hamiltonian is of the same order as the vacuum part, or when $A = 2\sqrt{2}G_f N_e E \approx \frac{\Delta m_{21}}{2E}$. We shall call this density the critical electron density, N_e^c. Below this density, the neutrino oscillations are mostly driven by the vacuum mixing angle(s), whereas they are dominated by the matter oscillations when the density is larger. This can be seen in Figure (1), where the survival probability is plotted as a function of distance. The left panel shows essentially vacuum oscillations at a density of $N_e = 0.01N_e^c$ and the right panel shows matter oscillations when the density is increased to $N_e = 5N_e^c$. The neutrinos have an energy of $10MeV$ consistent with solar neutrinos. For simplicity, Figure (1) is calculated assuming two flavours of neutrinos, so that the mixing angle can easily be calculated.

The expression given in equation (38) for the mixing angle is singular when $A = \Delta m_{21}\cos(2\theta)$ and corresponds to a maximum amplitude of the oscillations (when $\theta_m = \frac{\pi}{4}$). This is the MSW resonance which can be seen when $\sin^2(\theta_m)$ is plotted as a function of A, as in Figure (2).

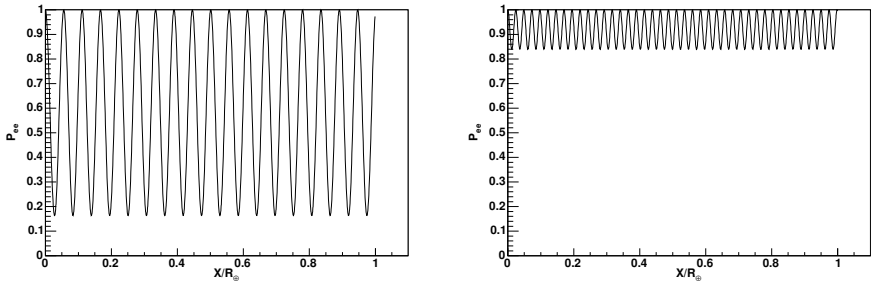

(a) $N_e = 0.01N_e^c$ (b) $N_e = 5N_e^c$

Figure 1: Survival probability below (a) and above (b) the critical density as a function of distance expressed in units of the Earth's radius for two flavours of neutrinos. The mixing angle is chosen as $\sin^2(2\theta) = 0.833$, which is consistent with the mixing angle for solar neutrinos ([22]). The mass squared difference is also taken from experimental data to be $\Delta m_{21} = 7 \times 10^{-5} eV^2$, and the energy is set to $10MeV$. The matter mixing angle in the left panel is given by $\sin^2(2\theta_m) = 0.837$, which is the same as for vacuum oscillations. In the right panel, the matter mixing angle is given by $\sin^2(2\theta_m) = 0.160$ and matter is seen to have a large effect.

One notes that as $A \to 0$, $\theta_m \to \theta$ (matter oscillations become vacuum oscillations) and that when $A \to \infty$, $\theta_m \to \frac{\pi}{2}$ (no oscillations).

In Figure (3), one sees the effects of going through the MSW resonance. The upper left panel shows $A - \Delta m_{21} \cos(2\theta)$ as a function of distance (in units of the Earth's radius), and the density was chosen to be a linear function of distance. The resonance occurs when $A - \Delta m_{21} \cos(2\theta) = 0$, at $X \approx 0.2$, that is, when the resonant density, $N_e^r \equiv \frac{1}{2} \cos(2\theta) N_e^c$, is reached. The bottom left panel shows the electron neutrino survival probability and one notes that the center of the oscillations shifts around the resonance. The upper right panel shows the matter mass eigenvalues (minus the common term, see equation (37)) and one clearly sees that these are closest in energy at the resonance. Finally, the bottom right panel of Figure (3) shows the probability of detecting the first matter mass eigenstate ($| < \nu_1^m | \nu(t) > |^2$) as a function of distance, which appears to be roughly constant.

We see that, throughout the propagation, the neutrino is mostly in the $|\nu_1^m >$ state, even though this state is time dependent. In fact, one easily makes the connection with the adiabatic approximation (see for example [30]) since the Hamiltonian is time dependent and the neutrino remains in the same energy eigenstate (of the time-independent Hamiltonian at the beginning of the slab). If the density profile is such that the propagation is adiabatic, one only needs to calculate the matter mixing angle at the production and detection points to find the probability for a flavour transition.

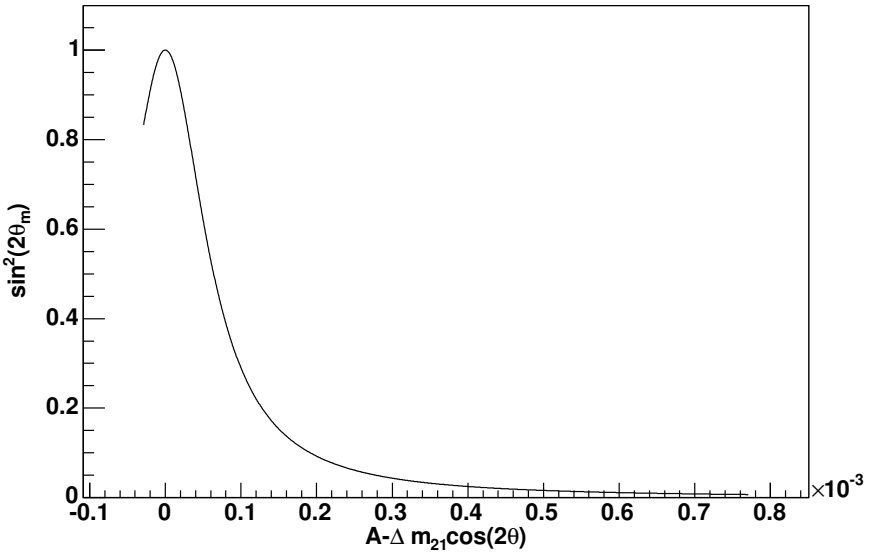

Figure 2: This plot is reproduced from [29] and shows how the matter mixing angle exhibits a resonant behavior as a function of density. The plot shows the amplitude of the matter oscillations ($\sin^2(2\theta_m)$), as a function of $A - \Delta m_{21}\cos(2\theta)$, so that the resonance occurs at zero. At the resonance, the probability for flavour change is maximized. The mixing parameters were chosen with $\sin^2(2\theta) = 0.833$ and $\Delta m_{21} = 7 \times 10^{-5} eV^2$. One notes that when $A = 0$, the matter mixing angle is indeed the same as the vacuum mixing angle. Also, at very high density, the matter oscillations have an amplitude of zero, and the survival probability does not oscillate any more.

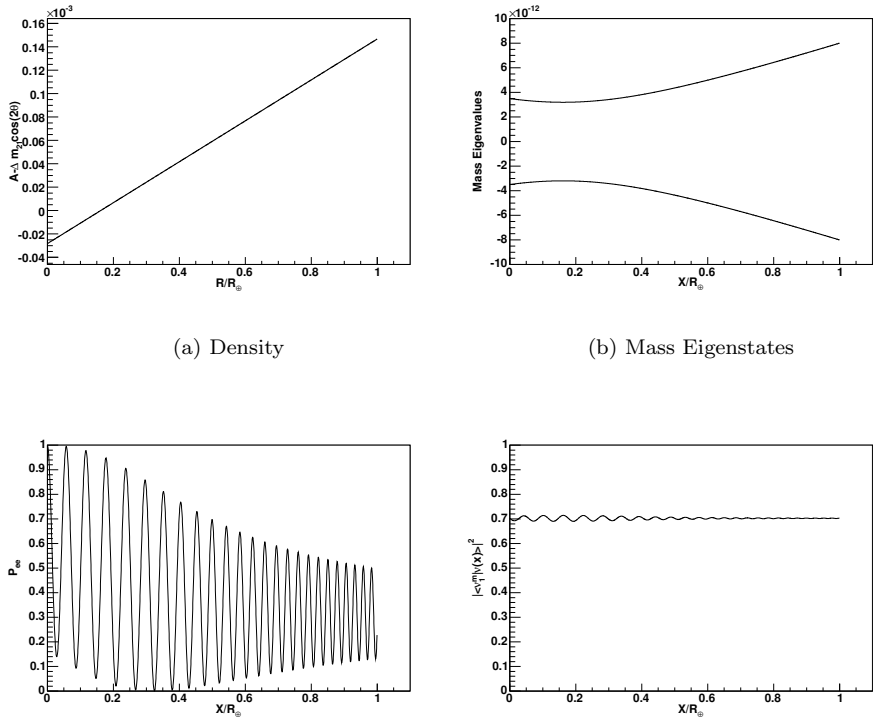

(a) Density

(b) Mass Eigenstates

(c) Survival Probability

(d) Matter Mass Eigenstate Content

Figure 3: Two flavour calculation. Panel (a) shows the density profile used to calculate the other panels. One notes that the resonance is crossed around $X = 0.2$. The density increases linearly from $N_e = 0.01N_e^c$ to $N_e = 5N_e^c$, which are the two extreme cases shown in Figure (1). Panel (b) shows the eigenvalues of the Hamiltonian in (34), and these become closest at the resonance. Panel (c) shows the survival probability, and one notes that the oscillations have a maximum amplitude at the resonance. Finally, panel (d) shows the content of the first matter mass eigenstate, and one notes that it remains roughly constant. The same mixing parameters as in Figure (1) are used.

At the resonance, the two matter states are closest in energy (see Figure (3 (b)), and it is possible for the neutrino to jump (tunnel) between states, in a manner exactly analogous to Landau-Zener level-crossing [31]. This effect depends on the width of the resonance, which in this case is quite large, and the difference in energy between the eigenstates. The small oscillation in the $|\nu_1^m>$ content thus come from the two mass eigenstates jumping back and forth between each other while the energy difference between them is a minimum.

In three flavours, the situation is qualitatively different, as there are two possible resonances, corresponding to the two mass squared differences. In Figure (4) the survival probability is plotted in three flavours as a function of distance (in units of the Earth's radius) for a density varying exponentially from $N_e = 10^{-1}N_e^r$ to $N_e = 10^{3.5}N_e^r$, with N_e^r given as the two flavour resonant density from the above discussion. One notes that the average value of the survival probability shifts two times, once at each resonance. The small oscillations superimposed on the longer wavelength ones come from Δm_{31}. Figure (5) shows the energy eigenvalues as a function of distance, and one notes that there are indeed two resonances, that occur when two of the energy eigenvalues become closest. The energy is set to $10MeV$ and the mixing parameters are $\sin^2(2\theta_{12}) = 0.833$, $\Delta m_{21} = 7 \times 10^{-5}eV^2$, $\sin^2(2\theta_{13}) = 0.1$ and $\Delta m_{31} = 1 \times 10^{-3}eV^2$. Again, we note by considering Figure (6), that the propagation is adiabatic, as the matter mass eigenstate contents do not change very much over the range of the medium. It seems however that the oscillations in the matter mass eigenstate contents have a fairly big amplitude compared to the two-flavour case scenario discussed above. This behavior is again consistent with the eigenstates tunneling into each other when the difference in energy is minimal between them. The oscillations between $|\nu_1^m>$ and $|\nu_2^m>$ also have a larger amplitude because the energy difference is smaller than between $|\nu_2^m>$ and $|\nu_3^m>$ at the corresponding resonance. In addition, the length over which these 'tunneling' oscillations take place is longer because the resonance between $|\nu_1^m>$ and $|\nu_2^m>$ is broader.

2.2.2 Adiabatic Propagation

We now consider the case of adiabatic propagation, mostly following the derivations from [29], and for simplicity, examining the two flavour-case.

We start with the Schrödinger equation in matter for the neutrino in the flavour basis:

$$i\frac{d}{dt}\vec{\nu}^f = H^f\vec{\nu}^f \tag{40}$$

where $\vec{\nu}^f$ is the neutrino state vector in the flavour basis and H^f is the Hamiltonian in the flavour

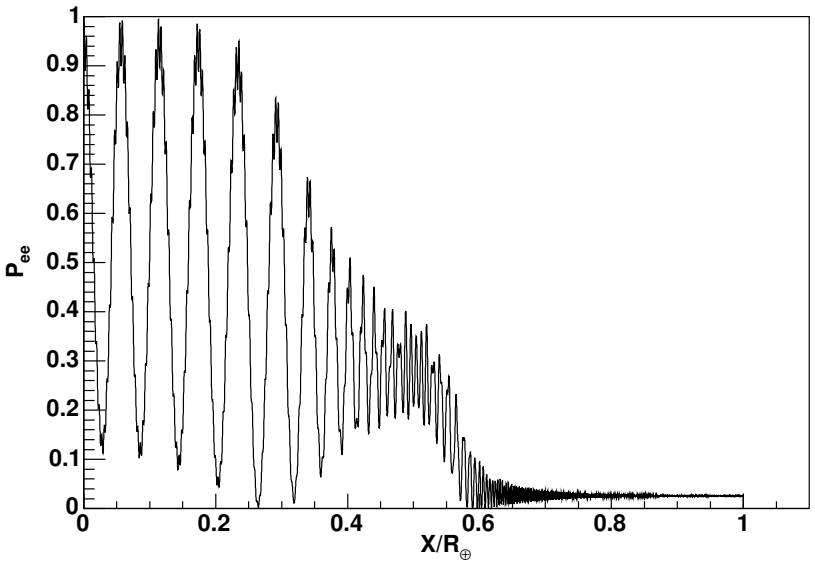

simply

Figure 4: Three-flavour calculation. Survival probability as a function of distance in a medium with density increasing exponentially from $N_e = 10^{-1}N_e^r$ to $N_e = 10^{3.5}N_e^r$, such that the two resonant densities are encountered. The energy is set to $10MeV$ and the mixing parameters are $\sin^2(2\theta_{12}) = 0.833$, $\Delta m_{21} = 7 \times 10^{-5}eV^2$, $\sin^2(2\theta_{13}) = 0.1$ and $\Delta m_{31} = 1 \times 10^{-3}eV^2$.

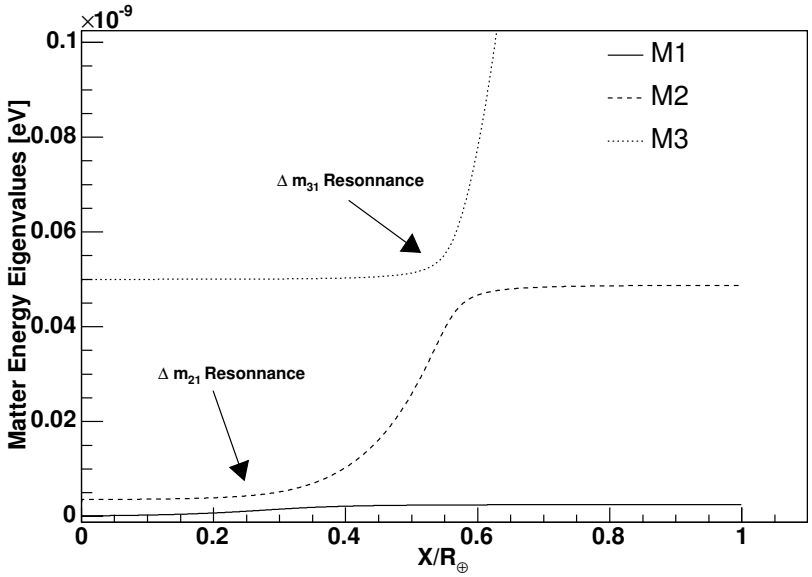

Figure 5: Three flavour calculation. Matter energy eigenvalues as a function of distance in a medium with density increasing exponentially from $N_e = 10^{-1}N_e^r$ to $N_e = 10^{3.5}N_e^r$, such that the two resonant densities are encountered. The energy is set to $10MeV$ and the mixing parameters are $\sin^2(2\theta_{12}) = 0.833$, $\Delta m_{21} = 7 \times 10^{-5}eV^2$, $\sin^2(2\theta_{13}) = 0.1$ and $\Delta m_{31} = 1 \times 10^{-3}eV^2$.

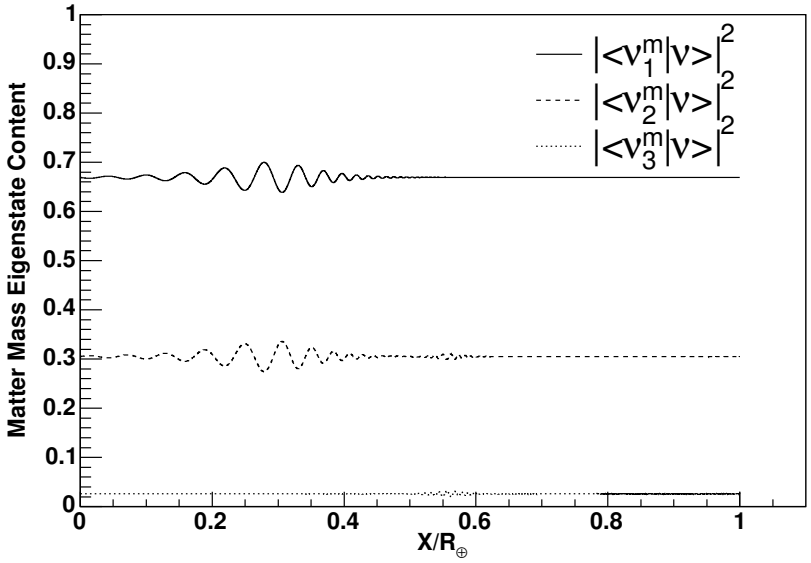

Figure 6: Three-flavour calculation. Matter mass eigenstate content as a function of distance in a medium with density increasing exponentially from $N_e = 10^{-1}N_e^r$ to $N_e = 10^{3.5}N_e^r$, such that two resonant densities are encountered. The energy is set to $10MeV$ and the mixing parameters are $\sin^2(2\theta_{12}) = 0.833$, $\Delta m_{21} = 7 \times 10^{-5}eV^2$, $\sin^2(2\theta_{13}) = 0.1$ and $\Delta m_{31} = 1 \times 10^{-3}eV^2$.

basis given by equation (36). If we let T be the transformation from the matter basis $\vec{\nu}^m$ to the flavour basis ($\vec{\nu}^f = T\vec{\nu}^m$) we can then write the propagation equation as:

$$\begin{aligned} i\frac{d}{dt}\vec{\nu}^f &= TH^mT^\dagger\vec{\nu}^f \\ i\frac{d}{dt}T\vec{\nu}^m &= TH^m\vec{\nu}^m \\ iT\frac{d}{dt}\vec{\nu}^m + i\left(\frac{d}{dt}T\right)\vec{\nu}^m &= TH^m\vec{\nu}^m \end{aligned} \tag{41}$$

where we have used the fact that $H^f = TH^mT^\dagger$ and H^m is the diagonalized Hamiltonian with the eigenvalues given by equation (37). Finally, using the fact that $T^\dagger T = 1$ one can write this in the form:

$$i\frac{d}{dt}\vec{\nu}^m = \left(H^m - iT^\dagger\left(\frac{d}{dt}T\right)\right)\vec{\nu}^m$$

$$
\begin{aligned}
&= \begin{pmatrix} M_1 & 0 \\ 0 & M_2 \end{pmatrix} \vec{\nu}^m \\
&- i \begin{pmatrix} \cos(\theta_m) & -\sin(\theta_m) \\ \sin(\theta_m) & \cos(\theta_m) \end{pmatrix} \begin{pmatrix} -\sin(\theta_m)\frac{d\theta_m}{dt} & \cos(\theta_m)\frac{d\theta_m}{dt} \\ -\cos(\theta_m)\frac{d\theta_m}{dt} & -\sin(\theta_m)\frac{d\theta_m}{dt} \end{pmatrix} \vec{\nu}^m \\
&= \begin{pmatrix} M_1 & -i\frac{d\theta_m}{dt} \\ i\frac{d\theta_m}{dt} & M_2 \end{pmatrix} \vec{\nu}^m
\end{aligned} \tag{42}
$$

As usual, we can factor out an overall phase ($=M_1$), by subtracting a term proportional to the identity matrix from the Hamiltonian and obtain:

$$
\begin{aligned}
i\frac{d}{dt}\vec{\nu}^m &= \begin{pmatrix} 0 & -i\frac{d\theta_m}{dt} \\ i\frac{d\theta_m}{dt} & \frac{\Delta M_{21}}{2E} \end{pmatrix} \vec{\nu}^m \\
&= \begin{pmatrix} 0 & -i\frac{\Delta m_{21}\sin(2\theta)}{2\Delta^2 M_{21}}\frac{dA}{dt} \\ i\frac{\Delta m_{21}\sin(2\theta)}{2\Delta^2 M_{21}}\frac{dA}{dt} & \frac{\Delta M_{21}}{2E} \end{pmatrix} \vec{\nu}^m
\end{aligned} \tag{43}
$$

where we have used equations (37) and (38) in the second line to calculate the derivative. The propagation is thus adiabatic when the off-diagonal terms are small, hence when the density varies slowly as a function of time (distance). More precisely, one can compare the scale over which the mixing angle changes with the wavelength in matter, $\lambda_m = \frac{4\pi E\hbar c}{\Delta M_{21}}$:

$$
\frac{d\theta_m}{dx} << \frac{1}{\lambda_m} \tag{44}
$$

When this condition is satisfied, the propagation is adiabatic and the survival probability can be found simply by knowing the mixing angles at the start (say θ_1) and end of the medium (say θ_2). If one averages over the phase, the classical survival probability is then simply given by:

$$
\begin{aligned}
P_{ee} &= \sum_i^2 P_{\nu_e\to\nu_i}(\theta_1)P_{\nu_i\to\nu_e}(\theta_2) \\
&= \cos^2(\theta_1)\cos^2(\theta_2) + \sin^2(\theta_1)\sin^2(\theta_2) \\
&= \frac{1}{2} + \frac{1}{2}\cos(2\theta_1)\cos(2\theta_2)
\end{aligned} \tag{45}
$$

As we have seen previously, the most likely point for the propagation to be the least adiabatic

is when the matter mass (energy) eigenvalues are closest, as this allows for a tunneling transition between those eigenstates. It is then convenient to introduce an adiabatic parameter, γ, evaluated at the resonance, using equation (44) and the fact that $\lambda_m = \frac{4\pi E\hbar c}{\Delta m_{21}\sin(2\theta)}$

$$\gamma \equiv \frac{\Delta m_{21}\sin^2(2\theta_{12})}{2\hbar cE\cos(2\theta_{12})}\left(\frac{1}{Ne}\frac{dNe}{dx}\right)^{-1} \tag{46}$$

so that the propagation is adiabatic when $\gamma >> 1$. This choice follows from others in the literature ([29],[14]) and will be examined in section (2.3).

Figure (7) compares the survival probability from Figure (3) (through a slab with density varying linearly across the resonance) along with the result calculated using the adiabatic approximation as well as a numerical phase average (the neutrino content is averaged over the phase at each position). The curves agree quite well indicating that the propagation is indeed adiabatic, as suspected earlier. One notes that the adiabatic approximation becomes less accurate after the resonance and misses some small oscillations in the survival probability. These oscillations (in the phase-averaged curve) come from the mass eigenstate content oscillating slightly, as will be recalled from Figure (3).

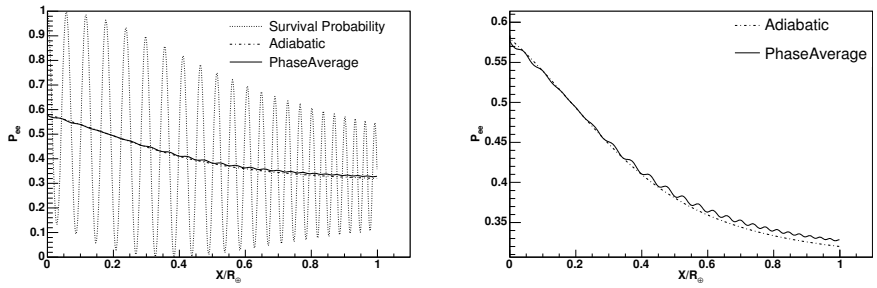

(a) (b)

Figure 7: Comparison of the adiabatic approximation in two flavours with a numerical phase average. The neutrino traverses a medium of length $R_\oplus$ with a density varying linearly from $0.01N_e^c$ to $5N_e^c$. The left panel shows the fully numerical survival probability and the right panel is drawn with a scale that highlights the differences between the adiabatic and the (exact) phase averaged curves.

2.2.3 Deviations from Adiabaticity-Jump Probability

We now examine the case when the propagation deviates slightly from being fully adiabatic, particularly in the case where the MSW resonance is encountered during the propagation. As stated before, this case is analogous to Landau-Zener level crossing. In fact, panel (b) of Figure (3) is almost the same as Figure(2) in [31] where the level crossing problem is considered for colliding molecules.

The Hamiltonian is also similar to that in [31] and the problem can be solved in a similar fashion. One would generally approximate the terms varying in space by a linear function which then yields coupled equations that can be solved exactly. This is the approach first taken by Haxton [32] and Parke [14] when they considered solar neutrinos and approximated the density as varying linearly at the resonance. Kuo and Pantaleone have derived the solutions for various other analytical forms for the density and a summary is provided in [29].

When the propagation is non-adiabatic at the resonance, there exists a probability, P_j, of 'jumping' from one mass eigenstate to the other. This can only be found by solving the differential equations (43) and this is only possible for (some) analytic forms of the electron density. One can define P_j as the probability $| < \nu_1(\theta_1)|\nu_2(\theta_2) > |^2 = | < \nu_2(\theta_2)|\nu_1(\theta_1) > |^2$ for the eigenstates on each side of the resonance to have been converted into each other at the resonance, where $\theta_{1(2)}$ is the mixing angle at the production (detection) point. Equation (45) is then modified such that:

$$\begin{aligned} P_{ee} &= \sum_{i,k}^{2} P_{\nu_e \to \nu_i}(\theta_1) P_{\nu_i \to \nu_k}(N_e^r) P_{\nu_k \to \nu_e}(\theta_2) \\ &= \cos^2(\theta_1)(1-P_j)\cos^2(\theta_2) + \cos^2(\theta_1)(P_j)\sin^2(\theta_2) \\ &+ \sin^2(\theta_1)(1-P_j)\sin^2(\theta_2) + \sin^2(\theta_1)(1-P_j)\cos^2(\theta_2) \\ &= \frac{1}{2} + (\frac{1}{2} - P_j)\cos(2\theta_1)\cos(2\theta_2) \end{aligned} \tag{47}$$

where N_e^r is the density at the resonance and, by unitarity, $(1 - P_j)$ is the probability of one mass eigenstate remaining in that state through the resonance. In this 'corrected adiabatic' approximation, one then calculates the mixing angles at the starting and ending points as well as a jump probability at the resonance point. This can speed up numerical calculations substantially since one doesn't need to solve the propagation equation numerically at each point, but only in three locations in the medium. One should also note that this equation breaks down when the neutrino phase cannot be averaged out, which happens if the neutrinos are produced in a small region or close to the resonance. Other relevant limits of this calculation are discussed in [33].

If one applies the result from Landau and Zener [31] to a medium with density varying linearly, as was first suggested by Haxton [32] and Parke [14], one finds that the jump probability is simply given by:

$$P_j^{Parke} = e^{-\frac{\pi}{2}\gamma(x_{res})} \tag{48}$$

in exact analogy to the result from Landau and Zener, where x_{res} indicates that the the adiabaticity parameter, γ, (defined above) is to be evaluated at the resonance.

2.2.4 Three-Flavour Case

In three flavours, the adiabatic approximation can still apply as well as the 'corrected adiabatic' approximation. In the case of adiabatic propagation, one solves for the mixing matrix at the production point (say $T^{(1)}$) and detection point (say $T^{(2)}$) so that the classical electron survival probability can be written as:

$$\begin{aligned} P_{ee} &= \sum_i^3 P_{\nu_e \to \nu_i}(T^{(1)}) P_{\nu_i \to \nu_e}(T^{(2)}) \\ &= |T_{e1}^{(1)}|^2 |T_{e1}^{(2)}|^2 + |T_{e2}^{(1)}|^2 |T_{e2}^{(2)}|^2 + |T_{e3}^{(1)}|^2 |T_{e3}^{(2)}|^2 \end{aligned} \tag{49}$$

Figure(8) shows a comparison of the adiabatic approximation with the phase-averaged survival probability from the case in Figure (4), where the density increased exponentially with distance. We see that, even in the case where two resonances are crossed, the adiabatic approximation provides an excellent approximation to the full numerical calculation. In addition, from Figure (6), it appeared that the propagation was less adiabatic than in the example with the linear density, considered previously, but the adiabatic approximation is still very accurate. In fact, it only misses small oscillations in the mass eigenstate content, which are visible in the phase-averaged curve as well as Figure (6).

In the case of a slight deviation from adiabaticity in three flavours, one can rewrite equation (47) in the form:

$$P_{ee} = \sum_{i,k}^3 P_{\nu_e \to \nu_i}(T^{(1)}) P_{\nu_i^{(1)} \to \nu_k^{(2)}}(N_e^r(\Delta m_{ik})) P_{\nu_k \to \nu_e}(T^{(2)}) \tag{50}$$

where the resonant density is now a function of the mass-squared difference that is relevant for the transition. This modification arises since there can be more than one resonant density corresponding to the different mass-squared differences. One must then solve the differential equations for the three

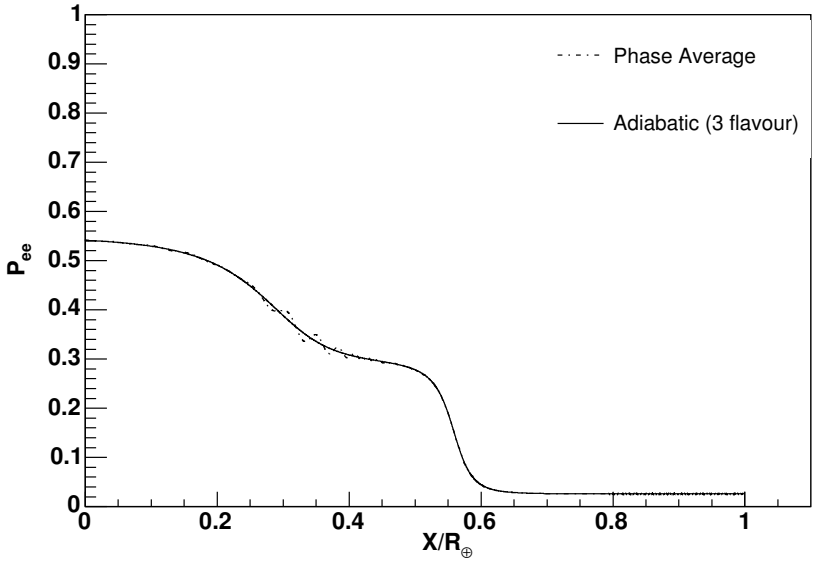

Figure 8: Comparison of the adiabatic approximation in three flavours with a numerical phase average for the same situation as in Figure (4). The neutrino traverses a medium of length $R_\oplus$ with a density increasing exponentially from $N_e = 10^{-1}N_e^r$ to $N_e = 10^{3.5}N_e^r$. The mixing parameters are the same as in Figure (4)

possible mass eigenstate transitions at the resonances. We will however see in section (2.3) that this is unnecessary in the case of solar neutrinos, and that an excellent approximation can be achieved by using only the transition between the first two eigenstates.

2.2.5 Three-Flavour Case - Decoupling

To better understand the three-flavour case, we follow work from [12] and [34] and consider situations that are well approximated by equivalent two-flavour models. We recall the equation (34) for propagation in matter for three flavours of neutrinos expressed in the flavour basis:

$$i\frac{d}{dt}\vec{\nu^f} = \frac{1}{2E}\left(R_{23}R_{13}R_{12}H_1^v R_{12}^\dagger R_{13}^\dagger R_{23}^\dagger + H_2^f\right)\vec{\nu^f} \tag{51}$$

where we have expanded the mixing matrix U in terms of the rotation matrices,R_{ij}, that generate it. One can now introduce a new basis $\{|\nu_i^Z>\}|_{i=1,2,3}$ that is given by the transformation $\vec{\nu^f} = Z\vec{\nu^Z}$, where Z is defined as $Z = R_{23}R_{13}$. In this new basis, the θ_{23} mixing angle disappears [1], and the Hamiltonian, H^Z, is given by:

[1] As noted earlier (section (2.1)), the electron survival probability will never depend on θ_{23} in the chosen parametrization of U.

$$\begin{aligned} H^Z &= Z^\dagger H^f Z = R_{13}^\dagger R_{23}^\dagger H^f R_{23} R_{13} \\ &= \frac{1}{2E}\begin{pmatrix} Ac_{13}^2 + \Delta m_{21} s_{12}^2 & \Delta m_{21} s_{12} c_{12} & Ac_{13}s_{13}e^{-i\delta} \\ \Delta m_{21} s_{12} c_{12} & c_{12}^2 \Delta m_{21} & 0 \\ Ac_{13}s_{13}e^{i\delta} & 0 & As_{13}^2 + \Delta m_{31} \end{pmatrix} \end{aligned} \tag{52}$$

where Z is given by:

$$Z = \begin{pmatrix} c_{13} & 0 & s_{13}e^{-i\delta} \\ -s_{23}s_{13}e^{i\delta} & c_{23} & s_{23}c_{13} \\ -c_{23}s_{13}e^{i\delta} & -s_{23} & c_{23}c_{13} \end{pmatrix} \tag{53}$$

In the case where Δm_{12} and A are small compared to Δm_{31}, the three-flavour oscillations effectively decouple into one single neutrino and a standard two-neutrino oscillation scheme. To zeroth order in $Ac_{13}s_{13}e^{-i\delta}$ the Hamiltonian then becomes:

$$H_{dec}^Z = \frac{1}{4E}\begin{pmatrix} 2Ac_{13}^2 + \Delta m_{21}(1 - \cos(2\theta_{12})) & \Delta m_{21}\sin(2\theta_{12}) & 0 \\ \Delta m_{21}\sin(2\theta_{12}) & \Delta m_{21}(1 + \cos(2\theta_{12})) & 0 \\ 0 & 0 & \Delta m_{31} \end{pmatrix} \tag{54}$$

which is exactly the same Hamiltonian (in block form) as given by equation (34) in two flavours, if the substitution $A \to Ac_{13}^2$ is made. This situation is relevant when the density is such that A never becomes of order Δm_{31}. One notes that the block part of the Hamiltonian cannot be neglected as the eigenvalues would become degenerate. There is thus an inherent error of order $Ac_{13}s_{13}$ in the approximation, which is acceptable, since current bounds on θ_{13} are consistent with zero. The eigenvalues of this Hamiltonian are then given by:

$$\begin{aligned} M_{1,2}^{3f} &= \frac{1}{4E}\left(\Delta m_{21} + c_{13}^2 A \mp \Delta M_{21}^{3f}\right) \\ M_3^{3f} &= \frac{1}{4E}\Delta m_{31} \\ \Delta M_{21}^{3f} &\equiv \sqrt{\Delta^2 m_{21} + A^2 c_{13}^4 - 2Ac_{13}^2 \Delta m_{21}\cos(2\theta_{12})} \end{aligned} \tag{55}$$

and the phase differences acquired between the matter mass eigenstates are thus:

$$\begin{aligned} \phi_1 &= \frac{\Delta M^{3f}_{21}}{2E} \\ \phi_2 &= \frac{\Delta m_{31}}{4E} \end{aligned} \tag{56}$$

and the third neutrino does not mix with the first two. As usual, we can define a matrix T that diagonalizes H^Z and relates the matter mass eigenstates $\vec{\nu^m}$ to the basis $\vec{\nu^Z}$, so that $\vec{\nu^Z} = T\vec{\nu^m}$:

$$\begin{aligned} T &= \begin{pmatrix} \cos(\theta_m) & \sin(\theta_m) & 0 \\ -\sin(\theta_m) & \cos(\theta_m) & 0 \\ 0 & 0 & 1 \end{pmatrix} \\ \tan(2\theta_m) &= \frac{\Delta m_{21}\sin(2\theta_{12})}{\Delta m_{21}\cos(2\theta_{12}) - Ac^2_{13}} \end{aligned} \tag{57}$$

Finally, one can go from the matter mass basis to the original flavour basis using the relation $\vec{\nu^f} = M\nu^m$, where M is given by $M = ZT$ (and has the same form as U with the replacement $\theta_{12} \to \theta_m$), so the survival probability is then given by (recall equations (28) and (17)):

$$\begin{aligned} P_{ee} &= \left| |M_{e1}|^2 + |M_{e2}|^2 e^{-i\frac{\phi_1}{\hbar}t} + |M_{e3}|^2 e^{-i\frac{\phi_2}{\hbar}t} \right|^2 \\ &= \left| |c^2_{13}\cos^2(\theta_m) + c^2_{13}\sin^2(\theta_m) e^{-i\frac{\phi_1}{\hbar}t} + s^2_{13} e^{-i\frac{\phi_2}{\hbar}t} \right|^2 \\ &= s^4_{13} + c^4_{13}\left[\cos^4(\theta_m) + \sin^4(\theta_m) + 2\cos^2(\theta_m)\sin^2(\theta_m)\cos\left(\frac{\phi_1 t}{\hbar}\right)\right] \\ &+ 2s^2_{13}c^2_{13}\cos^2(\theta_m)\cos\left(\frac{\phi_2 t}{\hbar}\right) + 2s^2_{13}c^2_{13}\sin^2(\theta_m)\cos\left(\frac{(\phi_2-\phi_1)t}{\hbar}\right) \\ &\approx s^4_{13} + c^4_{13} P^{2f}_{ee}|_{A\to Ac^2_{13}} + 2c^2_{13}s^2_{13}\cos\left(\frac{\phi_2 t}{\hbar}\right) \\ &\approx s^4_{13} + c^4_{13} P^{2f}_{ee}|_{A\to Ac^2_{13}} \end{aligned} \tag{58}$$

where we have assumed $\phi_2 >> \phi_1$ in the second-last line and then dropped the rapidly oscillating term ($\cos\left(\frac{\phi_2 t}{\hbar}\right)$). $P^{2f}_{ee}|_{A\to Ac^2_{13}}$ is the standard two-flavour survival probability in matter with the replacement of A with Ac^2_{13}. This approximation was first derived in [12] and is often used to correct the two-flavour formulas for solar neutrinos, as it is believed that θ_{13} is small but might have a slight

effect at the order of this correction. The validity of this formula will be examined in more detail in section (2.3). Equation (58) is relevant when the matter potential, A, can become of order Δm_{21}, which is the MSW resonance. In this case, the adiabatic approximation may also be used in three flavours with a two-flavour jump probability, since the oscillations to the third mass eigenstate are decoupled. In summary, equation (58) is appropriate when the neutrino propagates through the Δm_{21} resonance and $\Delta m_{21} << \Delta m_{31}$ with small θ_{13}. This will be examined in section (2.3) and is discussed substantially in the literature, ([34],[35]).

Lim, Ogure and Tsujimoto ([34]) have derived the formula to the next leading order for the same case as above and showed some improvement in accuracy. The essential feature is in modifying θ_{13} at the production point and adding a small correction, ϵ. These formulas will be compared in section (2.3) and are discussed substantially in their paper, so we will just present their version without deriving it:

$$\begin{aligned} A_{eff} &\equiv c_{13}^2 A - \frac{\sin^2(2\theta_{13})A^2}{4\Delta m_{31}} \\ \tan(2\epsilon(t)) &\equiv \frac{A(t)\sin(2\theta_{13})}{\Delta m_{31} - s_{12}^2\Delta m_{21} - A(t)\cos(2\theta_{13})} \\ P_{ee} &= s_{13}^2\sin^2(\theta_{13}+\epsilon(0)) + c_{13}^2\cos^2(\theta_{13}+\epsilon(0))P_{ee}^{2f}|_{A\to A_{eff}} \end{aligned} \tag{59}$$

We note that the expression for ϵ will be singular when:

$$\sin^2(2\theta_{12})\Delta m_{21} = A(t)\cos(2\theta_{13}) - \Delta m_{31} \tag{60}$$

corresponding to a large correction to θ_{13}, and this formula will break down.

The reduction formulas that have been presented so far are relevant when the neutrino traverses a matter resonance where the matter potential is of the same order as the first mass-squared difference or when it sees no resonances. It is natural to consider the case when a resonance with the second mass squared difference is encountered. In this case, a similar derivation can be done, setting $Z = R_{23}$. The Hamiltonian then becomes:

$$H^{Z(2)} = \tfrac{1}{2E} \times$$

$$\begin{pmatrix} s_{12}^2 c_{13}^2 \Delta m_{21} + s_{13}^2 \Delta m_{31} + A & s_{12} c_{12} c_{13} \Delta m_{21} & c_{13} s_{13} e^{-i\delta} (\Delta m_{31} - s_{12}^2 \Delta m_{21}) \\ s_{12} c_{12} c_{13} \Delta m_{21} & c_{12}^2 \Delta m_{21} & -s_{12} c_{12} s_{13} e^{-i\delta} \Delta m_{21} \\ c_{13} s_{13} e^{i\delta} (\Delta m_{31} - s_{12}^2 \Delta m_{21}) & -s_{12} c_{12} s_{13} e^{i\delta} \Delta m_{21} & s_{13}^2 s_{12}^2 \Delta m_{21} + c_{13}^2 \Delta m_{31} \end{pmatrix} \tag{61}$$

In this case, we still assume $\Delta m_{31} >> \Delta m_{21}$ and drop the terms of leading order in $s_{12} c_{12} \Delta m_{21}$ (since these are negligible compared to A and Δm_{31}) and obtain the Hamiltonian:

$$H_{dec}^{Z(2)} = \tfrac{1}{2E} \times$$
$$\begin{pmatrix} s_{12}^2 c_{13}^2 \Delta m_{21} + s_{13}^2 \Delta m_{31} + A & 0 & c_{13} s_{13} e^{-i\delta} (\Delta m_{31} - s_{12}^2 \Delta m_{21}) \\ 0 & c_{12}^2 \Delta m_{21} & 0 \\ c_{13} s_{13} e^{i\delta} (\Delta m_{31} - s_{12}^2 \Delta m_{21}) & 0 & s_{13}^2 s_{12}^2 \Delta m_{21} + c_{13}^2 \Delta m_{31} \end{pmatrix} \tag{62}$$

which once again decouples into one uncoupled neutrino and a set of two-neutrino oscillations with eigenvalues:

$$\begin{aligned} M_{1,3}^{dec} &= \frac{1}{2E} \left(\Delta m_{31} + A + \Delta m_{21} s_{12}^2 \pm M_{31}^{3f} \right) \\ M_2^{3f} &= \frac{1}{2E} \Delta m_{21} c_{12}^2 \\ \Delta M_{31}^{3f} &\equiv \\ &\sqrt{\Sigma - 2\Delta m_{21} s_{12}^2 (A + \Delta m_{31}) - 4\Delta m_{21} A s_{12}^2 c_{13}^2 + 2\Delta m_{31} A (1 - 4c_{13}^2) + \Delta^2 m_{21} c_{12}^2 (c_{12}^2 - 2)} \\ \Sigma &\equiv \Delta^2 m_{31} + \Delta^2 m_{21} + A^2 \end{aligned} \tag{63}$$

The main point is that the equations can be decoupled when the mass-squared differences are well separated and only one of the resonances is encountered. If both resonances are traversed by the neutrino, these formulas can still be applied, provided that the neutrino can propagate adiabatically between them. In this case, one can use each Hamiltonian at the relevant resonance. The subject of passing through both resonances is well discussed in [34] and [29].

2.2.6 Boundary Between Layers

We now consider what happens at the boundary between two slabs of (different) constant densities. The left panel of Figure (9) shows the survival probability through a medium whose density changes in the middle (at $X = 0.5$) from $N_e = 0.01N_e^c$ to $N_e = 5N_e^c$. The right panel show the corresponding $|\nu_1^m >$ content. The length of each slab is $0.325R_\oplus$, where $R_\oplus$ is the radius of the Earth. One notes that the neutrino is mostly in the $|\nu_1^m >$ eigenstate before the interface (at $X = 0.5$) and mostly in the $|\nu_2^m >$ state after the density change. The propagation between the slabs is thus strongly non-adiabatic. In the first slab, the oscillations are essentially vacuum oscillations and $\theta_m < \frac{\pi}{4}$ so a pure electron neutrino is mostly in the first mass eigenstate. In the second slab, $\theta_m > \frac{\pi}{4}$ and the neutrino is mostly in the second mass eigenstate, because, at the interface, the neutrino is mostly in the electron flavour eigenstate (this comes from the specific lengths of the slabs that were chosen). Although the parameters are the same as in Figure (1), one immediately notes that the oscillations in the second slab have a different amplitude than in Figure (1b), and that this amplitude is not simply given by $\sin^2(2\theta_m)$. This arises from the fact that the oscillation formula in the second slab is not given by equation (39). The reason for this is simply that in the second slab, the neutrino does not start as a pure flavour eigenstate. If the neutrino arrives in the second slab with a mix of flavour eigenstates given by:

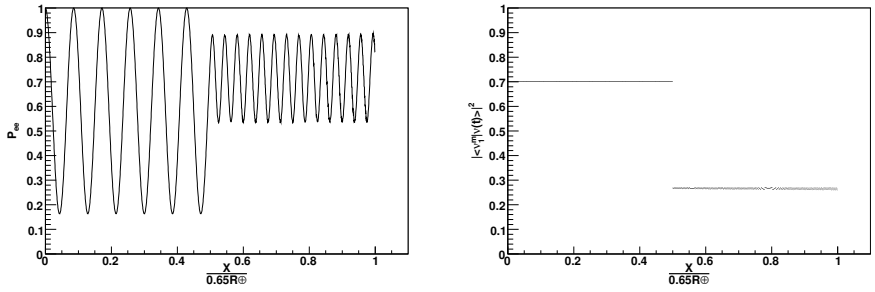

(a) (b)

Figure 9: Probabilities as a function of distance, over a range of $0.65R_\oplus$, through two slabs of constant density, $N_e = 0.01N_e^c$ and $N_e = 5N_e^c$. Panel (a) shows the survival probability and panel (b) the first matter mass eigenstate content. The same parameters as those of Figure (1) were used. One notes that the amplitude of the oscillations in the survival probability in the second slab is no longer given by $\sin^2(2\theta_m) = 0.160$, since the neutrino is not in a pure electron flavour state at the beginning of the second slab. The transition between the two slabs is strongly non-adiabatic, as can be seen in panel (b) where the neutrino is mostly in the $|\nu_1^m >$ state in the first slab and mostly $|\nu_2^m >$ in the second slab.

$$|\nu(0)>= A_e|\nu_e> + A_\mu|\nu_\mu> \tag{64}$$

then equation (15) is modified to:

$$\begin{aligned} k_1^m &= A_e\cos\theta_m - A_\mu\sin\theta_m \\ k_2^m &= A_e\sin\theta_m + A_\mu\cos\theta_m \end{aligned} \tag{65}$$

and the probability of detecting an electron type neutrino, P_e, then becomes:

$$\begin{aligned} P_e(t) &= |A_e(\cos^2\theta_m + \sin^2\theta_m e^{-i\frac{\Delta^2 M_{21}}{2E\hbar}t}) + A_\mu\cos\theta_m\sin\theta_m(e^{-i\frac{\Delta^2 M_{21}}{2E\hbar}t} - 1)|^2 \\ &\propto \frac{1}{2}\sin^2(2\theta_m)\cos\left(\frac{\Delta^2 M_{21}}{2E\hbar}t\right) + 2\cos^3\theta_m\sin\theta_m\Re(A_e A_\mu^* e^{-i\frac{\Delta^2 M_{21}}{2E\hbar}t}) \\ &+ 2\cos\theta_m\sin^3\theta_m\Re(A_e^* A_\mu e^{-i\frac{\Delta^2 M_{21}}{2E\hbar}t}) \end{aligned} \tag{66}$$

where $\Re$ denotes the real part of an expression and only the oscillating terms are shown. Clearly, the amplitude of the oscillations also depends on the initial flavour content. This is the reason the slabs in Figure (9) were chosen to each have a length of $0.325R_\oplus$, since it resulted in the neutrino entering the second slab as mostly $|\nu_e>$. In Figure (10), the slabs are slightly longer ($0.425R_\oplus$) so that the neutrino exits the first slab as mostly $|\nu_\mu>$ and one notes that in the right panel, the neutrino stays mostly in the $|\nu_1^m>$ state. In this case, we see that the energy eigenstate content changes less and conclude that the phase of the neutrinos at the boundary is important, since varying the length of a slab of constant density is equivalent to changing the phase that was acquired through the slab.

When it comes to the numerical accuracy of crossing the boundary, one can easily guarantee a smooth behavior in the evolution of the flavour content. In order to do this, one writes a computer program that tracks the flavour content. At the beginning of the slab, the matter mass eigenstate content can be calculated from the matter mixing angle and the initial flavour content. The neutrino can then be propagated through the slab, according to equation (14), and the flavour content can then be updated. Hence, if one imposes the boundary condition that the flavour content is continuous at the interface between slabs, a smooth survival probability is automatically achieved, even in the case of a strongly non-adiabatic density change. The only numerical issue is then to make sure that

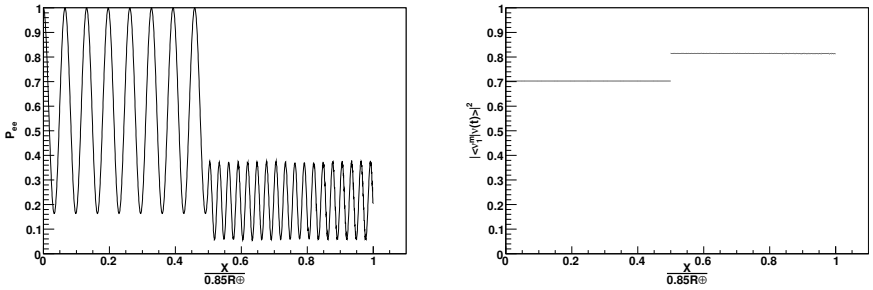

(a) Survival Probability (b) First matter mass eigenstate content

Figure 10: Probabilities as a function of distance, over a range of $0.85R_{\oplus}$, through two slabs of constant density, $N_e = 0.01N_e^c$ and $N_e = 5N_e^c$. Panel (a) shows the survival probability and panel (b) the first matter mass eigenstate content. The same parameters as those of Figure (9) were used.

the oscillation length does not change very much across the length of the slabs.

2.2.7 The Effect of the Phase on Propagation Across Boundaries

We now briefly consider an interesting effect arising from the neutrino phase when crossing a boundary between two different electron densities. As was noted from Figures (9) and (10), the phase has an effect on the propagation through a boundary. We examine this further by considering a neutrino propagated through vacuum, then through the same medium as in Figure (10) and then vacuum again. That is, the density goes from 0 to $0.01N_e^c$ then $5N_e^c$ and finally back to 0. The survival probability is plotted for such a situation in Figure (11) where the two vacuum parts are each one Earth radius in length and the non-zero density part is also one Earth radius in length with a density change at $X = 0$. The mixing parameters are set to $\Delta m_{21} = 2 \times 10^{-5} eV^2$ and $\tan^2(\theta) = 0.42$ with an energy of $10MeV$. The left panel shows the survival probability and the right panel shows the first matter-mass eigenstate content. The first slab of non-zero density does not affect the propagation very much, as we have seen earlier that when $N_e = 0.01N_e^c$, the neutrino is essentially in the vacuum regime.

The calculation was done by starting the neutrino in the electron flavour state and solving for the mass eigenstate contents k_1 and k_2:

$$|\nu(0)> = |\nu_e> = k_1|\nu_1> + k_2|\nu_2> \tag{67}$$

The neutrino is then initialized to have mass eigenstate contents k_1 and k_2, which is the same as

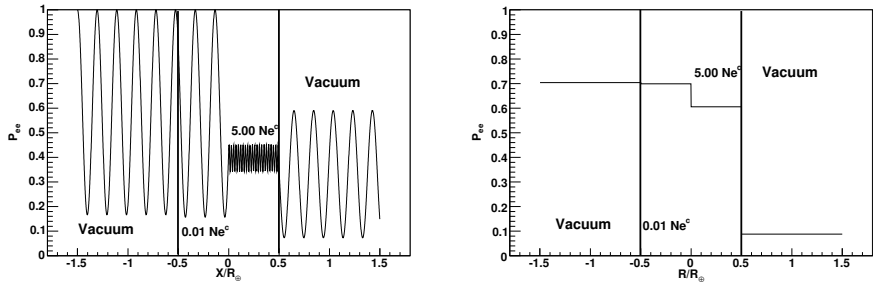

(a) Survival Probability (b) First mass eigenstate content

Figure 11: Probabilities as a function of distance (in units of the Earth radius), through vacuum then two different slabs of constant density and finally through vacuum again. Panel (a) shows the survival probability and panel (b) the first mass eigenstate content. The mixing parameters are $\Delta m_{21} = 2 \times 10^{-5} eV^2$ and $\tan^2(\theta) = 0.42$ with an energy of $10 MeV$. The neutrino starts in vacuum in the electron flavour according to equation (67). The propagation is physically analogous to that of a coherent beam of neutrinos.

having a beam of coherent (electron flavour) neutrinos, and then propagating it through the medium.

We now consider the probability of detecting an electron neutrino that started in the state defined by equation (67), but shifted by half a wavelength, hence, with the replacement $k_2 \rightarrow k_2 e^{i\pi}$. When one looks at the probability of detecting an electron type neutrino, Figure (12a), one is not surprised to see that the oscillations in the vacuum part before the medium are now out of phase when compared to Figure (11). One does however note that the oscillations in the medium are not exactly out of phase. Introducing this phase shift is analogous to the change in length we imposed on the medium in going from Figure (9) to Figure (10).

The interesting aspect of this calculation arises when one averages over the phase (ϕ) of the initial mass content, $k_2 \rightarrow k_2 e^{i\phi}$. This is physically equivalent to considering a beam of incoherent neutrinos. Figure (13) shows the probability of detecting an electron neutrino and the first mass eigenstate content in such a situation. We see that in the vacuum part before the medium, the probability of detecting an electron neutrino is now constant (as expected), however, the medium reintroduces coherence and the neutrino beam becomes coherent after leaving the medium. This situation happens in Nature when solar neutrinos, which are incoherent (as they originated in different parts of the Sun), traverse the Earth and oscillate coherently in vacuum once they have left the Earth. The explanation lies in the fact that as the beam enters the medium, there is now a common point in space (time) for all the neutrinos. At this point, one of the mass eigenstates ($|\nu_2>$ in the above example) gets created coherently for all the neutrinos. This surprising result will be examined

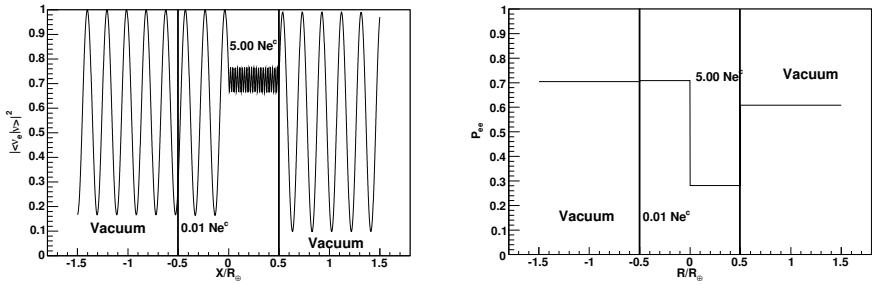

(a) Probability of detecting ν_e (b) First mass eigenstate content

Figure 12: Probabilities as a function of distance (in units of the Earth radius), through vacuum then two different slabs of constant density and finally through vacuum again. Panel (a) shows the survival probability and panel (b) the first mass eigenstate content. The mixing parameters are $\Delta m_{21} = 2 \times 10^{-5} eV^2$ and $\tan^2(\theta) = 0.42$ with an energy of $10 MeV$. The neutrino starts in vacuum as an electron neutrino that has traveled half of a wavelength in vacuum, that is, in the state defined by equation (67) with $k_2 \rightarrow k_2 e^{i\pi}$. The propagation is physically analogous to that of a coherent beam of neutrinos, out of phase compared to Figure (11).

when neutrinos traversing the Earth are considered. It is also interesting to note that the part of the medium with $Ne = 0.01 N_e^c$ actually does have an effect on the neutrino propagation, and one can clearly see that this is where the coherent regeneration begins. We first used this density to show that below the critical density, the matter oscillation regime is almost the same as in vacuum. We now see that this has to be a qualified statement, and a small density is not the same as a zero density, as it can reintroduce coherence.

2.2.8 Flux at SNO

We now briefly consider the steps needed in order to calculate the flux of solar electron flavour neutrinos at the SNO detector. If one considers a distributed source of neutrinos (which is the case for the ^8B neutrinos that SNO sees), one must integrate the flux over the source distribution, $\phi(\vec{r})$. In the case of solar neutrinos, an azimuthally symmetric distribution can be assumed so that the total flux, Φ, can be written as:

$$\Phi(x) \propto \int_0^{\pi} \int_0^{R_\odot} P_{ee}(d_{SNO}(\vec{r}_0, L))\ \phi(r_0) r_0^2 \sin(\theta_\odot)\ dr_0\ d\theta_\odot \tag{68}$$

where $\vec{r}_0$ is the point in the Sun where the neutrino was produced and d_{SNO} is the distance from that position to the SNO detector, which depends on the earth-sun distance L. Since the oscillation lengths relevant in the Sun are smaller than the solar radius, one must also integrate over the polar

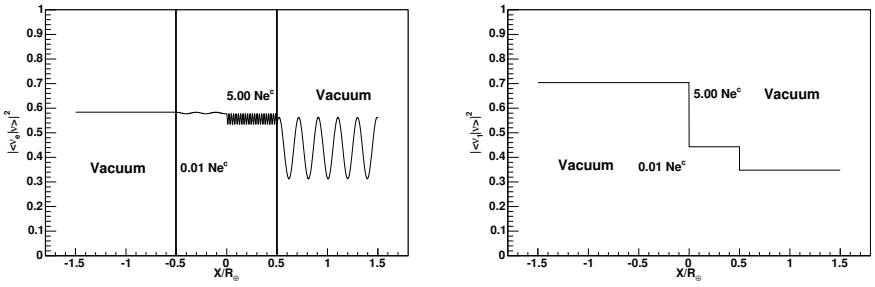

(a) Probability of detecting ν_e (b) First mass eigenstate content

Figure 13: Probabilities as a function of distance (in units of the Earth radius), through vacuum, then two different slabs of constant density and finally through vacuum again. Panel (a) shows the survival probability and panel (b) the first mass eigenstate content. The mixing parameters are $\Delta m_{21} = 2 \times 10^{-5} eV^2$ and $\tan^2(\theta) = 0.42$ with an energy of $10 MeV$. The neutrino starts in vacuum as an incoherent superposition of neutrinos that originated at different locations (spread over one wavelength) in the electron flavour. The calculation was done using equation (67) with the substitution $k_2 \to k_2 e^{-i\pi}$ and the result was then averaged over ϕ.

angle, $\theta_\odot$ of the initial position (to model neutrinos from the far side of the sun, see Figure (14).

We are interested in yearly averages at SNO, so we must also integrate the flux over the earth-sun distance:

$$\Phi(x) \propto \int_{1AU(1-\epsilon)}^{1AU(1+\epsilon)} \int_0^{\pi} \int_0^{R_\odot} P_{ee}(d_{SNO}(\vec{r}_0, L))\, \phi(r_0) r_0^2 \sin(\theta_\odot)\, dr_0\, d\theta_\odot\, dL \tag{69}$$

where $1AU$ is 1 astronomical unit and ϵ is the Earth's orbit's eccentricity. We have made the assumption that the distribution of earth-sun distances is constant. This is motivated by the fact that the neutrino oscillation wavelength in vacuum is smaller than this variation for the best-fit mixing parameters. This assumption then allows one to change the average over earth-sun distances into a simple average over one wavelength in vacuum. In effect, the mass eigenstates in the neutrino beam then become incoherent (phase-averaged). Finally, in doing a yearly averaged flux, one must also average over the trajectories through the Earth, which can be labeled by the Nadir angle η, (see Figure (14)), which is just π minus the zenith angle of the sun. It is reasonably straightforward to calculate the theoretical distribution, $\zeta(\eta)$, of these trajectories over a year for a particular location by using simple geometry and the parameters describing the Earth's orbit. One typically refers to this distribution as the zenith angle exposure function. For example, SNO has its own experimental zenith angle exposure function, which is essentially just a histogram of the live-time of the detector at each zenith angle of the sun. The total yearly flux is then obtained through the following 4-

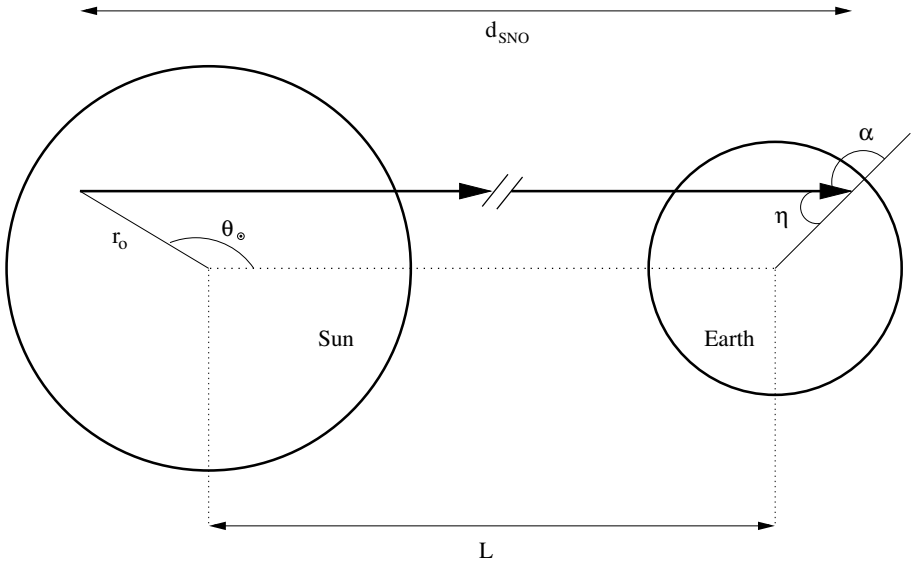

Figure 14: Diagram showing a possible trajectory for a neutrino. All the neutrinos are assumed to follow parallel trajectories and originate from the upper half of the Sun. The neutrino starting position is labeled by the polar angle $\theta_\odot$ and it's starting radius r_o. In the Earth part, the trajectory is labeled by the Nadir angle η, which is π minus the zenith angle α. Spherical symmetry is assumed in the Earth so that the Earth trajectories only depend on the Nadir angle. The general case of an underground detector is shown. One notes that for a surface detector, one can define a day (night) trajectory depending on whether the Nadir angle is bigger (smaller) than $\frac{\pi}{2}$.

dimensional integral:

$$\Phi(x) \propto \int_0^{\pi} \zeta(\eta) \int_{1AU(1-\epsilon)}^{1AU(1+\epsilon)} \int_0^{\pi} \int_0^{R_\odot} P_{ee}(d_{SNO}(r_0, \theta_\odot, L, \eta))\ \phi(r_0) r_0^2 \sin(\theta_\odot) \sin(\eta)\ dr_0\ d\theta_\odot\ dL\ d\eta \tag{70}$$

In a numerical calculation, this involves calculating $P_{ee}(d_{SNO})$ many times, since it is different for each parameter over which the flux is integrated. A basic program will then have four nested loops in order to calculate an average flux, which we have noted to be a very CPU-intensive task. One is then motivated to find ways to speed up such calculations, which is the main theoretical focus of this thesis.

2.3 Neutrino Propagation in the Sun

In this section we examine the propagation of neutrinos through the Sun. We will start by briefly introducing the relevant parts of the standard solar model that treat ^8B neutrinos whose energy is in the range that the SNO detector can see. We will then give an overview of numerical propagation in the Sun, and show the influences of this medium on the survival probability. We will also examine numerically the dependence on the mixing parameters. Various algorithms for numerical propagation through the Sun will then be presented. Finally, the approximations presented in section (2.2) will be examined in the context of propagation through the Sun and we will conclude by recommending the most computationally efficient and numerically accurate methods for the calculation of solar neutrino fluxes in three flavours.

2.3.1 The Solar Model

Much work has been done in trying to model the Sun, and we will limit the discussion to aspects relevant to ^8B neutrinos. Most of the leading research on solar physics has been carried out by the late John Bahcall and his collaborators who have been publishing up-to date solar models roughly every two years since 1998 ([36], [37]). The work in this thesis has mostly been carried out using the 2000 Bahcall-Pinsonneault solar model [36], which will be referred to as the BP2000 model.

We will not go into the details of solar physics and simply state that the hydrodynamic stability of the Sun results from the balance between its self-gravity and the outward pressure of the nuclear fusion reactions that take place in the interior. The nuclear reactions produce neutrinos, and some produce intermediate states that β-decay and produce additional neutrinos. For example, the ^8B neutrinos are produced through the following branch of reactions in the p-p chain:

$$\begin{aligned}
H + H &\longrightarrow {}^2H + e^+ + \nu_e \\
{}^2H + H &\longrightarrow {}^3He + \gamma \\
{}^3He + {}^3He &\longrightarrow H + H + {}^4He \\
{}^4He + {}^3He &\longrightarrow {}^7Be + \gamma \\
{}^7Be + H &\longrightarrow {}^8B + \gamma \\
\\
{}^8B &\longrightarrow {}^8Be^* + e^+ + \nu_e
\end{aligned} \tag{71}$$

Figure (15) shows the energy spectra of all the neutrinos produced in the Sun and is taken from the 2005 solar model [37]. One notes that ^8B neutrinos are responsible for most of the flux that SNO sees, since the detector is sensitive to energies between approximately $4MeV$ and $15MeV$ (for the Charged-Current reaction). One also notes that the uncertainty on the number of ^8B neutrinos is 16%, which is bigger than the uncertainty on the flux as measured by SNO [8].

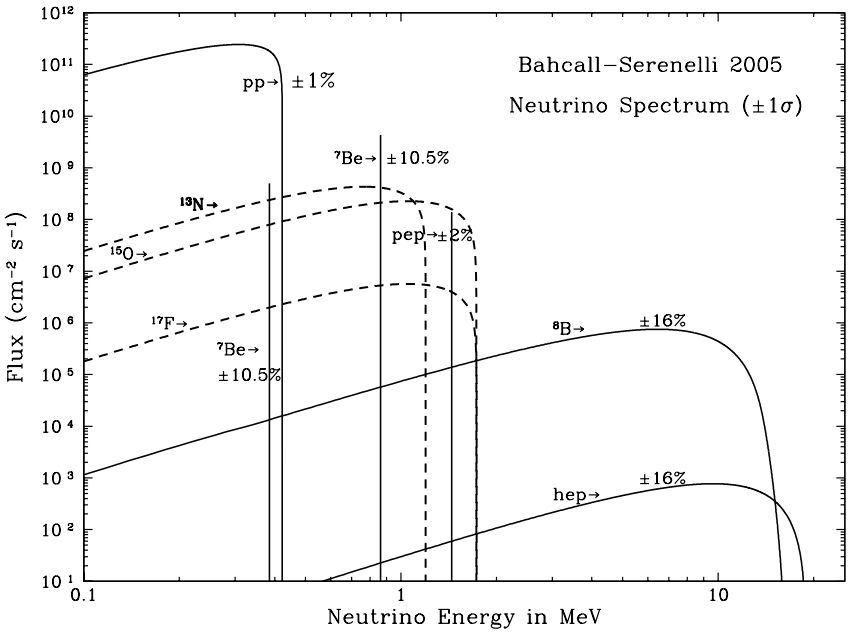

Figure 15: Solar neutrino fluxes with uncertainties as a function of energy at $1AU$, taken from [37]. Above $2MeV$, the flux is dominated by ^8B neutrinos.

The ^8B neutrino production region is required in order to calculate the flux of electron-flavour neutrinos using equation (70) and is shown in Figure (16) where the fraction of ^8B neutrinos produced at each radius ($\phi(r)r^2\ dr$) as a function solar radius is plotted. One notes that the source of these neutrinos is reasonably well localized.

The final piece of data required from solar physics in order to calculate neutrino fluxes is the density profile of the Sun. This is shown in Figure (17) where the logarithm (base 10) of the electron density is plotted as a function of solar radius. One notes that the density decreases exponentially throughout most of the Sun.

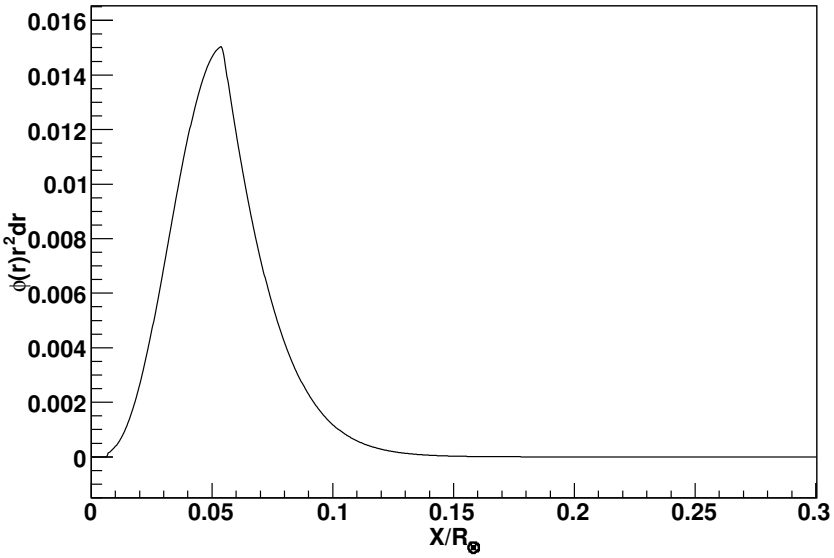

Figure 16: Fraction of ^8B neutrinos produced at each solar radius, from [36]. The distribution of ^8B is actually peaked at the center of the Sun, but most neutrinos come from a little further out, simply due to the volume of the shells at the center being essentially zero. This is why the fraction of neutrinos produced, $\phi(r)r^2\ dr$, is plotted instead of the ^8B distribution, $\phi(r)$.

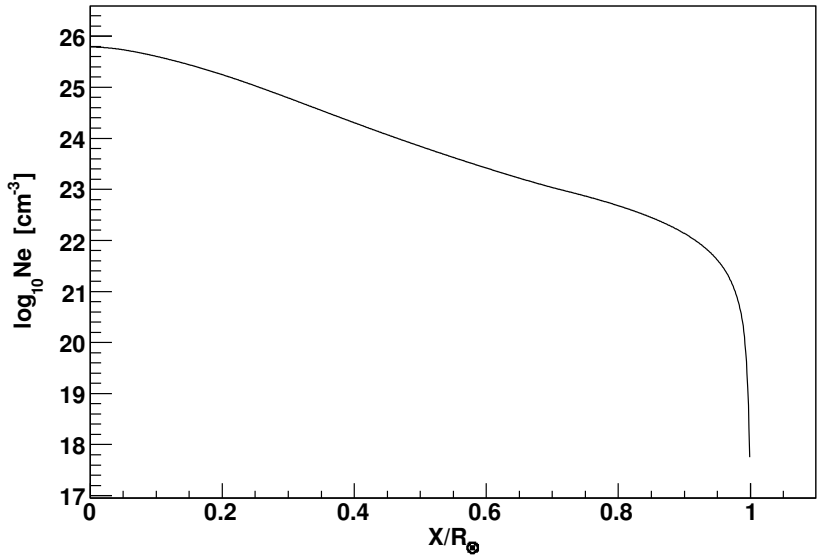

Figure 17: Logarithm (base 10) of the electron density (in cm^{-3}) in the Sun as a function of solar radius, from [36]. The density decreases exponentially from the center, except close to the outer edge.

2.3.2 Numerical Survival Probabilities: Overview with Mixing Parameters Consistent with Experimental Data (Two Flavours)

In the following sections, we examine the dependence of the survival probability through the Sun on the mixing parameters in a two-flavour scheme. We will assume that neutrinos are produced in the center and consider how the solar medium affects the neutrino flavour content. We will start by considering the case where the mixing parameters are consistent with experimental data, then consider the more general case, for completeness.

In Figure (18), the survival probability through the Sun is plotted in two flavours for a neutrino that started at the center with an energy of $10MeV$ and mixing parameters set to $\Delta m_{21} = 7 \times 10^{-5} eV^2$ and $\tan^2(\theta_{12}) = 0.42$. Figure (19) shows the same plot for a neutrino with an energy of $5MeV$ and the same mixing parameters. One notes that the oscillation wavelength is much smaller than the radius of the Sun as well as the size of the region where ^8B neutrinos are produced in either case. In Figure (20) the matter-mass squared difference is plotted as a function of radius for $5MeV$ and $10MeV$ energy neutrinos, and one notes that the solar density is such that the MSW resonance occurs (when the mass squared difference is a minimum). One also notes that the resonance is reached at lower radii for lower energies and that the matter mass-squared difference reaches its vacuum value about half-way through the Sun. That is, matter effects (at these energies and mixing parameters) become negligible at a radius, R, bigger than $0.5R_\odot$. The resonances are seen more clearly in Figure (21) where the matter mixing angle is plotted as a function of distance.

Figure (22) shows the second matter mass eigenstate content, which is almost constant, indicating an adiabatic propagation. The neutrino thus starts off in mostly the $|\nu_2^m>$ eigenstate and remains that way throughout the Sun, indicating that the adiabatic approximation is well suited for solar neutrinos at these energies and mixing parameters.

Finally, Figure (23) shows the survival probability as a function of energy for the mixing parameters $\Delta m_{21} = 7 \times 10^{-5} eV^2$ and $\tan^2(\theta_{12}) = 0.42$, integrated (numerically) over the Sun according to equation (68), using the ^8B distribution from Figure (16). This is the spectral distortion expected for ^8B neutrinos and will be referred to as the 'LMA plot' (Large Mixing Angle). The transition from vacuum oscillations at low energy to matter oscillations at higher energies is clearly visible. At low energies, one indeed notes that $P_{ee} \approx 1 - \frac{1}{2}\sin^2(2\theta_{12}) = 0.58$ (for $\tan^2(\theta_{12}) = 0.42$) (recall equation (18)).

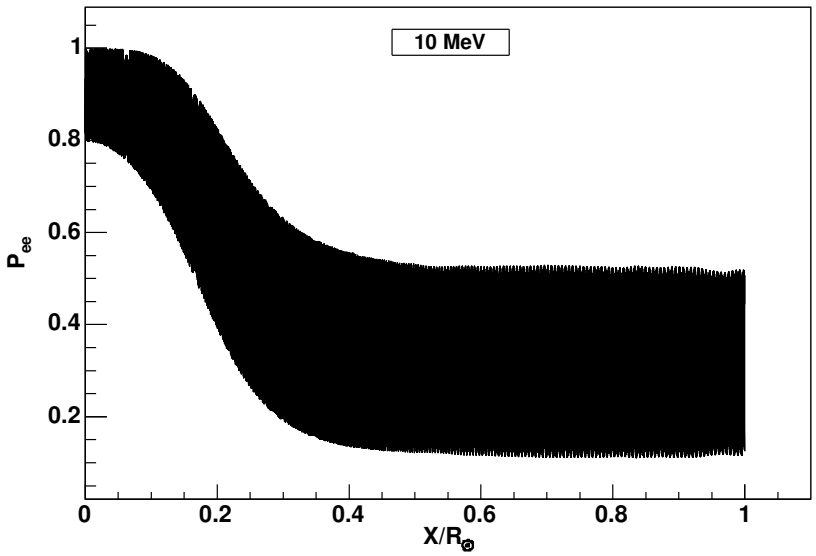

Figure 18: Survival probability in two flavours through the Sun for a $10MeV$ neutrino with $\Delta m_{21} = 7 \times 10^{-5} eV^2$ and $\tan^2(\theta_{12}) = 0.42$. One notes the oscillation length is very small compared to the region where ^8B neutrinos are produced (see Figure(16)).

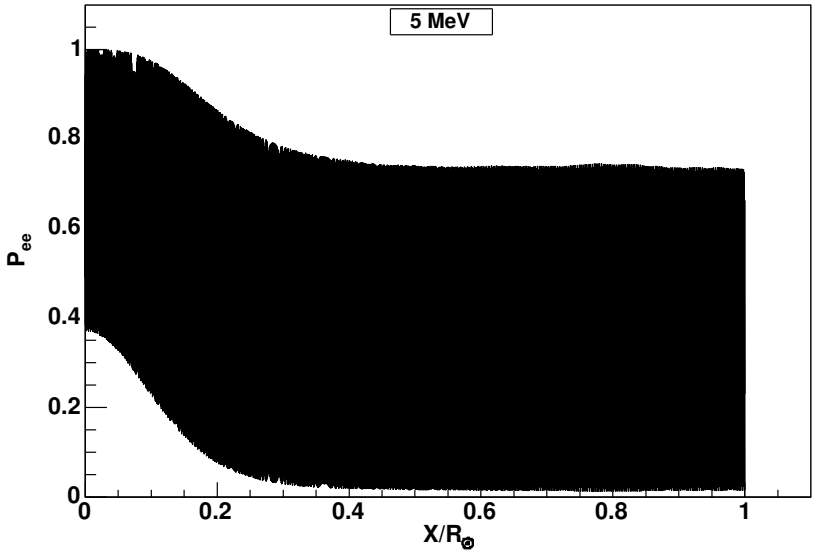

Figure 19: Survival probability in two flavours through the Sun for a $5MeV$ neutrino with $\Delta m_{21} = 7 \times 10^{-5} eV^2$ and $\tan^2(\theta_{12}) = 0.42$. The oscillation amplitude is larger than at higher energies, Figure (18).

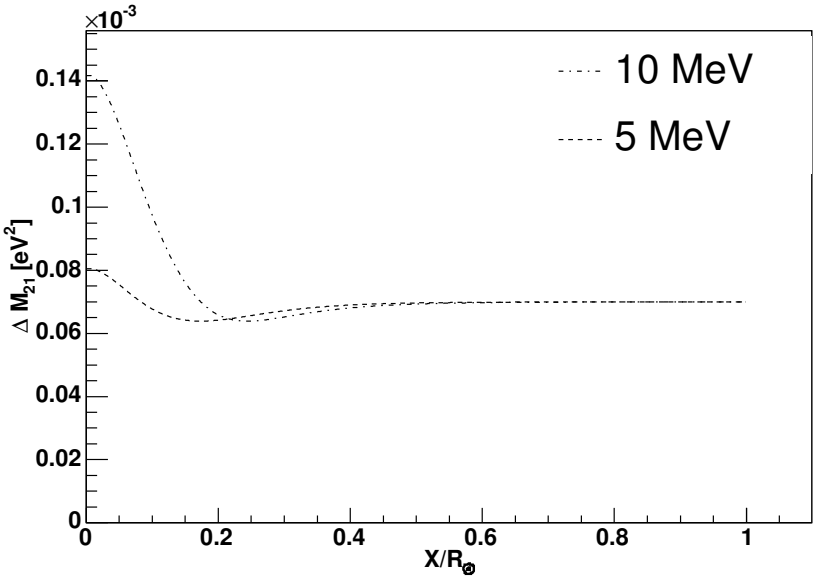

Figure 20: Matter mass-squared difference as a function of distance through the Sun for neutrino energies of $5MeV$ and $10MeV$ with mixing parameters $\Delta m_{21} = 7 \times 10^{-5} eV^2$ and $\tan^2(\theta_{12}) = 0.42$. The MSW resonance occurs at the local minima.

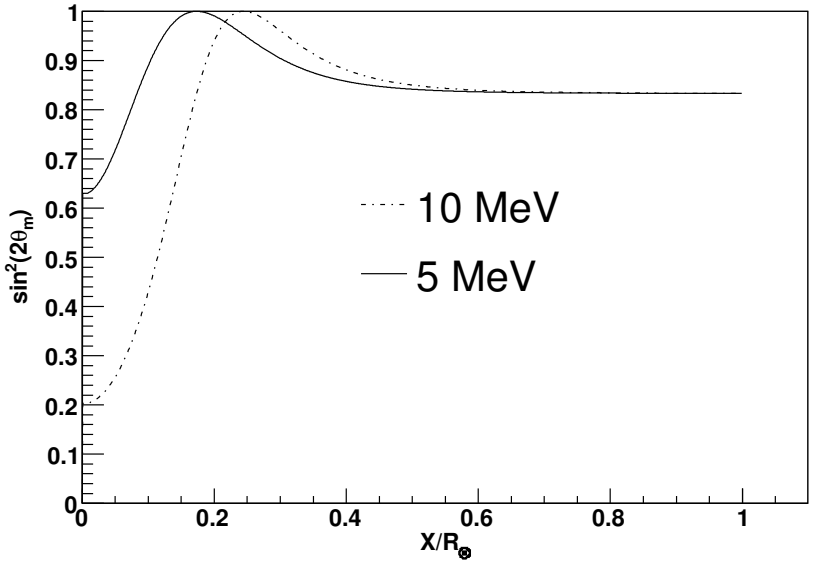

Figure 21: Matter mixing angle as a function of distance through the Sun for neutrino energies of $5MeV$ and $10MeV$ with mixing parameters $\Delta m_{21} = 7 \times 10^{-5} eV^2$ and $\tan^2(\theta_{12}) = 0.42$. The MSW resonance occurs at the local maxima.

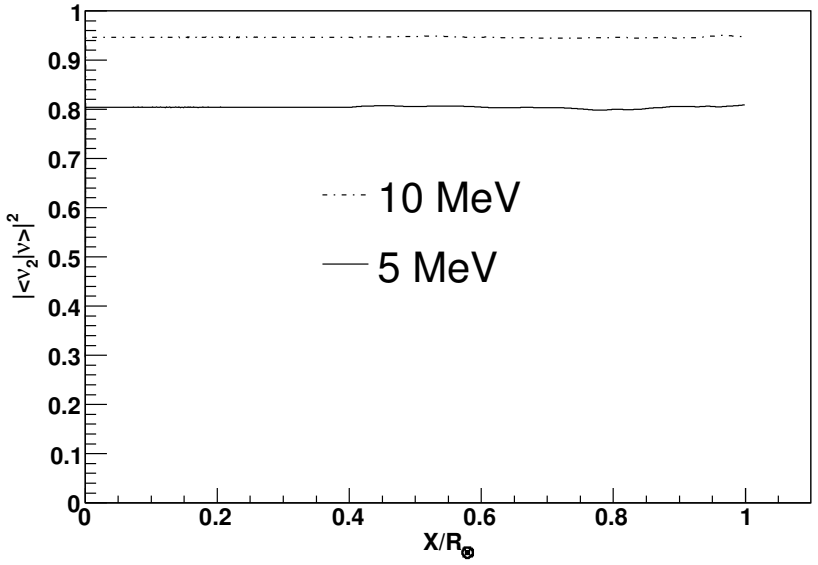

Figure 22: Second matter-mass eigenstate content as a function of distance through the Sun for neutrino energies of $5MeV$ and $10MeV$ with mixing parameters $\Delta m_{21} = 7 \times 10^{-5} eV^2$ and $\tan^2(\theta_{12}) = 0.42$. The propagation is very close to being adiabatic as the mass eigenstate content does not change very much.

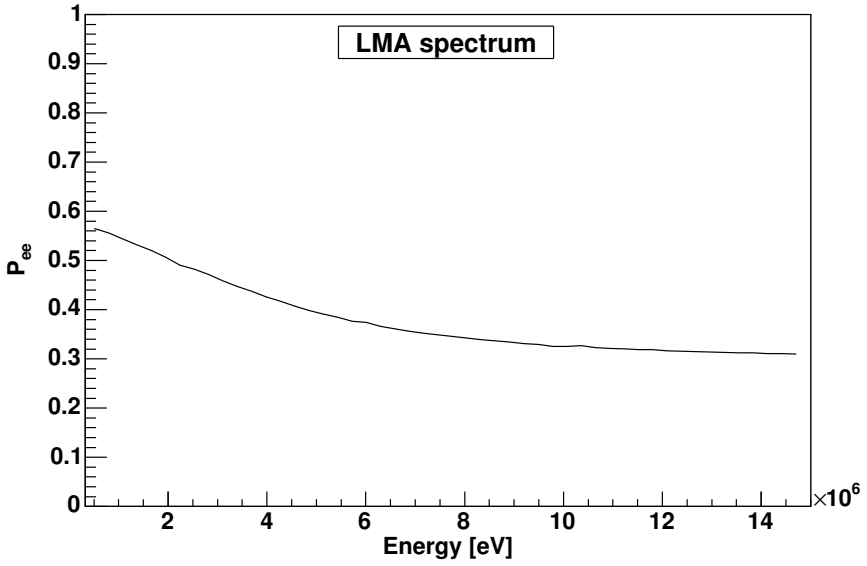

Figure 23: Solar neutrino LMA energy spectral distortion calculated numerically with two flavours, averaged over ^8B production region (r and θ) and Earth-Sun distance in vacuum. Mixing parameters are set to their experimental values, $\tan^2(\theta_{12}) = 0.42$ and $\Delta m_{21} = 7 \times 10^{-5} eV^2$.

2.3.3 Numerical Survival Probabilities: Dependence on Mixing Parameters (Two Flavours)

The calculations through the Sun so fa were focused on the mixing parameters consistent with current experimental limits. The behavior can change dramatically depending on the mixing angle and mass-squared difference and we will only briefly examine these changes in this section, as the main focus is to perfect three-flavour calculations within the current range of experimental parameters.

We will note the amazing consequence of the MSW solution, as it allows large flavour changing oscillations even with a very small mixing angle. Before the measurement of mixing parameters by experiments such as SNO, it was assumed that the mixing between flavour generations would be small, in analogy to the already known mixing matrix elements in the quark sector. When neutrino oscillations were first proposed, it thus seemed unlikely that they would cause the factor of three depletion in the solar flux that was measured. However, Mikheyev, Smirnov and Wolfenstein ([25], [26]) proposed the matter-enhanced oscillations that could cause large flavour conversion even with very small mixing angles. This is illustrated in Figure (24) where the survival probability is plotted as a function of distance through the Sun for $10MeV$ neutrinos created in the center with $\Delta m_{21} = 7 \times 10^{-5} eV^2$ and $\sin^2(2\theta_{12}) = 0.039$. If only vacuum oscillations take place, one would expect a classical survival probability of the order $P_{ee} \approx 1 - \frac{1}{2} \times 0.039 = 0.98$, however, it is clear that after going through the MSW resonance, the electron neutrinos become almost entirely converted into muon type neutrinos.

Since the oscillation lengths in the Sun are small, it is more convenient to look at the phase averaged survival probabilities to make comparisons for different values of the mixing angle. That is, at each point in the propagation, the electron flavour content is calculated by averaging over the phase between mass eigenstate contents. This is done in Figure (25) where P_{ee} is plotted as a function of distance through the Sun for $10MeV$ neutrinos with $\Delta m_{21} = 7 \times 10^{-5} eV^2$ and various mixing angles. We have chosen to label the curves with $\tan^2(\theta_{12})$ since $\sin^2(2\theta_{12})$ is degenerate for $\theta_{12} > \frac{\pi}{4}$. One notes that the survival probability is close to one for (very) large mixing angles.

We now consider the influence of the vacuum mass-squared difference. One should recall that as the mass-squared difference becomes smaller, the resonant density also becomes smaller and moves to a higher radius in the Sun. Inversely, as the mass-squared is increased, a point will be reached where the resonance does not occur in the Sun (as is the case with Δm_{31}). This is illustrated in Figure (26) where the survival probability as a function of distance in the Sun is plotted for different values of the mass squared difference for $10MeV$ neutrinos with $\tan^2(\theta_{12}) = 0.42$. For the resonance to

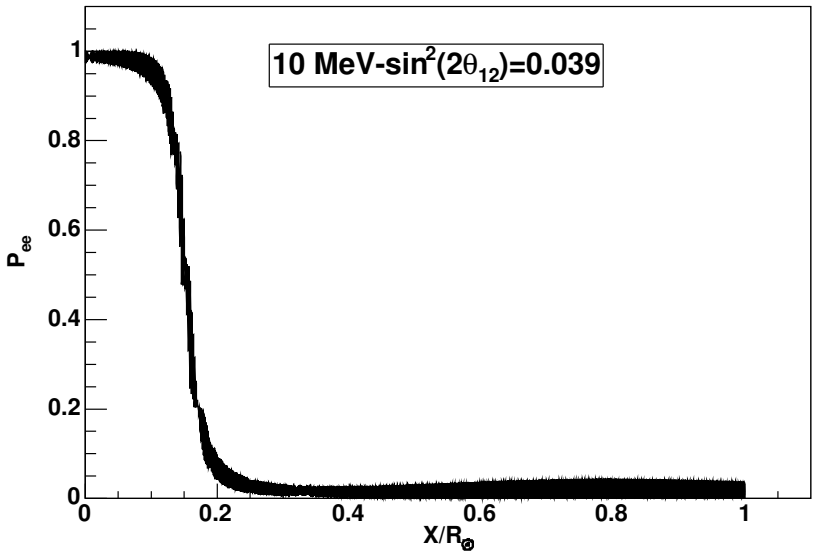

Figure 24: Survival probability through the Sun for a very small vacuum mixing angle for a $10MeV$ neutrino with $\Delta m_{21} = 7 \times 10^{-5} eV^2$ and $\sin^2(2\theta_{12}) = 0.039$. The important effect of the MSW resonance is illustrated.

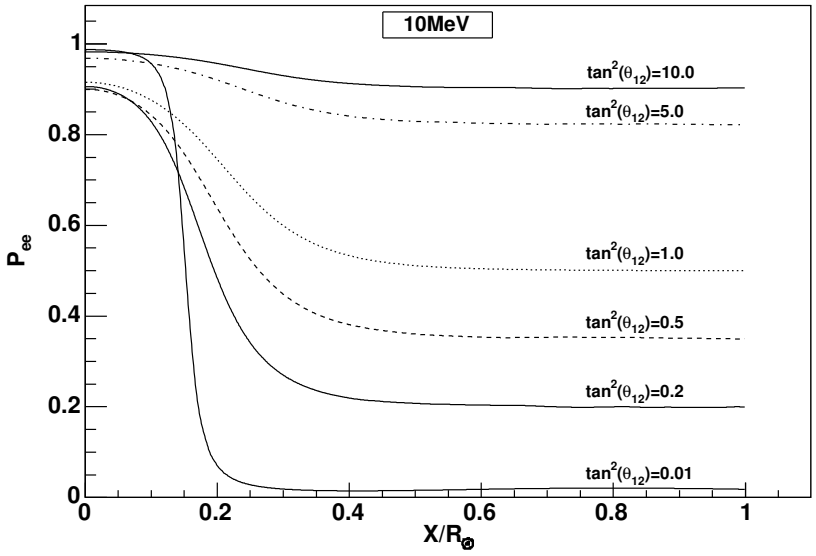

Figure 25: Phase-averaged survival probability through the Sun for $10MeV$ neutrinos with $\Delta m_{21} = 7 \times 10^{-5} eV^2$ and different values of the mixing angle.

occur at the center of the Sun, a mass-squared difference of $\Delta m_{21} \approx 3.8 \times 10^{-4} eV^2$ is required (with the given mixing angle). One notes from Figure (26) that for the curve with $\Delta m_{21} = 7 \times 10^{-4} eV^2$, matter has a small effect and the phase-averaged probability is almost equal to that in vacuum.

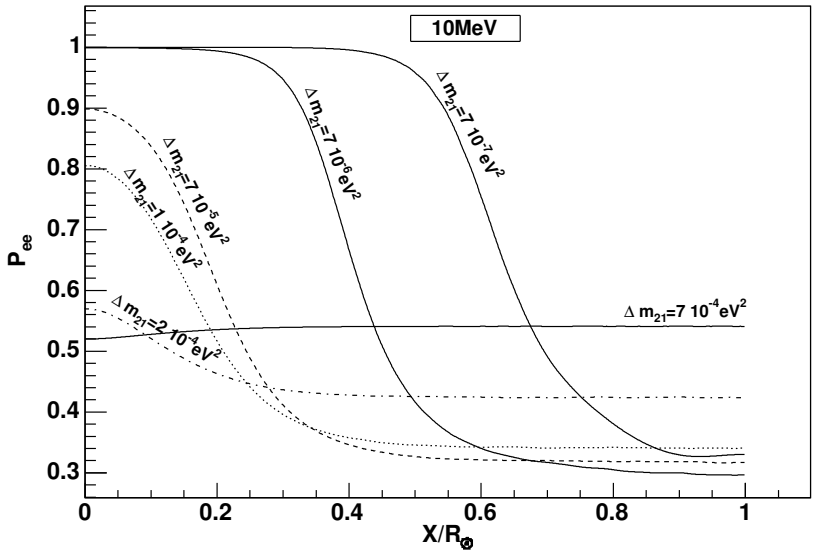

Figure 26: Phase-averaged survival probability through the Sun for $10MeV$ neutrinos with $\sin^2(2\theta_{12}) = 0.833$ and different values of the mass-squared difference. The mass-squared differences are chosen so that the MSW resonance occurs throughout the Sun.

The resonant radius is plotted as a function of θ_{12} and $\frac{\Delta m_{21}}{E}$ in Figure (27). The current experimental value is approximately marked by a star for an energy of $10MeV$. One should recall that there is no resonant radius if $\theta_{12} > \frac{\pi}{4}$, since the resonance is given by $\Delta m_{21} \cos(2\theta_{12}) = A$ and would then occur at a negative value of A. As Δm_{21} becomes large, the solar density is never large enough to have a resonance. However, since the solar density decreases exponentially, there is always a point on the edge where the density is small enough to produce a resonance for very low values of Δm_{21}.

Finally, Figure (28) shows the phased-average probability for neutrinos that started in the center of the Sun as a function of θ_{12} and $\frac{\Delta m_{21}}{E}$, and the features discussed earlier are visible over the entire range of mixing parameters. We will adopt this type of contour plot throughout most of the following sections, as it conveniently shows the dependence on both mixing parameters.

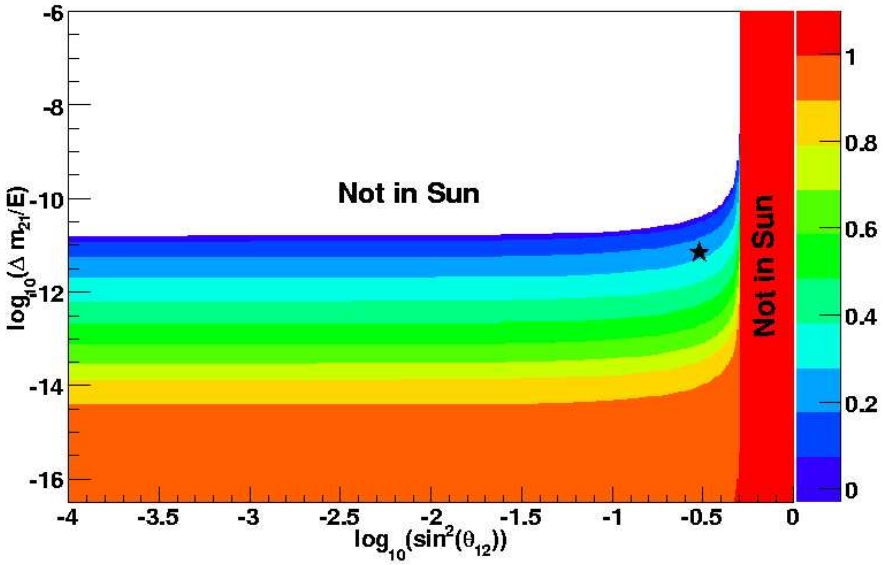

Figure 27: Contour plot of the location of the MSW resonance (in units of the solar radius) as a function of $\log_{10}(\sin^2(\theta_{12}))$ and $\log_{10}(\frac{\Delta m_{21}}{E})$. The point marked with a star is for $\Delta m_{21} = 7 \times 10^{-5} eV^2$ and $\tan^2(2\theta_{12}) = 0.42$ at an energy of $10 MeV$.

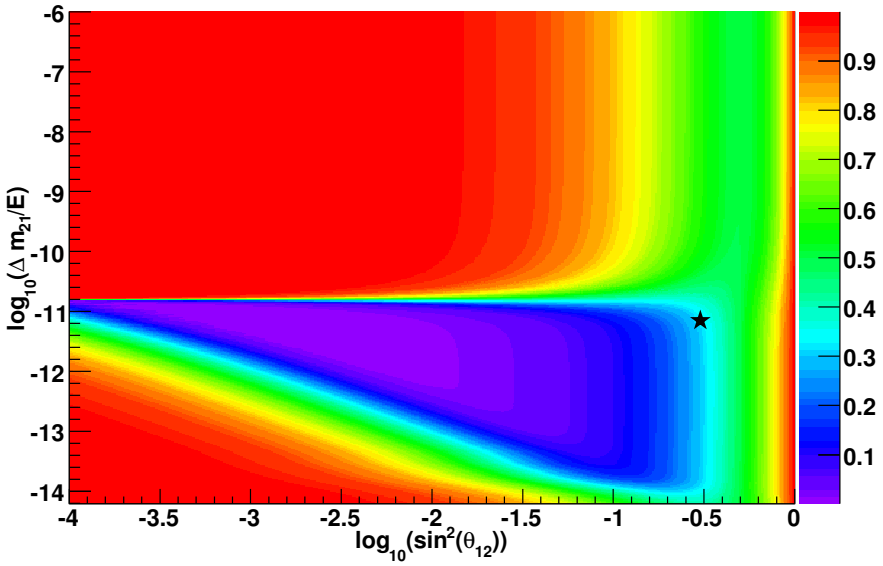

Figure 28: Contour plot of the phase-averaged P_{ee} for neutrinos originating in the center of the Sun as a function of $\log_{10}(\sin^2(\theta_{12}))$ and $\log_{10}(\frac{\Delta m_{21}}{E})$. The point marked with a star is for $\Delta m_{21} = 7 \times 10^{-5} eV^2$ and $\tan^2(2\theta_{12}) = 0.42$ at an energy of $10 MeV$.

2.3.4 Numerical Survival Probabilities: Dependence on Mixing Parameters (Three Flavours)

We proceed in a similar fashion as the previous section to examine the dependence of the survival probability on the mixing parameters with three flavours of neutrinos. That is, we will focus on phase-averaged survival probabilities for neutrinos that started in the center of the Sun. We will fix the two-flavour mixing parameters to their best-fit experimental values ($\Delta m_{21} = 7 \times 10^{-5} eV^2$ and $\tan^2(2\theta_{12}) = 0.42$) throughout this section, unless stated otherwise.

Figure (29) shows the phased average survival probability as a function of distance through the Sun for different values of θ_{13} compared to the two-flavour solution ($\theta_{13} = 0$) at an energy of $10MeV$. The second mass-squared difference is set to $\Delta m_{31} = 1 \times 10^{-3} eV^2$, consistent with results from atmospheric neutrinos ([10]) and long-baseline experiments ([38]). One notes that as the mixing angle is increased, P_{ee} decreases, since there is now another flavour to oscillate into; as the mixing angle increases, so does the possibility of mixing with the extra flavour.

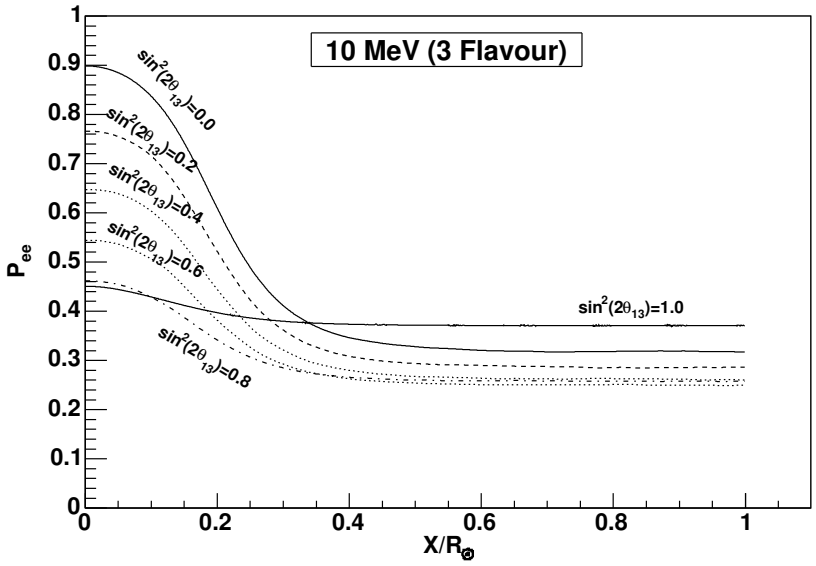

Figure 29: Phase-averaged survival probability as a function of distance through the Sun for different values of $\sin^2(2\theta_{13})$ at an energy of $10MeV$ and $\Delta m_{31} = 1 \times 10^{-3} eV^2$.

We now consider the dependence on the second mass-squared difference. To illustrate this, we have chosen the usual two-flavour mixing parameters ($\Delta m_{21} = 7 \times 10^{-5} eV^2$ and $\tan^2(2\theta_{12}) = 0.42$) as well as $\sin^2(2\theta_{13}) = 0.4$, which is unrealistically large but increases the effect of Δm_{31}. The results are shown in Figure (30) where one notices that as the mass-squared difference increases past

$1 \times 10^{-2} eV^2$, it ceases to have a perceptible effect. Also, Δm_{31} does not have a large influence on P_{ee} when it is varied about its experimental value.

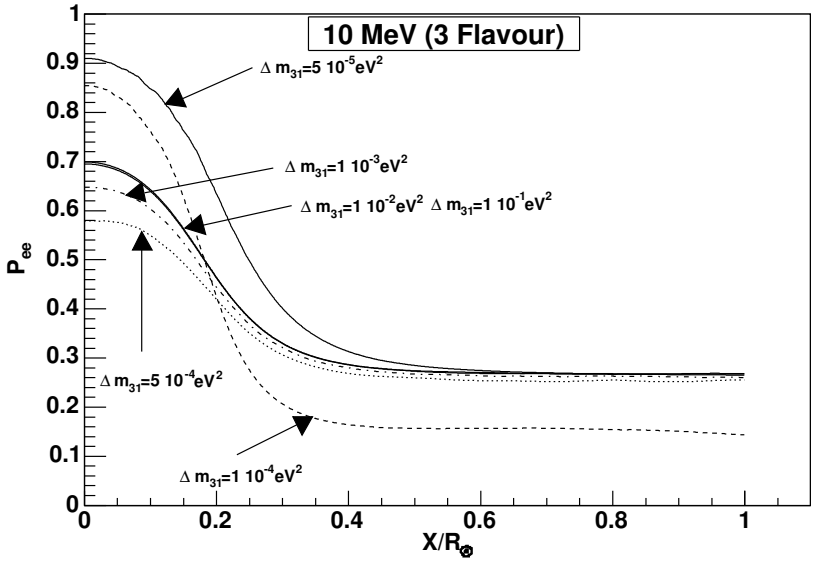

Figure 30: Phase-averaged survival probability as a function of distance through the Sun for different values of Δm_{31} at an energy of $10MeV$ with $\sin^2(2\theta_{13}) = 0.4$. The curves for $\Delta m_{31} = 1 \times 10^{-2} eV^2$ and $\Delta m_{31} = 1 \times 10^{-1} eV^2$ overlap.

Figure (31) shows the influence of θ_{13} on the phase-averaged survival probability when it is varied along with Δm_{21} for $\tan^2(\theta_{12}) = 0.42$. The general effect of increasing θ_{13} is to decrease the survival probability, as observed above. We note that this is more pronounced at lower values of Δm_{21}. Figure (32a) shows the contours in P_{ee} over the θ_{12}-Δm_{21} plane when $\sin^2(2\theta_{13}) = 0.5$. These contours are to be compared with Figure (28), and we see that the shape does not change very much, but that, as anticipated earlier, P_{ee} decreases by the same amount over most of the plane. Figure (32b) shows the difference between Figures (28) and (32a), and we note that adding θ_{13} does not change the survival probability very much in the range of the experimental parameters.

2.3.5 Numerical Algorithms for Propagation through the Sun

In this section, we examine numerical methods for propagating neutrinos through the Sun. The aim is to determine the fastest algorithms based on physical arguments that can be employed in numerical calculations. The most rudimentary approach for propagating a neutrino through the Sun is to divide each path that the neutrino takes into N steps and propagate through the Sun using brute force. One must determine the value of N through trial and error until the results converge

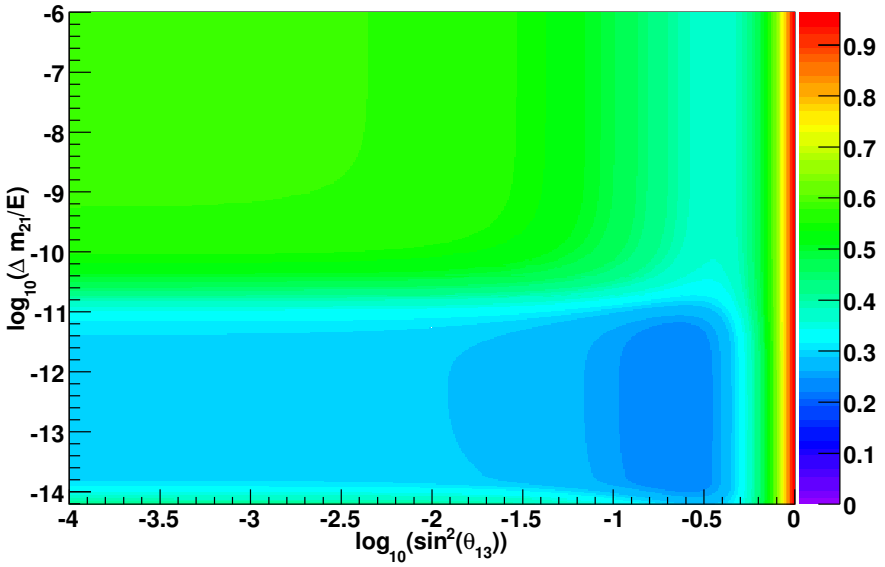

Figure 31: Contour plot of the phase averaged P_{ee} for neutrinos originating in the center of the Sun as a function of $\log_{10}(\sin^2(\theta_{13}))$ and $\log_{10}(\frac{\Delta m_{21}}{E})$.

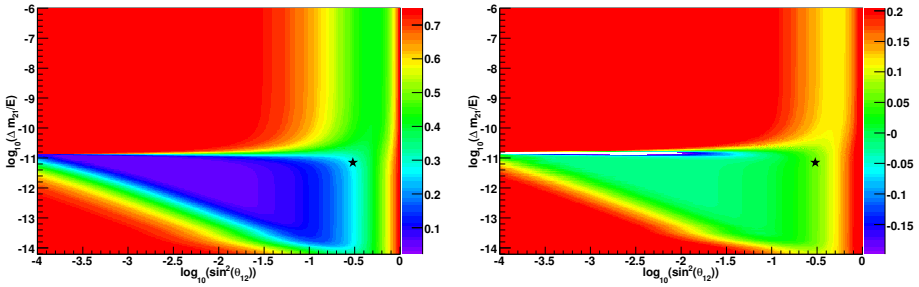

(a) (b)

Figure 32: Contour plot of the phase-averaged P_{ee} with $\sin^2(2\theta_{13}) = 0.5$ (left) and difference with P_{ee} when $\sin^2(2\theta_{13}) = 0.5$ for neutrinos originating in the center of the Sun as a function of $\log_{10}(\sin^2(\theta_{12}))$ and $\log_{10}(\frac{\Delta m_{21}}{E})$.

to the same value as when N is (almost) infinite. The number of steps to achieve convergence also depends on the mixing parameters and energy of the neutrino and one would have to set a very big value for N based on the least convergent situation, when this would be over calculating in other situations. Such an algorithm would look like:

$BRUTE\_FORCE()$
{
$RADIUS = 0$
$STEPSIZE = \frac{SUNRADIUS}{N}$
$FOR\ I\ = 1\ TO\ N$
    $RADIUS = RADIUS + STEPSIZE$
    $SET\_NEUTRINOPOSITION(RADIUS)$
    $STEP\_NEUTRINO(STEPSIZE)$
$END\ FOR$
}

where we have assumed the neutrino started at the center of the Sun. *STEP_NEUTRINO()* is a function that would calculate and diagonalize the Hamiltonian based on the neutrino position in the Sun and then evolve the mass eigenstate contents through a length *STEPSIZE* assuming a constant density for that length of slab, and finally update the flavour content:

$STEP\_NEUTRINO(STEPSIZE)$
{
$ELECTRON\_DENSITY = GET\_SOLARDENSITY(NEUTRINOPOSITION)$
$SET\_HAMILTONIAN(MIXING\_ANGLES, ELECTRON\_DENSITY)$
$SET\_MASSCONTENT(MIXING\_MATRIX, FLAVOURCONTENT)$
$DIAGONALIZE(HAMILTONIAN)$
$FOR\ I\ = 1\ TO\ NFLAVOURS$
    $PHASE[I] = EIGENVALUE[I] * STEPSIZE$
    $MASSCONTENT[I] = MASSCONTENT[I] * EXP(PHASE[I])$
$END\ FOR$
$SET\_FLAVOURCONTENT(MIXING\_MATRIX, MASSCONTENT)$
}

where we first calculate the mass eigenstate content based on the flavour content from the last

step (this guarantees a continuous flavour content through strongly non-adiabatic interfaces), then diagonalize the Hamiltonian to update the mixing matrix and energy eigenvalues.

However, from considering the solar (electron) density as a function of radius (see Figure (17)) as well as the fact that the propagation is mostly adiabatic (see Figure (22)), it is noted that a variable step size algorithm can be attempted. The aim is to take more steps where the flavour content changes the most, which is, in essence, a similar concept to using the jump probabilities, since this will happen at the MSW resonance. In this work, two such algorithms were created, and it was found that a combination of the two was actually the most efficient.

The first algorithm chooses the step size for the next step so that the density changes by a constant amount. Because the density decreases exponentially, the step size increases exponentially as the neutrino is further from the center of the Sun. The idea behind this algorithm is that more steps should be taken where the density changes most. We shall call this the *LOGSTEP* algorithm:

$LOGSTEP()$

{

$RADIUS = 0$

$STEPSIZE = \frac{SUNRADIUS}{N}$

$DENSITYCHANGE = 0.01 * GET\_SOLARDENSITY(0)$

DO

$RADIUS = RADIUS + STEPSIZE$

$SET\_NEUTRINOPOSITION(RADIUS)$

$STEP\_NEUTRINO(STEPSIZE)$

$STEPSIZE = FACTOR * \frac{DENSITYCHANGE}{ELECTRON\_DENSITY}$

$WHILE\ RADIUS < SUNRADIUS$

}

where *FACTOR* is just some numerical factor to convert a fractional change in density to a radial distance in appropriate units. In the above example, the density is required to change by 1% of the density at the center and the first step is carried out with the same step size as the *BRUTE_FORCE()* algorithm. The algorithm also assumes that the electron density was set by *STEP_NEUTRINO()* and will thus be different at each iteration. This algorithm does not need to be tuned for numerical accuracy once one has determined a suitable percent change in the electron density.

Figure (33) shows the step size as a function of solar radius as calculated by an algorithm similar to LOGSTEP. One notes that the step size increases exponentially with radius. At about $R = 0.8R_{\odot}$

the step size appears to become smaller again; this is simply because the algorithm prevents the step size from overshooting the edge of the Sun. The step size is logically independent of the neutrino energy and mixing parameters. Figure (34) shows a histogram of the number of steps carried out at each radius and one notes that only 1 step is taken after the step size starts to become smaller. This algorithm is thus very efficient at higher radii.

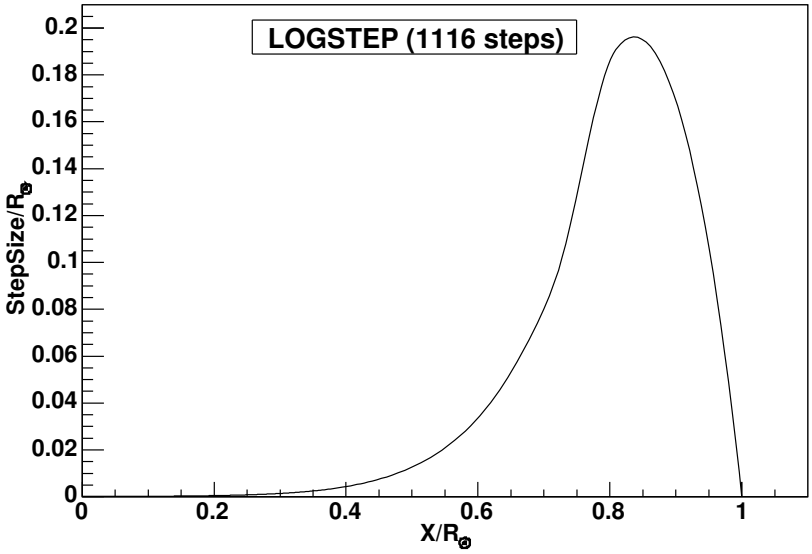

Figure 33: Step size (in units of $R_\odot$) as a function of distance through the Sun as calculated by an algorithm similar to *LOGSTEP*. The algorithm guards against overshooting the edge of the Sun and reduces the step size when appropriate.

The second algorithm that was designed calculates the step size based on the oscillation length in matter. The idea here is that steps should be slightly smaller than the distance over which the oscillation length in matter **changes**. As will be recalled from Figure (18), there are many oscillations in the Sun, but their average value only changes around the resonance. One can thus step over several oscillation lengths as long as it does not change very much over the step. We shall call this the *EIGENSTEP* algorithm, as it bases the step size on a difference in energy eigenvalues (as calculated by *STEP_NEUTRINO()*):

$EIGENSTEP()$

{

$RADIUS = 0$

$STEPSIZE = \frac{SUNRADIUS}{N}$

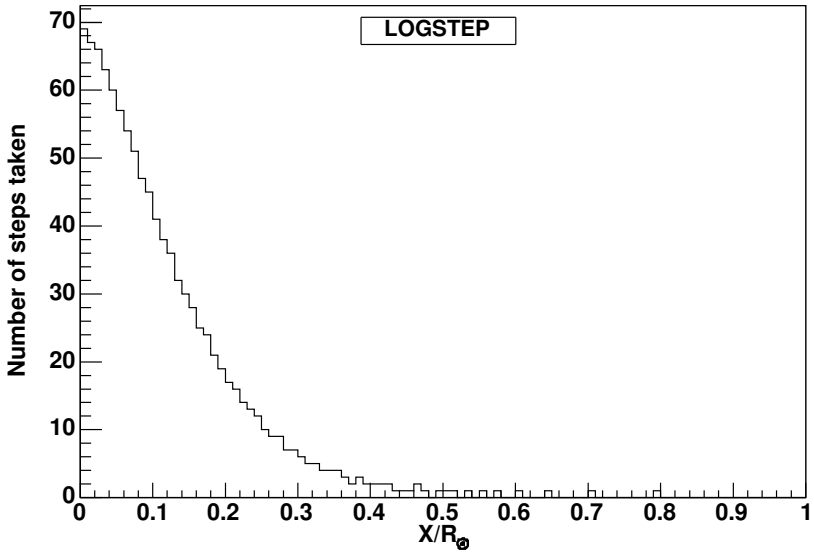

Figure 34: Histogram showing the number of steps taken at each radius by the *LOGSTEP* algorithm. The last step is taken at $0.8R_{\odot}$.

DO

$RADIUS = RADIUS + STEPSIZE$

$SET\_NEUTRINOPOSITION(RADIUS)$

$STEP\_NEUTRINO(STEPSIZE)$

$STEPSIZE = FACTOR * \frac{1}{PHASE}$

$WHILE\ RADIUS < SUNRADIUS$

}

where *FACTOR* is again some number to convert the oscillation phase into units of length. As it stands, this algorithm bases the step size on the oscillation length (proportional to the inverse of the phase) and steps over a 'few' wavelengths (determined by *FACTOR*). Again, this algorithm only needs to be tuned for the number of oscillation lengths to be stepped over. It also has the pleasing feature that the step size now depends on the mixing parameters.

Figure (35) shows the step size as a function of radius calculated using the EIGENSTEP algorithm for different energies with the mixing parameters set to $\Delta m_{21} = 7 \times 10^{-5} eV^2$ and $\tan^2(\theta_{12}) = 0.42$. One notes that the step size is smaller for lower energy neutrinos, because their oscillation length is smaller. The step size increases to a maximum value at the resonance, then becomes constant once the resonance is traversed, since the propagation is essentially in the vacuum regime. Figure (36) shows a histogram of the number of steps taken at each radius (for the same energies). One

notes that this algorithm takes fewer steps at low radius than *LOGSTEP*, and the reverse is true at higher radii. The problem with this algorithm is that it does not increase the step size once the vacuum regime is reached. The particular algorithm shown here set the step size to be ≈ 2.5 times the oscillation wavelength.

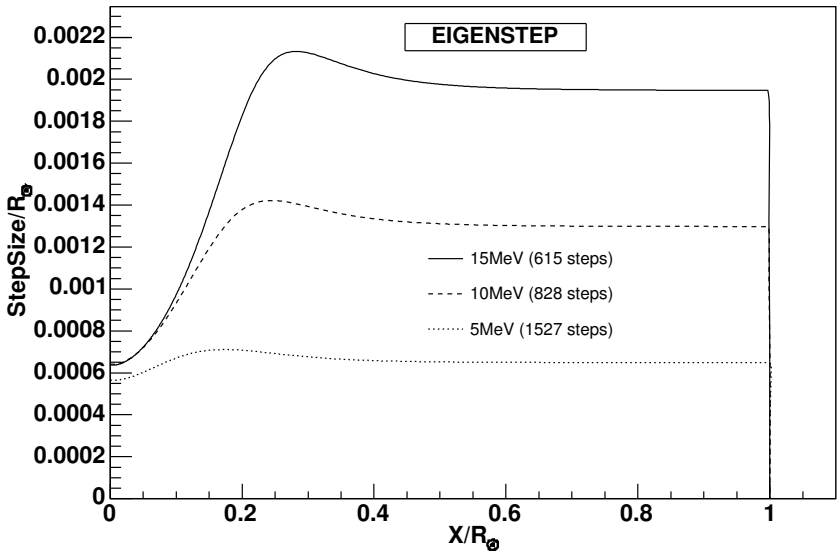

Figure 35: Step size (in units of $R_\odot$) as a function of distance through the Sun as calculated by an algorithm similar to *EIGENSTEP* for different energies and mixing parameters set to $\Delta m_{21} = 7 \times 10^{-5} eV^2$ and $\tan^2(\theta_{12}) = 0.42$.

As can be noted from Figures (33) and (35) the step size has different behaviors for the two algorithms. The goal is to have the longest step size possible throughout the Sun. In the *LOGSTEP* approach, the step size near the center of the Sun is very small, because the density changes significantly in that region, so *LOGSTEP* takes many steps in that region. The pitfall is that the oscillation amplitude does not change very much near the center of the Sun, because the density is so large that the matter mixing angle is small and completely dominates. The *LOGSTEP* approach then takes steps that are too small near the center. The *EIGENSTEP* approach takes steps that are too small after the resonance, since the steps are based on the oscillation length, which remains small throughout the Sun. The best approach is then to combine the two algorithms, by using *EIGENSTEP* near the center, before the resonant radius and then switch to *LOGSTEP* after the resonance, once the oscillations are essentially in the vacuum regime. We shall call this the *VARSTEP* algorithm:

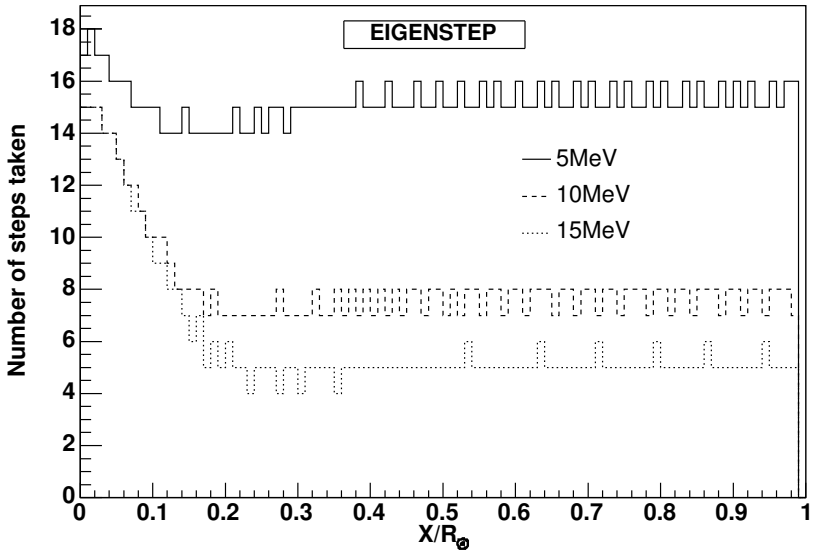

Figure 36: Histogram showing the number of steps taken at each radius by the *EIGENSTEP* algorithm for different energies and mixing parameters set to $\Delta m_{21} = 7 \times 10^{-5} eV^2$ and $\tan^2(\theta_{12}) = 0.42$.

$VARSTEP()$

{

$RADIUS = 0$

$STEPSIZE = \frac{SUNRADIUS}{N}$

$DENSITYCHANGE = 0.01 * GET\_SOLARDENSITY(0)$

$STEPTYPE = 0$

DO

$RADIUS = RADIUS + STEPSIZE$

$SET\_NEUTRINOPOSITION(RADIUS)$

$LASTPHASE = PHASE$

$STEP\_NEUTRINO(STEPSIZE)$

$CURRENTPHASE = PHASE$

$PHASECHANGE = CURRENTPHASE - LASTPHASE$

$IF\ STEPTYPE = 0$

$STEPSIZE = FACTOR1 * \frac{1}{PHASE}$

$IF\ \frac{PHASECHANGE}{CURRENTPHASE} > 0.01$

$STEPTYPE = 1$

$END\ IF$

$END\ IF$

$IF\ STEPTYPE = 1$

$STEPSIZE = FACTOR2 * \frac{DENSITYCHANGE}{ELECTRON\_DENSITY}$

$END\ IF$

$WHILE\ RADIUS < SUNRADIUS$

}

which starts off by setting the step size to be a 'few' wavelengths (using *EIGENSTEP*) at the beginning of the iteration. Once the algorithm detects that the phase (the difference between energy eigenvalues) did not change by more than 1% it switches to using *LOGSTEP*. This algorithm turns out to be very stable (numerically) and was used for all the solar numerical calculations presented in this thesis. The pleasing aspect of this algorithm is that it will change the step size to be suited for different mixing parameters and energies and really only needs to be tuned once.

Figure (37) shows the step size as a function of radius calculated using the *VARSTEP* algorithm for different energies with the mixing parameters set to $\Delta m_{21} = 7 \times 10^{-5} eV^2$ and $\tan^2(\theta_{12}) = 0.42$. The step size is small near the resonance and then switches to increasing exponentially with radius. The algorithm that was used switches from *EIGENSTP* to *LOGSTEP* when the matter mass squared difference changed by less than 1% from the previous step. It also forces the use of *EIGENSTEP* until the neutrino is at least $0.15 R_\odot$ out from the resonance, which can be seen in the sharp increase in stepsize around $0.4 R_\odot$. Figure (38) shows a histogram of the number of steps taken at each radius (for the same energies). One notes that this algorithm always takes fewer steps than either *LOGSTEP* or *EIGENSTEP*. It correctly takes more steps before and around the resonance and then changes to exponential steps when the vacuum oscillation regime is reached.

We thus conclude that a variable step algorithm is appropriate for propagating solar neutrinos numerically and recommend it be used. Through trial and error, it was determined that about 3000 steps need to be taken in the Sun for a brute force algorithm to converge consistently, but have shown here that a factor of ≈ 10 in speed can be gained by using variable step size routines.

2.3.6 Two-Flavour Approximations

We now consider various approximations in order to determine the best technique for calculating solar neutrino fluxes with three flavour of neutrinos. The goal is to define the fastest three-flavour algorithm that is still accurate.

We will follow the order of approximations presented in Section (2.2), and start by examining the adiabatic approximation in two flavours. We have already noted from Figure (22) that the

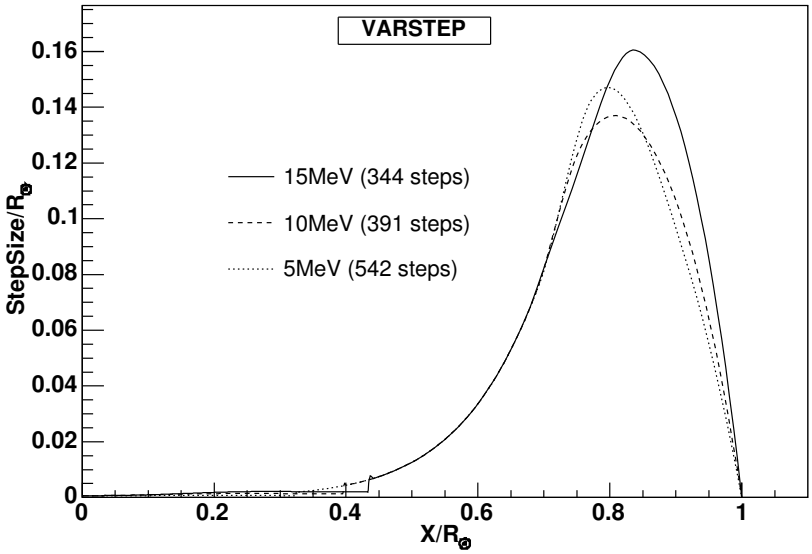

Figure 37: Step size (in units of $R_\odot$) as a function of distance through the Sun as calculated by an algorithm similar to *VARSTEP* for different energies and mixing parameters set to $\Delta m_{21} = 7 \times 10^{-5} eV^2$ and $\tan^2(\theta_{12}) = 0.42$. The steps size changes around $0.4 R_\odot$ from *EIGENSTEP* to *LOGSTEP*.

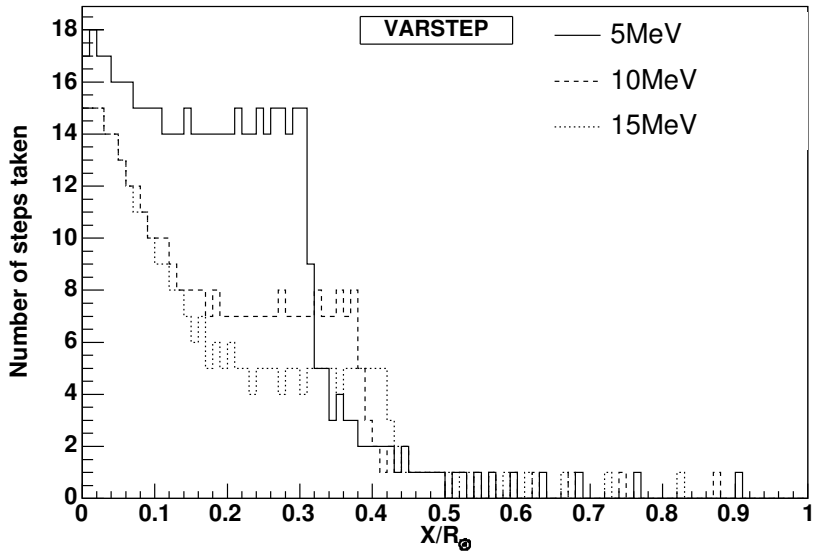

Figure 38: Histogram showing the number of steps taken at each radius by the *VARSTEP* algorithm for different energies and mixing parameters set to $\Delta m_{21} = 7 \times 10^{-5} eV^2$ and $\tan^2(\theta_{12}) = 0.42$. More steps are taken near the center of the Sun, then very few are taken after the resonance.

propagation in the Sun is very close to being adiabatic. This can be examined further by looking at the adiabatic parameter, γ, defined in section (2.2) for different mixing angles and mass squared differences. We recall the definition:

$$\gamma(x) \equiv \frac{\Delta m_{21} \sin^2(2\theta_{12})}{2\hbar c E \cos(2\theta_{12})} \left(\frac{1}{Ne} \frac{dNe}{dx} \right)^{-1} \tag{72}$$

Figure (39) shows how γ varies as a function of $\frac{\Delta m_{21}}{E}$ and $\sin^2(\theta_{12})$. The adiabatic parameter is evaluated at the resonance, since this is where the energy eigenvalues are closest to each other and the probability of tunneling is thus the largest. The contours where the adiabadicity parameter is of order unity is where the adiabatic approximation is expected to break down. One should note that the scale is set in order to highlight the region where $\gamma \sim 1$, and is thus misleading, since the adiabatic parameter actually becomes many orders of magnitudes larger than implied by the scale. One notes that the propagation is expected to be adiabatic over a fairly large range of mixing parameters, in particular in the region of the experimental parameters (indicated by the star for a $10MeV$ neutrino).

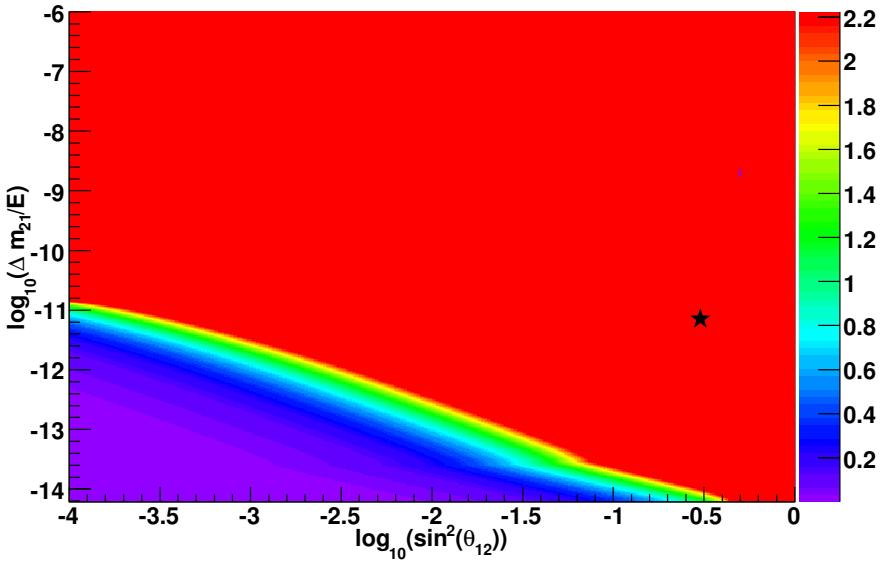

Figure 39: Adiabadicity parameter (as defined by equation (72)) plotted as a function of $\log_{10}(\sin^2(\theta_{12}))$ and $\log_{10}(\frac{\Delta m_{21}}{E})$. The scale is fixed so that the line where $\gamma \sim 1$ is clearly visible, and in some regions, the adiabadicity parameter is several orders of magnitudes bigger than indicated on the scale.

Figure (40a) shows the adiabatic survival probability over the same range of mixing parameters, and Figure (40b) shows the relative difference with the survival probability calculated with a nu-

merical phase average (Figure (28)). One notes that in the region where the current experimental parameters lie, the adiabatic approximation works very well. This was anticipated from Figure (39), and confirms that the adiabatic approximation breaks down when $\gamma \sim 1$.

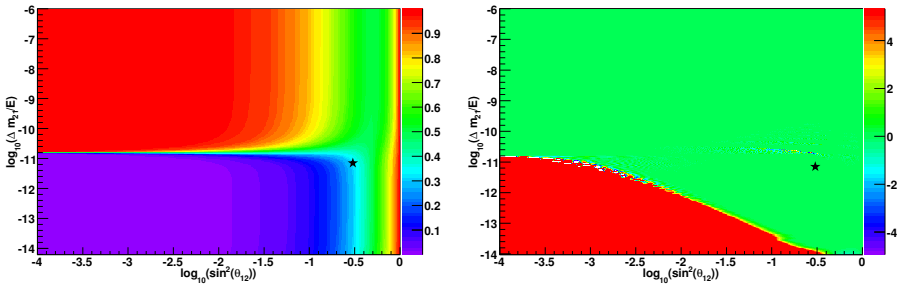

(a) Adiabatic approximation

(b) Relative difference from phase averaged P_{ee}

Figure 40: Contour plots of P_{ee} calculated with the adiabatic approximation (left) and relative difference from P_{ee} calculated with a phase average (right) for neutrinos originating in the center of the Sun as a function of $\log_{10}(\sin^2(\theta_{12}))$ and $\log_{10}(\frac{\Delta m_{21}}{E})$. The point marked with a star is for $\Delta m_{21} = 7 \times 10^{-5} eV^2$ and $\tan^2(2\theta_{12}) = 0.42$ at an energy of $10 MeV$.

We now consider the effect of modifying the adiabatic approximation by introducing the jump probability at the resonance. Several authors have derived analytical formulas for this result, depending on analytical descriptions of the density at the resonance. The most basic approach, first used by Landau and Zener, while considering atomic collisions, is to approximate the density as varying linearly with distance. This is a reasonable approach, as long as the resonance is narrow, which is often the case in Sun. Their result was first applied to neutrinos by Haxton [32] and Parke [14] for a linearly varying density who found the jump probability, P_j^{Parke} to be:

$$\begin{aligned} P_j^{Parke} &= e^{-\frac{\pi}{2}\frac{\Delta m_{21}\sin^2(2\theta_{12})}{2\hbar cE\cos(2\theta_{12})}\left|\frac{1}{Ne}\frac{dNe}{dx}|_{x=x_{res}}\right|^{-1}} \\ &= e^{-\frac{\pi}{2}\gamma(x_{res})} \end{aligned} \tag{73}$$

where the derivative of the density is evaluated at the resonance. Kuo and Pantaleone present more general formulas for various density profiles [29] in the form:

$$P_j^{KP} = e^{-\frac{\pi}{2}\gamma(x_{res})F} \tag{74}$$

where F depends on the specific density profile. For example, in the case of an exponentially decreasing density, $Ne \propto e^{-r}$, $F = 1 - \tan^2(\theta_{12})$. This particular case, which is most relevant for the Sun, was first solved by Petcov [13]. The survival probability is shown as a function of θ_{12} and $\frac{\Delta m_{21}}{E}$ in Figure (41), calculated using the two jump probabilities. We note that these agree quite well (with each other and with Figure (28)) and are valid over a much larger range than the adiabatic approximation, as expected. We did not plot the relative difference from the phase-averaged result as the agreement is to within fractions of a percent. There is a very small region of large disagreement (up to 80%) along the line where $\gamma \sim 1$, but we chose not to plot this, since the region is so small.

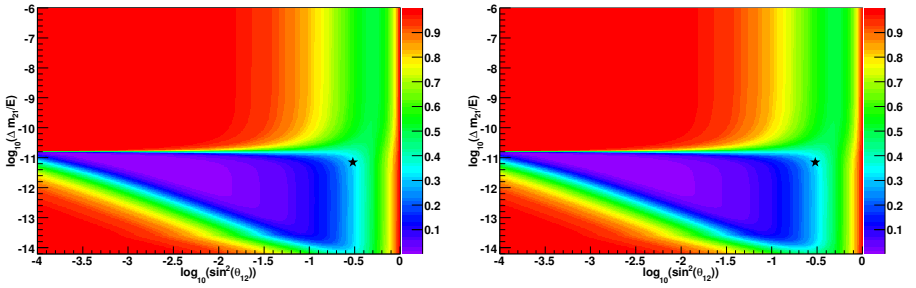

(a) Linear (Parke) (b) Exponential (Petcov)

Figure 41: Contour plot of P_{ee} calculated with the two jump probabilities (in two flavours), for neutrinos originating in the center of the Sun as a function of $\log_{10}(\sin^2(\theta_{12}))$ and $\log_{10}(\frac{\Delta m_{21}}{E})$. The point marked with a star is for $\Delta m_{21} = 7 \times 10^{-5} eV^2$ and $\tan^2(2\theta_{12}) = 0.42$ at an energy of $10 MeV$.

Figure (42) shows the percent difference between the survival probabilities calculated with the exponential and linear approximations to the density. We see that the region where these two disagree in the Sun is very small, far from the experimental parameter space and that the disagreement is mostly smaller than one percent.

At this point, we can finally understand all of the features in the Figures similar to Figure (41). The main triangular feature, often referred to as the MSW triangle, is the region of parameter space where matter has an important effect on the survival probability. The horizontal line at the top of the triangle delimits the region above which the MSW resonance cannot occur in the Sun (as illustrated by Figure (27)). The diagonal line on the bottom delimits the region below which the jump probability is non-negligible and, finally, the vertical line on the right of the triangle corresponds to a vacuum mixing angle of $\frac{\pi}{4}$. For mixing angles above this value, the MSW resonance cannot occur, as it would require a negative density or the neutrinos to be anti-neutrinos.

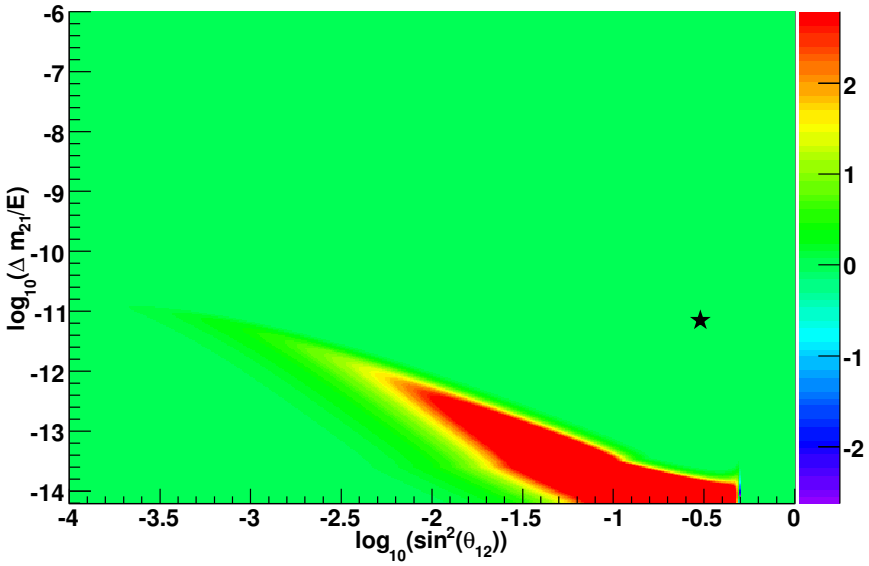

Figure 42: Percent difference between solar survival probability calculated with Petcov and Parke jump probabilities as a function of $\log_{10}(\sin^2(\theta_{12}))$ and $\log_{10}(\frac{\Delta m_{21}}{E})$.

2.3.7 Three-Flavour Approximations

We now consider the three flavour approximations presented earlier along with the adiabatic approximation in three flavours. We have noted that varying Δm_{31} around its experimental value does not have a large effect and we will hence only consider the influence of θ_{13}. Figure (43a) shows the survival probability calculated with the adiabatic approximation as a function of $\frac{\Delta m_{21}}{E}$ and θ_{13} for $\tan^2(\theta_{12}) = 0.42$, and we note that it agrees quite well with Figure (31). Figure (43b) shows the relative difference in percent between the two methods, and we note that for this value of θ_{12} the agreement is excellent over a large range of the plane.

Next, we consider using the adiabatic approximation in three flavours together with the jump probability in two flavours. This will work if the only important jump probability is between the first two eigenstates, as it will completely ignore the 2-3 transition. This is expected to be a valid assumption since only the 1-2 resonance is crossed in the Sun. We consider this approximation in the case where $\sin^2(2\theta_{13}) = 0.5$ so that the results can be compared to Figure (32). The results are shown in Figure (44), where the left panel is the survival probability calculated with the three-flavour adiabatic approximation with a two-flavour (Parke) jump probability and the left panel shows the relative difference (in percent) with the results from Figure (32). The agreement, once again, is seen to be excellent over most of the plane and we conclude that this is a very good approximation.

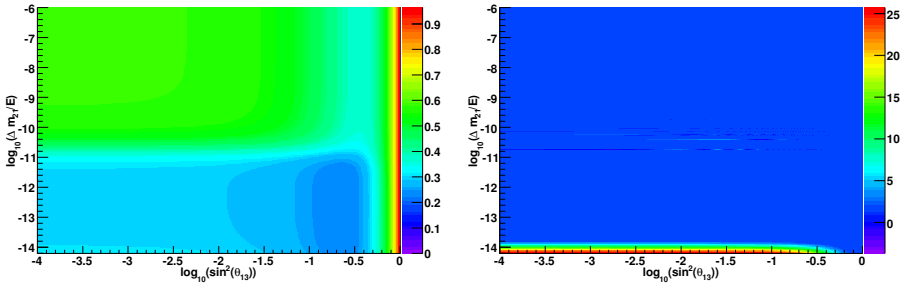

(a) Three-Flavour Adiabatic

(b) Percent difference with phase average

Figure 43: Contour plot of P_{ee} in the adiabatic approximation (left) and relative difference with the result calculated with a phase average (right) for neutrinos originating in the center of the Sun as a function of $\log_{10}(\sin^2(\theta_{13}))$ and $\log_{10}(\frac{\Delta m_{21}}{E})$ for $\tan^2(\theta_{12}) = 0.42$.

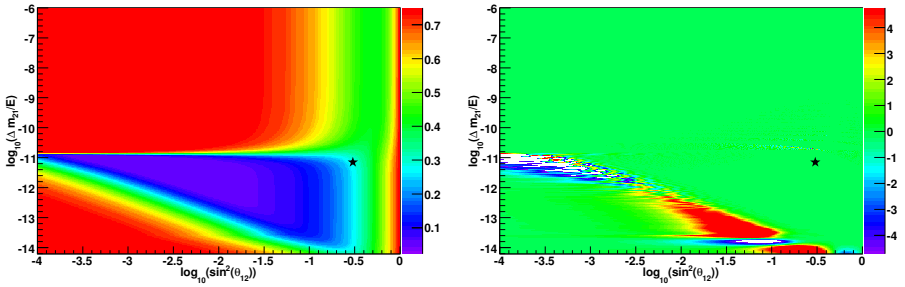

(a) Three-Flavour Adiabatic with Parke jump

(b) Percent difference with phase average

Figure 44: Contour plot of P_{ee} in the three-flavour adiabatic approximation using the two-flavour Parke jump probability (left) and relative difference with the result calculated with a phase average (right), as a function of $\log_{10}(\sin^2(\theta_{12}))$ and $\log_{10}(\frac{\Delta m_{21}}{E})$ for $\tan^2(\theta_{12}) = 0.42$ and $\sin^2(2\theta_{13}) = 0.5$.

Finally, we consider the approximations that correct the two-flavour calculation to include the effect of θ_{13} in the case when the three-flavour oscillations can be decoupled. We will refer to these at the first and second order approximations (see section (2.2)). We will use the Parke jump probability to calculate the two-flavour survival probability and compare the results with Figure (32), for the case where $\sin^2(2\theta_{13}) = 0.5$. The survival probability calculated with the first-order approximation is shown in Figure (45) along with the relative difference (in percent) from the numerical phase average. One notes that the results are almost the same as the three-flavour adiabatic with the two-flavour jump probability. This is to be expected and shows that the third neutrino is indeed decoupled. Figure (46) shows the same results when calculated with the second-order approximation. We note that both approximations agree very well in the region of experimental parameter space, and that the first-order approximation maps out the MSW triangle more accurately. The second-order approximation is seen to break down for a line where the expression for ϵ is singular (recall equation (60)). This only happens because we have chosen a particular neutrino energy when calculating the plot, and this singular line can easily be 'pushed out' of the graph by doing the calculation with a lower energy neutrino. It does however seem that the three-flavour adiabatic approximation using the two-flavour jump probability is a slightly more accurate approximation, which is the main conclusion of this section.

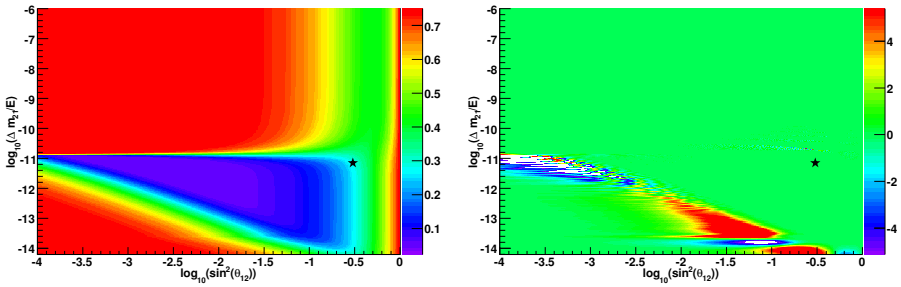

(a) First order correction to two-flavour P_{ee}

(b) Percent difference with phase-average

Figure 45: Contour plot of P_{ee} using the first-order correction for non zero θ_{13} and the two-flavour Parke jump probability (left) and relative difference with the result calculated with a phase average (right), as a function of $\log_{10}(\sin^2(\theta_{12}))$ and $\log_{10}(\frac{\Delta m_{21}}{E})$ for $\tan^2(\theta_{12}) = 0.42$ and $\sin^2(2\theta_{13}) = 0.5$.

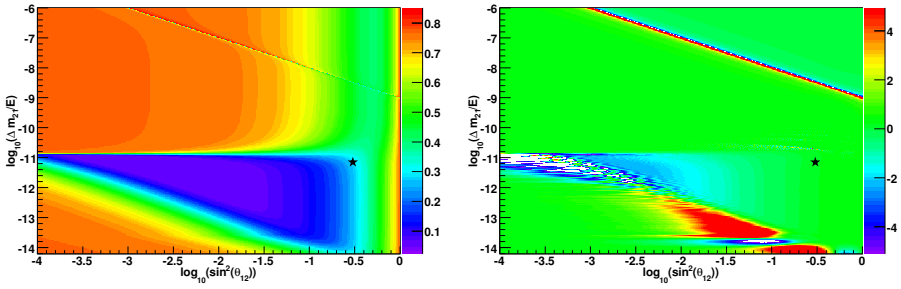

(a) Second-order correction to two-flavour P_{ee}

(b) Percent difference with phase average

Figure 46: Contour plot of P_{ee} using the second-order correction for non zero θ_{13} and the two-flavour Parke jump probability (left) and relative difference with the result calculated with a phase average (right), as a function of $\log_{10}(\sin^2(\theta_{12}))$ and $\log_{10}(\frac{\Delta m_{21}}{E})$ for $\tan^2(\theta_{12}) = 0.42$ and $\sin^2(2\theta_{13}) = 0.5$.

2.4 Neutrino Propagation in the Earth

In this section, we briefly examine the effect of the Earth on the propagation of neutrinos. We will see that the Earth has a small effect on the survival probability of neutrinos in the range of the experimental parameters and that the largest effect occur at energies higher than those of solar neutrinos.

The Earth is quite different than the Sun in the density profile that it presents to neutrinos. Figure (47) shows the electron density of the Earth as a function of radius and one notes that it contains several discontinuities. The Preliminary Earth Reference Model (PREM), [39] , from 1981 was used and seems to be the most widely accepted. The density profile is inferred from seismological considerations, and although it is named "Preliminary", most of the community still uses it to this day, and some authors just refer to it as the REM. Apart from the density discontinuities, we have also used a standard chemical composition to calculate the electron density as a function of mass density. This is a simple two layer chemical model where the ratio of protons to nucleons changes from $Z/A = 0.467$ to $Z/A = 0.497$ at an Earth radius of $3480km$, where the core-mantle interface is located. This is also consistent with approximations made by the rest of the neutrino physics community [40].

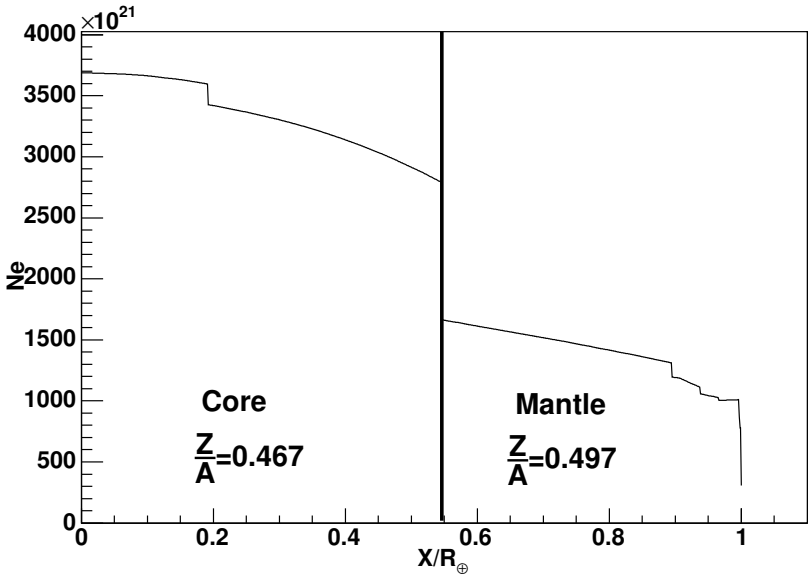

Figure 47: Electron density profile for the Earth based on the PREM model and a two layer chemical distribution where the ratio of protons to nucleons changes from $Z/A = 0.468$ to $Z/A = 0.497$ at an Earth radius of $3480km$, marked by the vertical line.

It was already argued in section (2.2) that the discontinuities do not present any inherent prob-

lems in numerical calculations as long as the flavour content is taken as continuous through any interface. In Figure (48), the survival probability is plotted for a neutrino that starts one Earth radius away from the Earth, then travels through the center and again one radius in vacuum after that. The energy is set to $10MeV$, with $\Delta m_{21} = 2 \times 10^{-5} eV^2$ and $\tan^2(\theta_{12}) = 0.42$. A smaller mass squared difference was chosen in order to make the wavelength bigger and the oscillations easier to see. One clearly notes the effect from the Earth's matter in the transition from vacuum oscillations to matter oscillations. The mantle-core interface is also visible and is the only point where the electron density changes enough to alter the matter oscillation amplitude significantly.

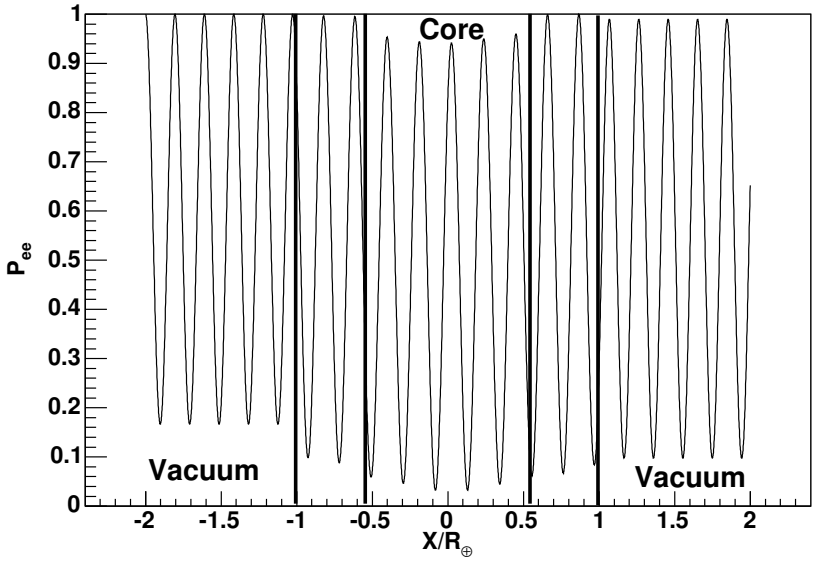

Figure 48: Survival probability (two flavours) for a neutrino that started one Earth radius away from the Earth, then traverses the Earth, and finally travels one more Earth radius in vacuum. The energy is set to $10MeV$, with $\Delta m_{21} = 2 \times 10^{-5} eV^2$ and $\tan^2(\theta_{12}) = 0.42$.

2.4.1 Incoherent Beam of Neutrinos arriving at Earth

When examining solar neutrinos, one must consider the effect from the Earth on an incoherent beam of neutrinos. The incoherence is due to neutrinos being generated in different locations in the Sun but can also arise from the fact that a detector will have a finite energy resolution and that the Earth-Sun distance varies. This section briefly introduces some of the surprising features that arise when an incoherent beam of neutrinos traverses the Earth. This discussion was already introduced in section (2.2).

Neutrinos from the Sun were shown to exit in mostly the $|\nu_2>$ eigenstate. We thus examine the

behavior of a neutrino that starts in vacuum in the following state:

$$|\nu >= \sqrt{0.1}|\nu_1 > +\sqrt{0.90}|\nu_2 > e^{-i\phi} \tag{75}$$

where we have chosen a mass content consistent with solar neutrinos and introduced a phase ϕ over which the results will be averaged. We have chosen a two flavour model as the addition of the third flavour does not introduce any qualitatively different behaviors. Figure (49) shows the probability of detecting an electron type neutrino as a function of distance for a neutrino that started out in the state given by equation (75) as well as the corresponding $|\nu_1^m >$ content. The neutrino is again started one Earth radius away in vacuum, it then goes through the center of the Earth and finally travels one more Earth radius in vacuum. The left panels of Figure (49) are done for a value of $\phi = 0$ and the right panels show the same plots for $\phi = \pi$. As expected, the vacuum oscillations in the two figures are out of phase. However one notes that the matter oscillations are not out of phase and that, in the case where $\phi = \pi$, the $|\nu_1^m >$ content is regenerated. One also notes that the $|\nu_1^m >$ oscillates and is not constant. This is because the density reaches the resonant density so that there is a non-negligible jump probability allowing the $|\nu_1^m >$ eigenstate to tunnel back and forth to the $|\nu_2^m >$ state. This can be seen more clearly in Figure (50) where the matter mixing angle and matter mass squared difference are plotted as a function of distance. One notes that the resonant density is reached in the core, which does not actually happen with a mass squared difference consistent with experimental limits. This will be examined further in the next section.

Finally, we can look at the probabilities averaged over the phase ϕ, shown in Figure (51), where we see that, as anticipated earlier, the Earth can reintroduce coherence into a beam of neutrinos. Again, this is because there is now a particular point in space (time) where the $|\nu_1^m >$ eigenstate is regenerated (coherently).

2.4.2 Survival Probability in the Earth : Dependence on Mixing Parameters

It is of interest to know the behavior of the survival probability through the Earth, for a neutrino that started at the edge of the Earth in the electron flavour. This is shown in Figure (52) where the survival probability is plotted along with its phase average, the $|\nu_1^m >$ content, the matter mixing angle and the matter mass squared difference for a $10MeV$ neutrino with $\Delta m_{21} = 7 \times 10^{-5} eV^2$ and $\tan^2(\theta_{12}) = 0.42$. We see that, in this case, the resonant density is never encountered and that the Earth has a very small effect on the average flavour content, which remains close to its vacuum average.

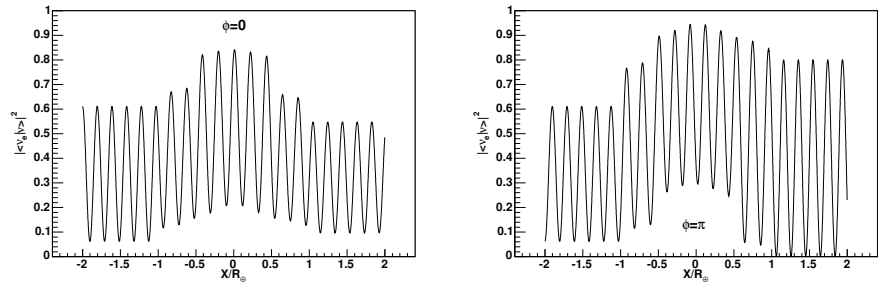

(a) $| < \nu_e | \nu > |^2$ (b) $| < \nu_e | \nu > |^2$

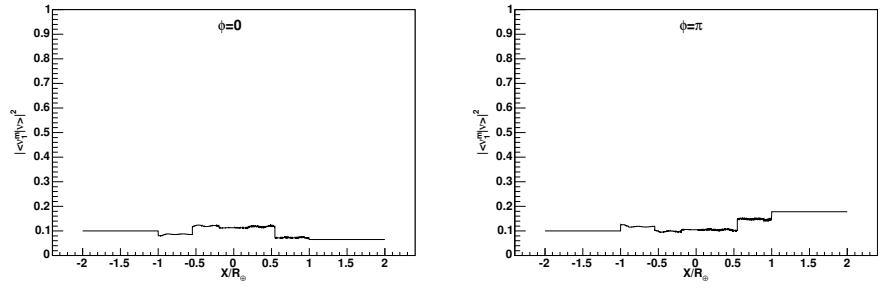

(c) $| < \nu_1^m | \nu > |^2$ (d) $| < \nu_1^m | \nu > |^2$

Figure 49: Survival probability and matter mass eigenstate content for a neutrino that started one Earth radius away from the Earth, then traverses the Earth, and finally travels one more Earth radius in vacuum. The energy is set to $10MeV$, with $\Delta m_{21} = 2 \times 10^{-5} eV^2$ and $\tan^2(\theta_{12}) = 0.42$ and the neutrino started in the state defined by equation (75) with the phase set to 0 (left) and π (right).

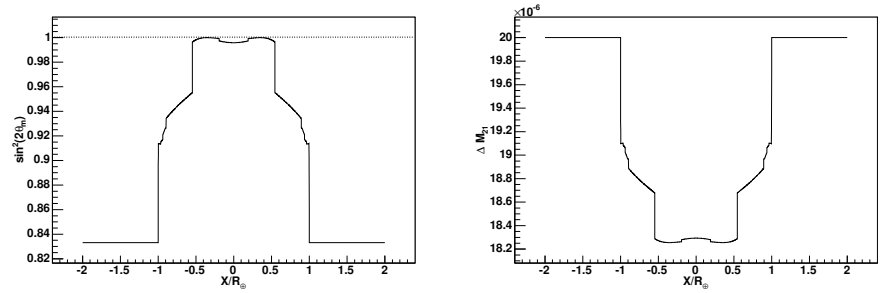

(a) Matter Mixing Angle (b) Matter Mass Squared Difference

Figure 50: $\sin^2(2\theta_m)$ and ΔM_{21} as a function of distance for the case illustrated in Figure (49).

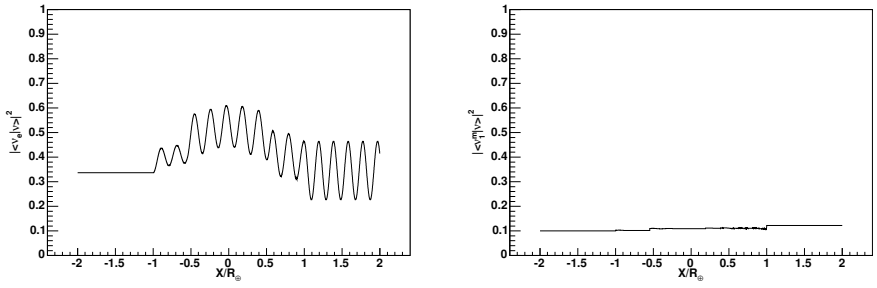

(a) $| < \nu_e | \nu > |^2$ (b) $| < \nu_1^m | \nu > |^2$

Figure 51: Survival probability and matter mass eigenstate content for a neutrino that started one Earth radius away from the Earth, then traverses the Earth, and finally travels one more Earth radius in vacuum. The energy is set to $10MeV$, with $\Delta m_{21} = 2 \times 10^{-5} eV^2$ and $\tan^2(\theta_{12}) = 0.42$ and the neutrino started in the state defined by equation (75) but the probabilities are averaged over the phase. One notes that the Earth reintroduces coherence in the neutrino beam.

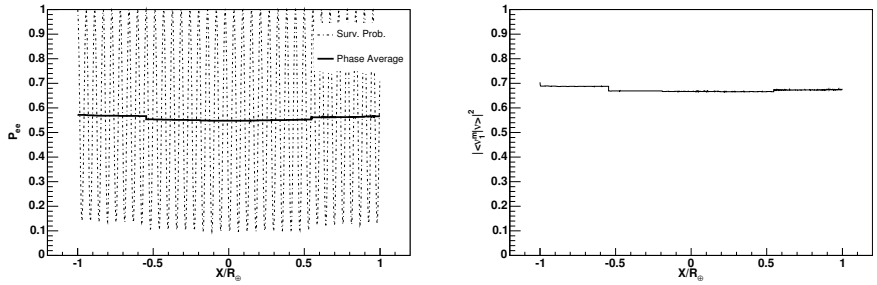

(a) Survival Probability and phase average (b) $| < \nu_1^m | \nu > |^2$

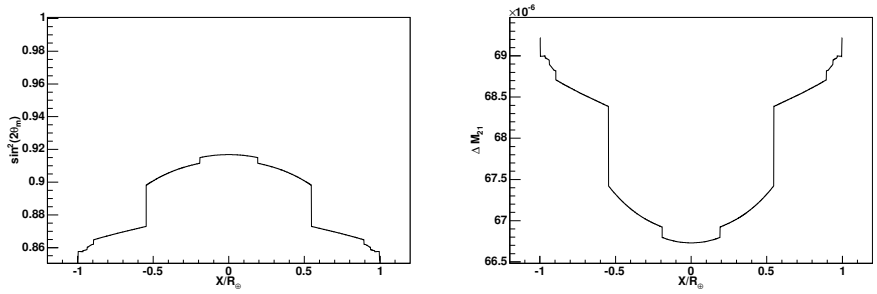

(c) Matter Mixing Angle (d) Matter-Mass Squared Difference

Figure 52: Survival probability, matter-mass eigenstate content, mixing angle and matter mass squared difference as a function of distance through the Earth for a $10MeV$ neutrino, with $\Delta m_{21} = 7 \times 10^{-5} eV^2$ and $\tan^2(\theta_{12}) = 0.42$. The Earth has a small influence on the flavour content.

Figure (53) shows the relative difference (in percent) between the phase averaged survival probability through the Earth (diametrical trajectories) and the classical survival probability in vacuum over a range of mixing parameters. This illustrates the range of parameter space where the Earth has a substantial influence beyond vacuum oscillations. One notes some regions at high energy where the difference is quite significant due to the resonance density being reached in the Earth. The effect is also more pronounced at small mixing angle where the oscillation length can become comparable to the lengths of the mantle and core. This has been termed the 'resonant wavelength' and is discussed in [40] and [41].

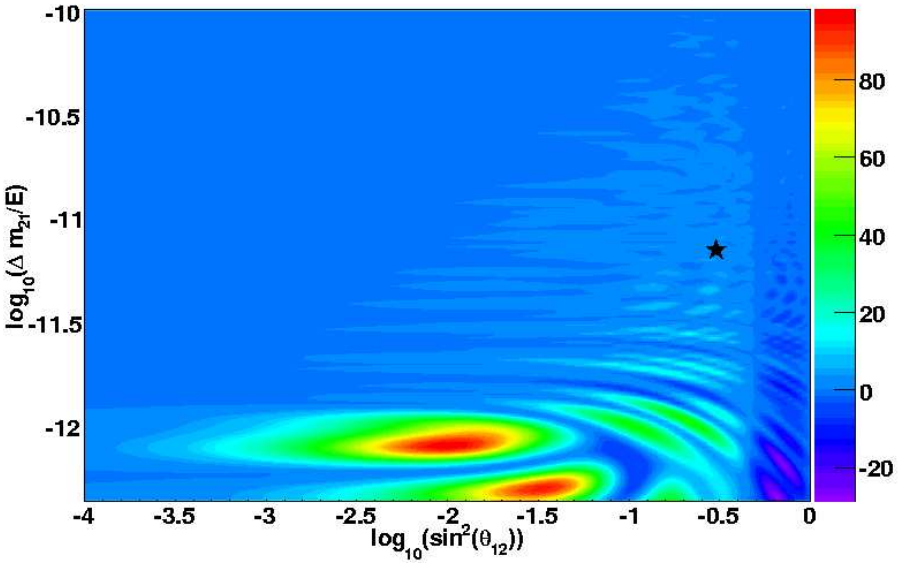

Figure 53: Relative difference (in percent) between vacuum classical survival probability and phase averaged survival probability for a trajectory through the Earth's core as a function of $\log_{10}(\frac{\Delta m_{21}}{E})$ and $\log_{10}(\sin^2(\theta_{12}))$. The star corresponds to the experimental parameters at an energy of $10MeV$. The Earth has the biggest effect at small mixing angles and large energies.

2.5 Solar Neutrinos Propagating Through the Earth

In this section we seek to derive a formalism for calculating fluxes of solar neutrinos when these also traverse the Earth. This is relevant in modeling the night flux at SNO and taking into account the effect of the Earth's matter on the survival probability. It will turn out that, in most cases, one need not do the lengthy integral presented at the end of Section (2.2) and that a very good approximation can be used. Instead, we will show how it is possible to calculate the average over the Earth trajectories separately from the average over the Sun. This will remove one of the nested integrals, which turns out to save considerable amounts of computing time. The theoretical motivation for this section is to consider the possible effects that θ_{13} can have on solar neutrino experiments and if a day-night asymmetry measurement can provide independent bounds on θ_{13}.

2.5.1 Introduction to PSE

The key to separating the Earth and solar integrals is the approximation that neutrinos from the Sun reach the Earth in an incoherent beam. Incoherence is achieved in several ways. Primarily, it comes from the neutrinos being produced in different locations in the Sun. As long as the neutrino wavelength in matter is small compared to the production region, incoherence will be assured. Furthermore, when one considers solar neutrino experiments such as SNO, even if the neutrinos are in a coherent beam, the detector will introduce an incoherence due to the energy resolution. That is, if an experiment is trying to measure neutrino oscillations by looking at the flux at different distances from a source, it will not be able to measure the oscillation length accurately if it has a poor energy resolution, since it depends on L/E (where L is the distance between the source and the detector). Hence, a detector with poor energy resolution will not necessarily be able to distinguish a coherent beam from an incoherent one. Another reason that a SNO type detector would introduce incoherence is from the fact that it does not see very many neutrino events per day (around 10 or so). Hence, to provide a statistically significant measure, many days of livetime need to be used. However, since the Earth-Sun distance will change over this livetime, a new incoherence is introduced.

One should thus be convinced that solar neutrinos reach the Earth incoherently. This condition is only violated if the neutrino energies are very large and result in an oscillation length that is comparable to the Earth-Sun distance. The particular requirements for solar neutrinos to reach the Earth in an incoherent beam are discussed in [42]

The goal of this section is thus to derive a formula for calculating the survival probability, P_{SE},

for solar neutrinos having traversed the Earth in the case when the solar neutrinos reach the Earth incoherently. The aim of this formula is to allow one to separate the Earth out from the integral in equation (70) and examine the dependence on θ_{13}.

2.5.2 Derivation of PSE

We will closely follow a derivation done by Baltz and Weneser in ([43], [44]), but extend their work to three flavours. A similar three-flavour derivation has already been done by Kim and Lee [16], although they did not consider the final result as a function of the mixing angles and sought a numerical method for the calculation. Similar work on the subject has also been carried out by Ohlsson *et. al.* in [15], who reach similar conclusions as us, although their approach is different.

We start by considering the wave-function for a single neutrino that exited the Sun, has traveled through vacuum and now reaches the Earth in the state:

$$|\nu^S >= f_i(t)k_i|\nu_i > \tag{76}$$

where $f_i(t)$ are the phases of the vacuum mass eigenstates $|\nu_i >$ acquired during the trajectory, and k_i are the vacuum eigenstate contents, which can be taken as real numbers. The index S on the neutrino wave-function indicates that this is the wave-function after the Sun, but before the Earth. Throughout this section, we will adopt the convention that repeated indices are to be summed over, roman letters run from 1 to 3 and Greek letters run over the neutrino flavours (e, μ, τ). One can re-express the neutrino wave-function in the flavour basis:

$$\begin{aligned} |\nu^S > &= \beta_\alpha|\nu_\alpha > \\ &= U^*_{\alpha i}f_i(t)k_i|\nu_i > \end{aligned} \tag{77}$$

where U is the PMNS mixing matrix from the vacuum to the flavour basis. Hence, the flavour contents, β_α, are given by:

$$\beta_\alpha = U^*_{\alpha i}f_i(t)k_i \tag{78}$$

In general, for an incoherent beam of neutrinos we then have:

$$|\beta_\alpha|^2 = U^*_{\alpha i}f^*_i(t)k^*_i U_{\alpha j}f_j(t)k_j$$

$$= |U_{\alpha i}|^2 |k_i|^2 \tag{79}$$

and

$$\begin{aligned} \beta_\alpha \beta_\gamma^* &= U_{\alpha i}^* f_i(t) k_i U_{\gamma j} f_j(t)^* k_j^* \\ &= U_{\alpha i}^* U_{\gamma i} |k_i|^2 \end{aligned} \tag{80}$$

where we have imposed $f_i(t)^* f_j(t) = \delta_{ij}$ and δ_{ij} is the Kronecker delta. This condition is valid if one can average over the neutrino phases as we have assumed an incoherent beam. One can thus identify some of these quantities with probabilities averaged over the Sun:

$$\begin{aligned} |\beta_e|^2 &= \bar{P}^{\odot}_{\nu_e \to \nu_e} \\ |\beta_\mu|^2 &= \bar{P}^{\odot}_{\nu_e \to \nu_\mu} \\ |\beta_\tau|^2 &= \bar{P}^{\odot}_{\nu_e \to \nu_\tau} = 1 - \bar{P}^{\odot}_{\nu_e \to \nu_e} - \bar{P}^{\odot}_{\nu_e \to \nu_\mu} \end{aligned} \tag{81}$$

where, for example $\bar{P}^{\odot}_{\nu_e \to \nu_e}$ is just the survival probability for neutrinos averaged over the Sun as well as the Earth-Sun distance, as given by equation (69).

We now introduce 'Earth Transmission' functions, $\Psi^{e(\mu,\tau)}$, to represent the wave-functions for a neutrino which has traversed the Earth having started out as an electron (muon, tauon) flavour neutrino. Expressed in the flavour basis, these can be written as:

$$|\Psi^\alpha >= C_e^\alpha |\nu_e > + C_\mu^\alpha |\nu_\mu > + C_\tau^\alpha |\nu_\tau > \tag{82}$$

and one can make the following identifications:

$$\begin{aligned} P^{\oplus}_{\nu_e \to \nu_e} &= |C_e^e|^2 \\ P^{\oplus}_{\nu_\mu \to \nu_e} &= |C_e^\mu|^2 \\ P^{\oplus}_{\nu_\tau \to \nu_e} &= |C_e^\tau|^2 = 1 - P^{\oplus}_{\nu_e \to \nu_e} - P^{\oplus}_{\nu_\mu \to \nu_e} \end{aligned} \tag{83}$$

We can now express the wave-function for a neutrino that arrived at the Earth in the state defined by equation (77) and has traversed the Earth. The result is simply a linear combination of the Earth Transmission functions:

$$|\nu^{SE}>=\beta_\alpha|\Psi^\alpha> \tag{84}$$

where we have now indexed the wave-function with SE, to indicate that the solar neutrino has now traversed the Earth. The probability of detecting an electron neutrino, P_{SE}, can now be expressed by separating out the Earth and Sun terms:

$$\begin{aligned}
P_{SE} &= |<\nu_e|\nu^{SE}>|^2 \\
&= |\beta_e C_e^e + \beta_\mu C_e^\mu + \beta_\tau C_e^\tau|^2 \\
&= |\beta_\alpha|^2|C_e^\alpha|^2 + \frac{1}{2}\Big((\beta_e\beta_\mu^* + c.c.)(C_e^e C_e^{\mu *} + c.c.) \\
&+ (\beta_e\beta_\tau^* + c.c.)(C_e^e C_e^{\tau *} + c.c.) + (\beta_\mu\beta_\tau^* + c.c.)(C_e^\mu C_e^{\tau *} + c.c.) \\
&+ (\beta_e\beta_\mu^* - c.c.)(C_e^e C_e^{\mu *} - c.c.) + (\beta_e\beta_\tau^* - c.c.)(C_e^e C_e^{\tau *} - c.c.) \\
&+ (\beta_\mu\beta_\tau^* - c.c.)(C_e^\mu C_e^{\tau *} - c.c.)\Big)
\end{aligned} \tag{85}$$

At this point, one can easily calculate the different quantities over the Sun and Earth separately. Since the terms separate, one can average (numerically) the quantities $|\beta_\alpha|^2$ and $\beta_\alpha\beta_\gamma^*$ ($|C_e^\alpha|^2$ and $C_e^\alpha C_e^{\gamma *}$) over the Sun (Earth) trajectories. This is essentially the point where the Kim and Lee derivation leads. We are however interested in examining how this formula depends on the various mixing angles and how it can be further simplified. We first note by considering equations (79) and (80) that one can re-express $\beta_\alpha\beta_\gamma^*$ in terms of solar probabilities, by using equation (79) to solve for the $|k_i|^2$. If we introduce the matrix $\mathcal{U}_{ij} = |U_{ij}|^2$ we have:

$$\begin{aligned}
|\beta_\lambda|^2 &= \mathcal{U}_{\lambda i}|k_i|^2 \\
|k_i|^2 &= \mathcal{U}_{i\lambda}^{-1}|\beta_\lambda|^2 \\
\beta_\alpha\beta_\gamma^* &= U_{\alpha i}U_{\gamma i}^*(\mathcal{U}_{i\lambda}^{-1}|\beta_\lambda|^2)
\end{aligned} \tag{86}$$

where we have assumed that $\mathcal{U}$ is an invertible matrix. One should thus keep in mind that this derivation cannot be done in the case where the determinant of $\mathcal{U}$ is zero. In this case, one must

keep everything in terms of the $|k_i|^2$, and this situation in two flavours is discussed in [42]. To lighten the notation, we will also introduce:

$$\begin{aligned} C^{\alpha\gamma} &\equiv C_e^{\alpha} C_e^{\gamma *} \\ \beta_{\alpha\gamma} &\equiv \beta_{\alpha}\beta_{\gamma}^{*} \end{aligned} \tag{87}$$

We can then rewrite equation (85) as:

$$\begin{aligned} P_{SE} &= |\beta_e|^2 \bar{P}^{\oplus}_{\nu_e\to\nu_e} + |\beta_\mu|^2 \bar{P}^{\oplus}_{\nu_\mu\to\nu_e} + |\beta_\tau|^2 \bar{P}^{\oplus}_{\nu_\tau\to\nu_e} \\ &+ 2\Big(\Re(\beta_{e\mu})\Re(C^{e\mu}) + \Re(\beta_{e\tau})\Re(C^{e\tau}) + \Re(\beta_{\mu\tau})\Re(C^{\mu\tau}) \\ &- \Im(\beta_{e\mu})\Im(C^{e\mu}) - \Im(\beta_{e\tau})\Im(C^{e\tau}) - \Im(\beta_{\mu\tau})\Im(C^{\mu\tau})\Big) \end{aligned} \tag{88}$$

where $\Re$ ($\Im$) stand for the real (imaginary) parts of an expression. We now use the property that, for two complex numbers, a and b, one has[2] :

$$\Re(a)\Re(b) - \Im(a)\Im(b) = \Re(ab) \tag{89}$$

so that one can rewrite P_{SE} as:

$$\begin{aligned} P_{SE} &= |\beta_e|^2 \bar{P}^{\oplus}_{\nu_e\to\nu_e} + |\beta_\mu|^2 \bar{P}^{\oplus}_{\nu_\mu\to\nu_e} + |\beta_\tau|^2 \bar{P}^{\oplus}_{\nu_\tau\to\nu_e} \\ &+ 2\Big(\Re(\beta_{e\mu}C^{e\mu}) + \Re(\beta_{e\tau}C^{e\tau}) + \Re(\beta_{\mu\tau}C^{\mu\tau})\Big) \\ &= |\beta_e|^2 \bar{P}^{\oplus}_{\nu_e\to\nu_e} + |\beta_\mu|^2 \bar{P}^{\oplus}_{\nu_\mu\to\nu_e} + |\beta_\tau|^2 \bar{P}^{\oplus}_{\nu_\tau\to\nu_e} \\ &+ 2\Re(U_{\alpha i}U^{*}_{\gamma i}C^{\alpha\gamma}\mathcal{U}^{-1}_{i\lambda})|\beta_\lambda|^2 \end{aligned} \tag{90}$$

where it is understood that each combination of flavour indices appears only once ($\alpha < \gamma$). It is now convenient to highlight the separation of earth and solar probabilities by explicitly writing out the linear combination of solar probabilities ($|\beta_\lambda|^2$) in the form:

[2]This relation was (re)discovered by accident and is shown here as it does not appear to be common knowledge!

$$\Re(U_{\alpha i}U^*_{\gamma i}C^{\alpha\gamma}\mathcal{U}^{-1}_{i\lambda})|\beta_\lambda|^2 = t_e|\beta_e|^2 + t_\mu|\beta_\mu|^2 + t_\tau|\beta_\tau|^2 \tag{91}$$

where the coefficients, t_λ are given by

$$t_\lambda \equiv 2\Re(C^{\alpha\gamma}U_{\alpha i}U^*_{\gamma i}\mathcal{U}^{-1}_{i\lambda}) \tag{92}$$

One can easily check from equation (92) that $t_e + t_\mu + t_\tau = 0$ from the orthogonality properties of the mixing matrix U. Thus, there are only two independent coefficients t_λ and these only depend on Earth probabilities, or cross-terms between them. In general, this shows that out of three possible Earth transmission functions, only two are independent, which is equivalent to the conclusion reached by [45]. If we now use equations (81) and (83), we can write P_{SE} as:

$$\begin{aligned} P_{SE} &= |\beta_e|^2\bar{P}^{\oplus}_{\nu_e\to\nu_e} + |\beta_\mu|^2\bar{P}^{\oplus}_{\nu_\mu\to\nu_e} + (1-|\beta_e|^2-|\beta_\mu|^2)(1-\bar{P}^{\oplus}_{\nu_e\to\nu_e}-\bar{P}^{\oplus}_{\nu_\mu\to\nu_e}) \\ &+ \Big(|\beta_e|^2(2t_e+t_\mu) + |\beta_\mu|^2(2t_\mu+t_e) - t_e - t_\mu\Big) \end{aligned} \tag{93}$$

which shows that one can now calculate the result by propagating one neutrino through the Sun and two through the Earth. Indeed, $|\beta_e|^2$ and $|\beta_\mu|^2$ can both be obtained from the same initial conditions in the Sun ($|\nu(0)>=|\nu_e>$), and we will show how one can calculate t_e and t_μ from two neutrinos propagated through the Earth instead of three, as suggested by equation (92). We will first demonstrate the use of this formalism in two flavours, where the algebra is significantly easier.

2.5.3 Interlude: Two-Flavour Case

In order to better understand the derivation and formula for P_{SE}, it is helpful to consider the two-flavour case. We start by rewriting equation (79) for two flavours of neutrinos:

$$\begin{aligned} |\beta_\alpha|^2 &= |U_{\alpha i}|^2|k_i|^2 \\ |\beta_e|^2 &= \cos^2(\theta)|k_1|^2 + \sin^2(\theta)|k_2|^2 \\ |\beta_\mu|^2 &= \sin^2(\theta)|k_1|^2 + \cos^2(\theta)|k_2|^2 \end{aligned} \tag{94}$$

One can then easily solve for the matrix $\mathcal{U}^{-1}$:

$$\mathcal{U}^{-1} = \frac{1}{\cos(2\theta)} \begin{pmatrix} \cos^2(\theta) & -\sin^2(\theta) \\ -\sin^2(\theta) & \cos^2(\theta) \end{pmatrix} \tag{95}$$

and note that this is only allowed when $\theta \neq \frac{\pi}{4}$. The expressions for t_e and t_μ, given by equation (92), are thus:

$$\begin{aligned} t_\lambda &\equiv 2\Re(C^{\alpha\gamma} U_{\alpha i} U^*_{\gamma i} \mathcal{U}^{-1}_{i\lambda}) \\ t_e &= \frac{1}{\cos(2\theta)} 2\Re\left(C^{e\mu}(-\cos(\theta)\sin(\theta)\cos^2(\theta) - \cos(\theta)\sin(\theta)\sin^2(\theta))\right) \\ t_\mu &= \frac{1}{\cos(2\theta)} 2\Re\left(C^{e\mu}(\cos(\theta)\sin(\theta)\sin^2(\theta) + \cos(\theta)\sin(\theta)\cos^2(\theta))\right) \end{aligned} \tag{96}$$

and one easily verifies that $t_\mu = -t_e$. We can now rewrite equation (93) in the two flavour case where we now have $|\beta_\mu|^2 = 1 - |\beta_e|^2$ and $t_\mu = -t_e$:

$$\begin{aligned} P^{2f}_{SE} &= |\beta_e|^2 \bar{P}^{\oplus}_{\nu_e \to \nu_e} + (1 - |\beta_e|^2)(1 - \bar{P}^{\oplus}_{\nu_e \to \nu_e}) + \left(|\beta_e|^2 t_e + (1 - |\beta_e|^2)(-t_e)\right) \\ &= 1 - |\beta_e|^2 + \bar{P}^{\oplus}_{\nu_e \to \nu_e}(2|\beta_e|^2 - 1) + t_e(2|\beta_e|^2 - 1) \end{aligned} \tag{97}$$

so that P_{SE} only depends on $|\beta_e|^2$ and t_e. We now show how one can express t_e in terms of a probability through the Earth and define P^{2f}_{E1} as the probability, averaged over the Earth trajectories, that a neutrino that started in the state with $|\beta_e|^2 = \chi_e$ is detected as an electron flavour neutrino after traversing the Earth:

$$\begin{aligned} P^{2f}_{E1} &\equiv P_{SE}(|\beta_e|^2 = \chi_e, |\beta_\mu|^2 = \chi_\mu = 1 - \chi_e) \\ &= 1 - |\chi_e|^2 + \bar{P}^{\oplus}_{\nu_e \to \nu_e}(2|\chi_e|^2 - 1) + t_e(2|\chi_e|^2 - 1) \end{aligned} \tag{98}$$

One can then trivially solve for t_e:

$$t_e = \frac{P^{2f}_{E1} - 1 + \chi_e}{2\chi_e - 1} - \bar{P}^{\oplus}_{\nu_e \to \nu_e} \tag{99}$$

and finally obtain the two-flavour formula for P_{SE}, where χ_e is simply a number between zero and one:

$$P_{SE}^{2f} = 1 - \bar{P}^{\odot}_{\nu_e \to \nu_e} + \frac{P_{E1}^{2f} - 1 + \chi_e}{2\chi_e - 1}(2\bar{P}^{\odot}_{\nu_e \to \nu_e} - 1) \tag{100}$$

In order to calculate the function P_{E1}^{2f}, one needs to know the mass eigenstate content that corresponds to the desired average flavour content (χ_e). This is required since we assumed an average flavour content, χ_e, in dropping the phases in equation (79). When one wants to calculate P_{E1}^{2f}, one then starts a neutrino in a state:

$$|\nu >= k_1|\nu_1 > + k_2 e^{i\phi}|\nu_2 > \tag{101}$$

and averages the electron flavour content, after the propagation, over the phase, ϕ as well as all the possible Earth trajectories. k_1 and k_2 are real numbers such that:

$$\begin{aligned} \chi_e &= \cos^2(\theta)|k_1|^2 + \sin^2(\theta)|k_2|^2 \\ \chi_\mu &= \sin^2(\theta)|k_1|^2 + \cos^2(\theta)|k_2|^2 \end{aligned} \tag{102}$$

In order to determine k_1 and k_2, one needs to invert equation (94). Several restrictions then become apparent; the determinant of the equation must be non-zero and most importantly, the solutions for k_1 and k_2 must be physical. This is not guaranteed since information was lost when the phases between mass eigenstates were dropped. For example, since all the terms in equation (102) must be positive, there is no way that one can solve for k_1 and k_2 if one of the χ is zero. One does however note that the sum of the $|k_i|^2$ is still guaranteed to be equal to one. Inverting equation (102) gives:

$$\begin{aligned} |k_1|^2 &= \frac{1}{\cos(2\theta)}\left(\cos^2(\theta)\chi_e - \sin^2(\theta)\chi_\mu\right) \\ |k_2|^2 &= \frac{1}{\cos(2\theta)}\left(-\sin^2(\theta)\chi_e + \cos^2(\theta)\chi_\mu\right) \end{aligned} \tag{103}$$

Then, if we assume that $\theta < \frac{\pi}{4}$ (thus restricting $\cos(2\theta)$ to be positive), and then require that $0 \leq |k_i|^2$, we obtain the following inequalities on the χ:

$$\sin^2(\theta) \leq \chi_e \leq \cos^2(\theta)$$

$$\sin^2(\theta) \quad \leq \quad \chi_\mu \ \leq \cos^2(\theta) \tag{104}$$

which are reversed if $\theta > \frac{\pi}{4}$. One notes that in the case where $\theta = \frac{\pi}{4}$, equation (103) breaks down, and one cannot use this derivation for P_{SE} in this case, which is discussed in [42]. This corresponds to the general case where the determinant of $\mathcal{U}$ is zero.

The two-flavour formula for P_{SE} is well know in the literature, it was first discovered by Baltz and Weneser ([43], [44]) who present a version that used two Earth transmission functions, and Mikheyev and Smirnov [46] first presented the formula that is presented here, although our formalism is more general. Mikheyev and Smirnov's formula corresponds to the choice where $\chi_e = \sin^2(\theta)$, where P^{2f}_{E1} is then the probability of detecting an electron flavour neutrino for a neutrino that entered the Earth in a pure $|\nu_2>$ eigenstate. This particular choice is advantageous due to the fact that one need not average over the phase in equation (101) to calculate P^{2f}_{E1} and is further motivated by the fact that neutrinos from the Sun were noted to emerge predominantly in the $|\nu_2>$ eigenstate. With this particular choice of χ_e, P_{SE} takes the simple form:

$$P_{SE} = \frac{\bar{P}^{\odot}_{\nu_e \to \nu_e} - \sin^2(\theta) - P^{\oplus}_{\nu_2 \to \nu_e}(2\bar{P}^{\odot}_{\nu_e \to \nu_e} - 1)}{\cos(2\theta)} \tag{105}$$

which is the version that appears most often in the literature and where we have relabeled P^{2f}_{E1} as $P^{\oplus}_{\nu_2 \to \nu_e}$, since it now represents the probability of detecting an electron neutrino from a neutrino that started in the $|\nu_2>$ mass eigenstate.

2.5.4 Back to Three Flavours

We now show how to re-express the t_λ in terms of simple probabilities in three flavours. We thus introduce two, new, functions, P_{E1} and P_{E2}. We will define P_{E1} as the probability averaged over the Earth of detecting an electron neutrino from a neutrino that started in a state with $|\beta_e|^2 = \chi_{1e}$ and $|\beta_\mu|^2 = \chi_{1\mu}$. Similarly, P_{E2} will correspond to the case of a neutrino entering the Earth in the state with $|\beta_e|^2 = \chi_{2e}$ and $|\beta_\mu|^2 = \chi_{2\mu}$. We thus define:

$$\begin{aligned} P_{E1} \quad &\equiv \quad P_{SE}(|\beta_e|^2 = \chi_{1e}, |\beta_\mu|^2 = \chi_{1\mu}) \\ &= \quad \chi_{1e}\bar{P}^{\oplus}_{\nu_e \to \nu_e} + \chi_{1\mu}\bar{P}^{\oplus}_{\nu_\mu \to \nu_e} + (1 - \chi_{1e} - \chi_{1\mu})(1 - \bar{P}^{\oplus}_{\nu_e \to \nu_e} - \bar{P}^{\oplus}_{\nu_\mu \to \nu_e}) \\ &+ \quad t_e(2\chi_{1e} + \chi_{1\mu} - 1) + t_\mu(2\chi_{1\mu} + \chi_{1e} - 1) \end{aligned} \tag{106}$$

and

$$\begin{aligned} P_{E2} &\equiv P_{SE}(|\beta_e|^2 = \chi_{2e}, |\beta_\mu|^2 = \chi_{2\mu}) \\ &= \chi_{2e}\bar{P}^{\oplus}_{\nu_e\to\nu_e} + \chi_{2\mu}\bar{P}^{\oplus}_{\nu_\mu\to\nu_e} + (1-\chi_{2e}-\chi_{2\mu})(1-\bar{P}^{\oplus}_{\nu_e\to\nu_e} - \bar{P}^{\oplus}_{\nu_\mu\to\nu_e}) \\ &+ t_e(2\chi_{2e}+\chi_{2\mu}-1) + t_\mu(2\chi_{2\mu}+\chi_{2e}-1) \end{aligned} \tag{107}$$

One can then easily solve equations (106) and (107) to express t_e and t_μ in terms of P_{E1} and P_{E2}. After some simple rearrangements, one finds that the dependence on $\bar{P}^{\oplus}_{\nu_e\to\nu_e}$ and $\bar{P}^{\oplus}_{\nu_\mu\to\nu_e}$ has vanished and that P_{SE} can be written as:

$$\begin{aligned} P_{SE} &= \frac{1}{W}\bar{P}^{\odot}_{\nu_e\to\nu_e}\left(P_{E2}(1-3\chi_{1\mu}) - P_{E1}(1-3\chi_{2\mu}) + \chi_{1\mu} - \chi_{2\mu}\right) \\ &+ \frac{1}{W}\bar{P}^{\odot}_{\nu_e\to\nu_\mu}\left(P_{E1}(1-3\chi_{2e}) - P_{E2}(1-3\chi_{1e}) + \chi_{2e} - \chi_{1e}\right) \\ &+ \frac{1}{W}P_{E1}(\chi_{2e}-\chi_{2\mu}) + P_{E2}(\chi_{1\mu}-\chi_{1e}) + \chi_{1e}\chi_{2\mu} - \chi_{1\mu}\chi_{2e} \end{aligned} \tag{108}$$

where we have defined:

$$W \equiv 3(\chi_{1e}\chi_{2\mu} - \chi_{1\mu}\chi_{2e}) + \chi_{1\mu} + \chi_{2e} - \chi_{1e} - \chi_{2\mu} \tag{109}$$

As in the two flavour case, one should note that not all choices of χ are permitted, since these must be consistent with equation (86). For example, none of them can be equal to zero or one, as there is no vacuum mass eigenstate content that, when averaged over the phases, will give a neutrino in a pure flavour eigenstate[3]. Again, one can write a set of inequalities that must be satisfied by the χ, simply by requiring that the mass eigenstate contents, as given by equation (86), be positive (the unitarity of U already guarantees that they will sum to one):

$$\begin{aligned} 0 \leq\ & \mathcal{U}_{1e}^{-1}\chi_e + \mathcal{U}_{1\mu}^{-1}\chi_\mu + (1-\mathcal{U}_{1e}^{-1}-\mathcal{U}_{1\mu}^{-1})(1-\chi_e-\chi_\mu) \\ 0 \leq\ & \mathcal{U}_{2e}^{-1}\chi_e + \mathcal{U}_{2\mu}^{-1}\chi_\mu + (1-\mathcal{U}_{2e}^{-1}-\mathcal{U}_{2\mu}^{-1})(1-\chi_e-\chi_\mu) \\ 0 \leq\ & \mathcal{U}_{3e}^{-1}\chi_e + \mathcal{U}_{3\mu}^{-1}\chi_\mu + (1-\mathcal{U}_{3e}^{-1}-\mathcal{U}_{3\mu}^{-1})(1-\chi_e-\chi_\mu) \end{aligned} \tag{110}$$

[3]This can only happen if the mixing matrix is the identity matrix, in which case the mass eigenstates are in fact the same as the flavour eigenstates

It is not helpful to solve these inequalities in the general case, since one does not know, a priori, the sign of the denominator of $\mathcal{U}$. One should however keep in mind when calculating P_{E1} and P_{E2} that not all choices are possible for the initial flavour contents.

2.5.5 Calculating and Choosing P_{E1} and P_{E2}

We now discuss P_{E1} and P_{E2} and how they are to be calculated. These functions were chosen to represent the probability of detecting an electron neutrino that entered the Earth in a given average flavour content, χ_e and χ_μ. In other words, we require that a neutrino starting in the state:

$$|\nu >= k_1|\nu_1 > +k_2 e^{i\phi_2}|\nu_2 > +k_3 e^{i\phi_3}|\nu_3 > \tag{111}$$

have the required average flavour content if one calculates the flavour content and then averages over the phases of the vacuum states. This is the requirement that we imposed in equation (79) so that we could express $\beta_\alpha \beta_\gamma^*$ in terms of $|\beta_\alpha|^2$ by relating both of these quantities to the $|k_i|^2$. The formula we derived for P_{SE} is thus only valid in this case, and represents the probability of detecting an electron neutrino from an incoherent beam of neutrinos emerging from the Sun.

P_{E1} and P_{E2} can then be calculated by starting a neutrino in the state given by equation (111), propagating it through the Earth, and averaging the resulting electron flavour content over all possible values of the phases, ϕ_2 and ϕ_3. Once this average over the phases is obtained, one then averages this result over all the possible Earth trajectories, which are determined by the zenith angle exposure function, to finally obtain P_{E1} and P_{E2}.

In order to calculate these probabilities quickly, it can be seen that choosing the initial content to be in a pure mass eigenstate eliminates the need to average over the phases. A particularly good choice is to calculate P_{E1} for a neutrino that starts in the $|\nu_1 >$ eigenstate and P_{E2} for a neutrino that starts in the $|\nu_3 >$ eigenstate, as this eliminates the need to calculate the phase average. This then corresponds to:

$$\begin{aligned}
\chi_{1e} &= |U_{e1}|^2 &&= c_{12}^2 c_{13}^2 \\
\chi_{1\mu} &= |U_{\mu 1}|^2 &&= |-s_{12}c_{23} - c_{12}s_{23}s_{13}e^{i\delta}|^2 = s_{12}^2 c_{23}^2 + c_{12}^2 s_{23}^2 s_{13}^2 + \xi \\
\chi_{2e} &= |U_{e3}|^2 &&= s_{13}^2 \\
\chi_{2\mu} &= |U_{\mu 3}|^2 &&= s_{23}^2 c_{13}^2
\end{aligned} \tag{112}$$

so that the final three-flavour formula for P_{SE} takes the form:

$$\begin{aligned}
P_{SE} &= \frac{1}{W}\bar{P}^{\odot}_{\nu_e\to\nu_e}\left[P^{\oplus}_{\nu_3\to\nu_e}(1-3s^2_{12}c^2_{23}-3c^2_{12}s^2_{23}s^2_{13}-3\xi)-P^{\oplus}_{\nu_1\to\nu_e}(1-3s^2_{23}c^2_{13})\right]\\
&+ \frac{1}{W}\bar{P}^{\odot}_{\nu_e\to\nu_e}\left[s^2_{12}c^2_{23}+c^2_{12}s^2_{23}s^2_{13}+\xi-s^2_{23}c^2_{13}\right]\\
&+ \frac{1}{W}\bar{P}^{\odot}_{\nu_e\to\nu_\mu}\left[P^{\oplus}_{\nu_1\to\nu_e}(1-3s^2_{13})-P^{\oplus}_{\nu_3\to\nu_e}(1-3c^2_{12}c^2_{13})+s^2_{13}-c^2_{12}c^2_{13}\right]\\
&+ \frac{1}{W}\left[P^{\oplus}_{\nu_1\to\nu_e}(s^2_{13}-s^2_{23}c^2_{13})+P^{\oplus}_{\nu_3\to\nu_e}(s^2_{12}c^2_{23}+c^2_{12}s^2_{23}s^2_{13}+\xi-c^2_{12}c^2_{13})\right]\\
&+ \frac{1}{W}\left[(c^2_{13}-s^2_{13})c^2_{12}s^2_{23}-s^2_{13}(s^2_{12}c^2_{23}+\xi)\right]\\
\\
W &= s^2_{13}+(1-3s^2_{13})(s^2_{12}c^2_{23}+c^2_{12}s^2_{23}+\xi)+c^2_{13}(3c^2_{12}s^2_{23}-c^2_{12}-s^2_{23})
\end{aligned} \tag{113}$$

where we have defined ξ as the term that depends on the CP violating phase:

$$\xi = \frac{1}{2}\sin(2\theta_{12})\sin(2\theta_{23})\sin(\theta_{13})\cos(\delta) \tag{114}$$

and renamed P_{E1} and P_{E2} with $P^{\oplus}_{\nu_1\to\nu_e}$ and $P^{\oplus}_{\nu_3\to\nu_e}$, respectively, since we have restricted them to correspond to probabilities for neutrinos that started in the first and third mass eigenstates. Equation (113) is the main theoretical result of this section.

2.5.6 Dependence of P_{SE} on the Mixing Parameters (Two Flavours)

In this section, we briefly examine how the formula for P_{SE} depends on the two-flavour mixing parameters, in analogy to section (2.3) where the dependence of the solar survival probability was examined. We will also introduce the day-night asymmetry, $\mathcal{A}_{\mathcal{N}-\mathcal{D}}$:

$$\mathcal{A}_{\mathcal{N}-\mathcal{D}} \equiv 2\frac{P_N - P_D}{P_N + P_D} \tag{115}$$

which is a measure of the relative difference between the solar neutrino flux at night-time (P_N) and in the day-time (P_D), when the neutrinos do not traverse the Earth. The day-night asymmetry is thus a measurable quantity that is proportional to $P_{SE} - \bar{P}^{\odot}_{\nu_e\to\nu_e}$. Solar neutrino experiments such as SNO can then make two independent measurements to constrain both the mixing angle and mass squared difference by measuring the daytime flux as well as the day-night asymmetry.

The easiest way to illustrate the effect of the Earth on solar neutrinos is to examine the spectrum

of the survival probability. This is shown in Figure (54a) where the probability of detecting an electron neutrino from a solar neutrino is plotted as a function of energy with $\Delta m_{21} = 4 \times 10^{-5} eV^2$ and $\tan^2(\theta) = 0.42$. The survival probability from the Sun is calculated using the two-flavour jump probability along with the adiabatic approximation. The three curves show the survival probability in the day (no Earth), at night and averaged over a year using the zenith angle exposure function (Figure (55)) for SNO. The night curve is also weighed by the zenith angle exposure function for nadir angles between 0 and π. The Earth is noted to have the largest effect at higher energies. Figure (54b) shows the corresponding day-night asymmetry as a function of energy.

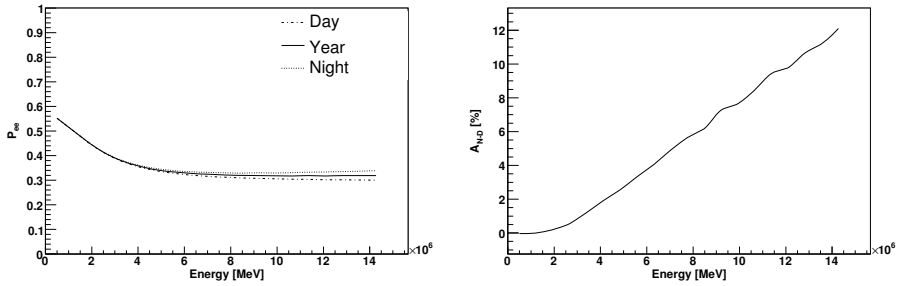

(a) Day, night and yearly average survival probability

(b) Day-Night Asymmetry

Figure 54: Survival probability of electron solar neutrinos as a function of energy at SNO with $\Delta m_{21} = 4 \times 10^{-5} eV^2$ and $\tan^2(\theta) = 0.42$ during the day, night and averaged over a year (left) and corresponding value of the day-night asymmetry (right) in percent. As expected, the yearly average curve lies between the day and night curves. The Earth is seen to have the largest effect at higher energies and regenerates the electron neutrino component of the beam. When integrated over the ^8B flux between $5MeV$ and $15MeV$, the total day-night asymmetry in this case is found to be 6.0%

Figure (56a) shows the day, night and yearly survival probabilities calculated using the best fit values of the two flavour mixing parameters. As one clearly notes, the day-night asymmetry is quite small (Figure (56b)), and SNO indeed measures a value that is consistent with zero [8].

Figure (57) shows how the day and night survival probabilities vary for different values of the mixing angle with $\Delta m_{21} = 7 \times 10^{-5} eV^2$ and Figure (58) shows the corresponding day-night asymmetry. One notes that the mixing angle has a rather small effect on the day-night asymmetry around the best fit value, so that a measurement of $\mathcal{A}_{\mathcal{N}-\mathcal{D}}$ does not constrain the mixing angle very much.

Figure (59) shows how the day and night time fluxes depend on the mass-squared difference and Figure (60) shows the corresponding day-night asymmetry. We note that in this case, the effect of the mass squared difference is large and conclude that measuring the day-night asymmetry constrains the mass-squared difference much better than the mixing angle.

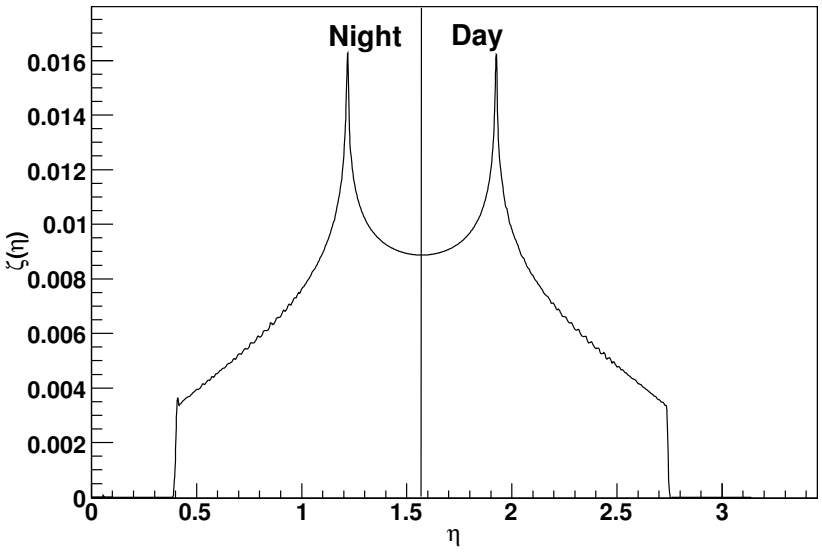

Figure 55: Zenith angle exposure function for SNO as a function of Nadir angle (in radians), taken from [1].

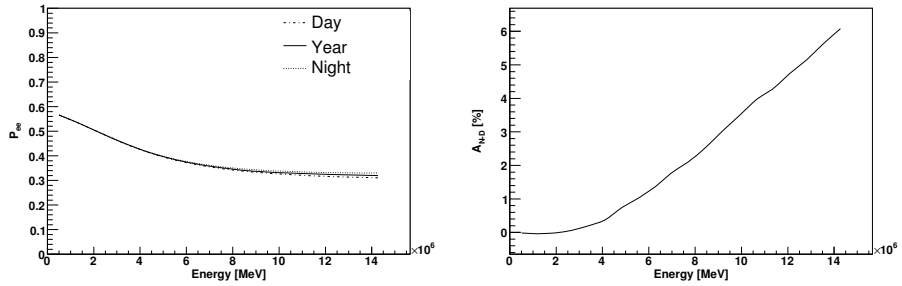

(a) Day, night and yearly average survival probability

(b) Day-Night Asymmetry

Figure 56: Survival probability of electron solar neutrinos as a function of energy at SNO with $\Delta m_{21} = 7 \times 10^{-5} eV^2$ and $\tan^2(\theta) = 0.42$ during the day, night and averaged over a year (left) and corresponding value of the day-night asymmetry (right) in percent. With the best fit values of the mixing parameters, there is almost no day-night asymmetry, as measured by SNO. When integrated over the ^8B flux between $5MeV$ and $15MeV$, the total day-night asymmetry in this case is found to be 2.3%

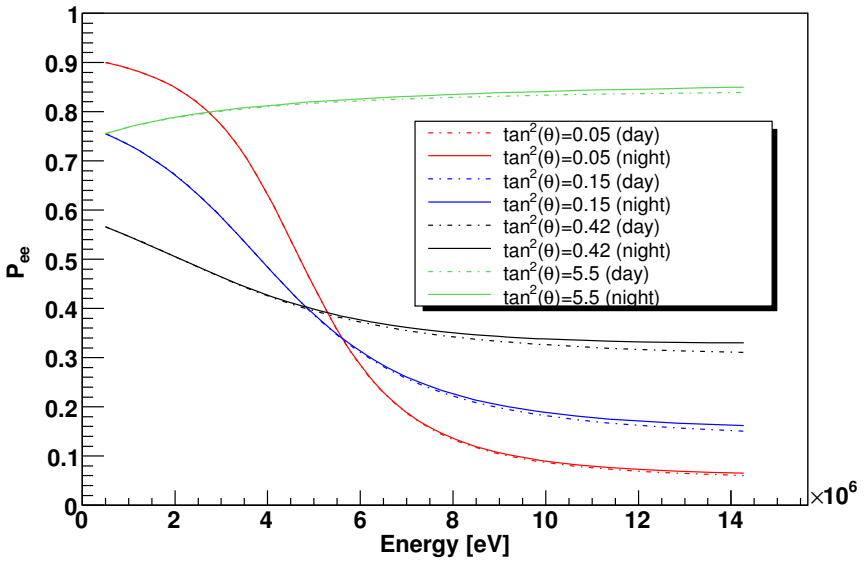

Figure 57: Day and night time survival probabilities as a function of energy for different values of the mixing angle with $\Delta m_{21} = 7 \times 10^{-5} eV^2$. The mixing angle is observed to have a small influence.

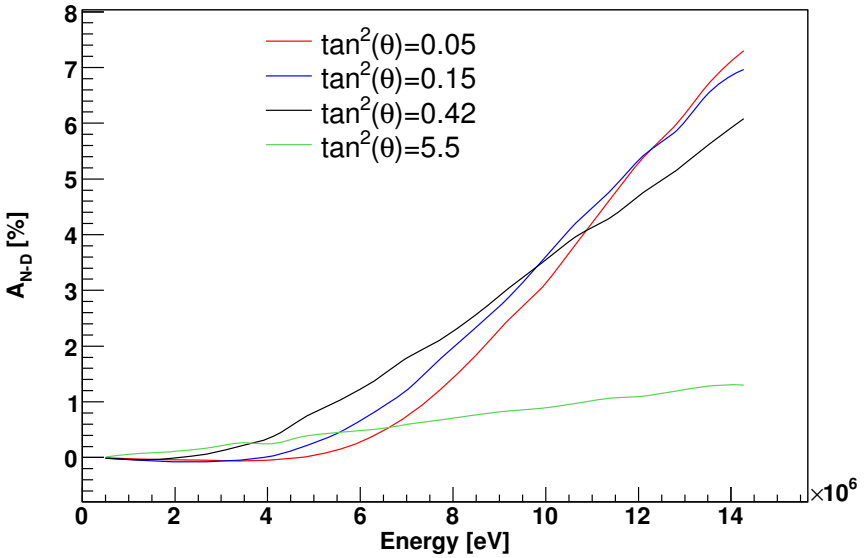

Figure 58: Day-night asymmetry as a function of energy for different values of the mixing angle with $\Delta m_{21} = 7 \times 10^{-5} eV^2$, corresponding to Figure (57). The mixing angle is observed to have a small influence when it is smaller than $\frac{\pi}{4}$.

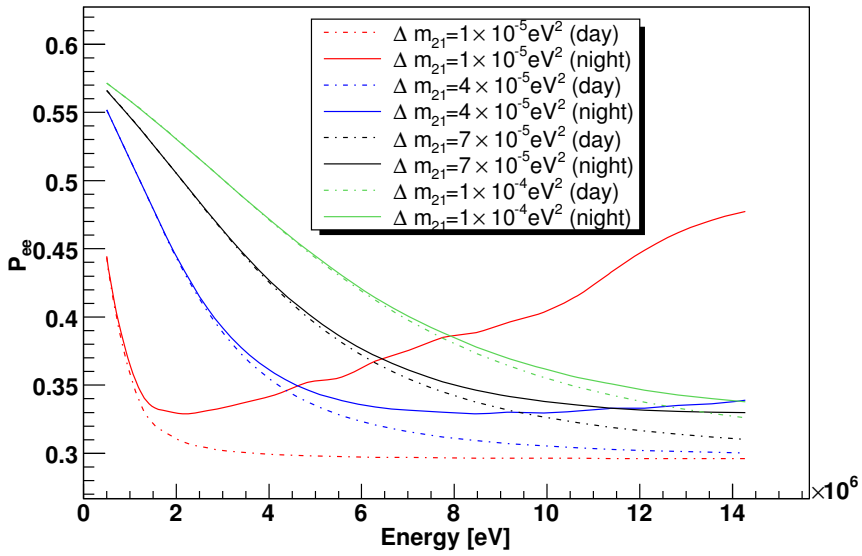

Figure 59: Day and night time survival probabilities as a function of energy for different values of the mass squared difference for $\tan^2(\theta) = 0.42$. The mass squared difference is seen to have a large effect.

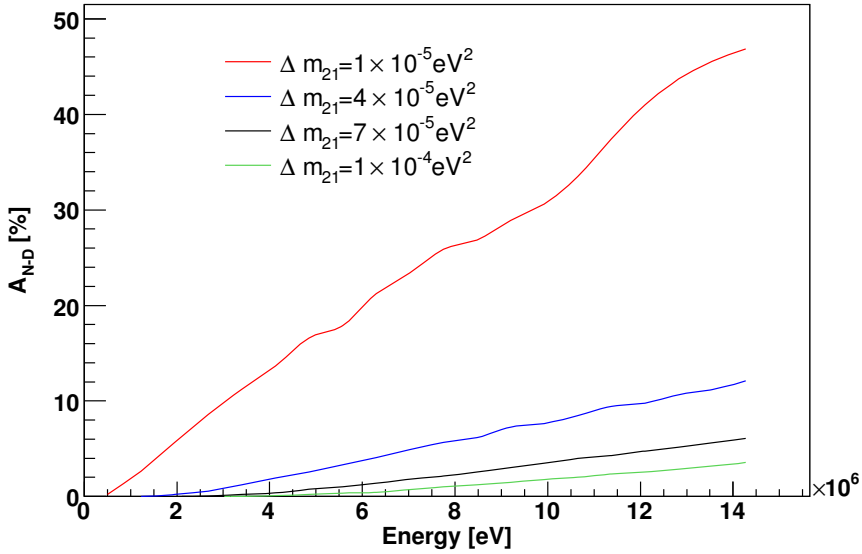

Figure 60: Day-night asymmetry as a function of energy for different values of the mass squared difference for $\tan^2(\theta) = 0.42$, corresponding to Figure (59). The mass squared difference is seen to have a large effect.

2.5.7 Dependence of P_{SE} on θ_{13}

In this section, we consider how the day-night asymmetry varies with θ_{13}. We will assume that Δm_{31} is fixed to $1 \times 10^{-3} eV^2$ by atmospheric neutrino experiments and have verified that, although the complex phase appears in the formula for P_{SE}, the day-night asymmetry does not vary as a function of δ. Furthermore, the mixing angle θ_{23} also has no influence on P_{SE}, even though it appears explicitly. The main goal is to consider whether solar neutrino experiments are sensitive (in principle) to θ_{13} when a measurement of the day-night asymmetry is made. Section (3.1) will focus more carefully on the measurement of θ_{13}, and we only intend a proof of principle in this section.

In general, it is difficult to factor out the θ_{13} dependence from our formula for P_{SE}. A qualitative idea on the dependence on θ_{13} can be obtained if one neglects the term ξ. It is then easy to show that P_{SE} can be parametrized in the form:

$$P_{SE} = \frac{c_{13}^2(A_1 P^{\oplus}_{\nu_1 \to \nu_e} + A_2 P^{\oplus}_{\nu_3 \to \nu_e} + A_3) + (B_1 P^{\oplus}_{\nu_1 \to \nu_e} + B_2 P^{\oplus}_{\nu_3 \to \nu_e} + B_3)}{D_1 c_{13}^2 + D_2} \tag{116}$$

where the A and B contain solar probabilities, mixing angles and Earth probabilities and the D contain only mixing angles. The authors in [47] have obtained approximations for the functions $P^{\oplus}_{\nu_1 \to \nu_e}$ and $P^{\oplus}_{\nu_1 \to \nu_e}$ that appear in the A and B by deriving series expansions in the matter potential term. We will not go into the details of their derivation, but simply quote their results:

$$\begin{aligned} P^{\oplus}_{\nu_1 \to \nu_e} &= c_{13}^2(a_1 c_{13}^2 + a_2) \\ P^{\oplus}_{\nu_3 \to \nu_e} &= 1 - c_{13}^2 \end{aligned} \tag{117}$$

where a_1 and a_2 depend on integrals of the matter potential through the Earth. We can then re-parametrize P_{SE} as:

$$P_{SE} = \frac{A_1 c_{13}^6 + A_2 c_{13}^4 + A_3 c_{13}^2 + B}{D_1 c_{13}^2 + D_2} \tag{118}$$

where A and B now depend only on solar survival probabilities and mixing angles. This is to be compared with the result in [15] where it is claimed that the day-night asymmetry is proportional to c_{13}^6. The authors in [15] make several approximations, in particular that the Earth has a constant density. Furthermore, they make the approximation that the third neutrino is decoupled (hence using the first-order formula that we presented in section (2.2)) and that the solar survival probability is then proportional to c_{13}^4. In our case, if we also assume that the solar survival probability goes as

c_{13}^4 we can express P_{SE} as an eighth order (even) polynomial in c_{13}:

$$P_{SE} = A_1 c_{13}^8 + A_2 c_{13}^6 + A_3 c_{13}^4 + A_4 c_{13}^2 + B_1 + \frac{B_2}{c_{13}} \tag{119}$$

This formula should give a qualitative idea on the dependence of the day-night asymmetry on θ_{13}, and it is not very enlightening to show the actual content of the coefficients A and D. In particular, we note that one expects a smaller asymmetry for large value of θ_{13}.

Figure (61) shows how the day and night time survival probabilities behave as a function of energy for different values of θ_{13}. The two-flavour mixing parameters were chosen as $\Delta m_{21} = 4 \times 10^{-5} eV^2$ and $\tan^2(\theta_{12}) = 0.42$, in order to amplify the day-night asymmetry. We note that the difference between the day and night flux is bigger for smaller θ_{13}, which is shown more clearly in Figure (62) where the corresponding day-night asymmetry is shown.

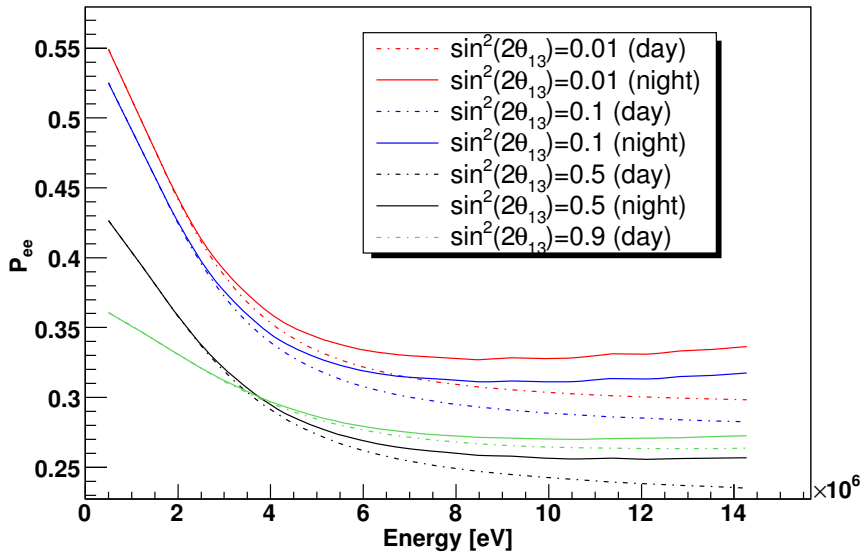

Figure 61: Day and night time survival probabilities as a function of energy for different values of θ_{13} with $\tan^2(\theta_{12}) = 0.42$ and $\Delta m_{21} = 4 \times 10^{-5} eV^2$. A larger θ_{13} is seen to decrease the effect of the Earth.

Figure (63) shows the day-night asymmetry as a function of θ_{13} divided by the corresponding day-night asymmetry with $\theta_{13} = 0$ for a neutrino energy of $10MeV$ with $\Delta m_{21} = 7 \times 10^{-5} eV^2$ and two different values of θ_{12} (30 and 40 degrees). This is to be compared with Figure (4) from [15] and we note that our agreement with their results is excellent. The small difference between our plot and theirs come from the fact that we have used a fully numerical calculation through the Earth

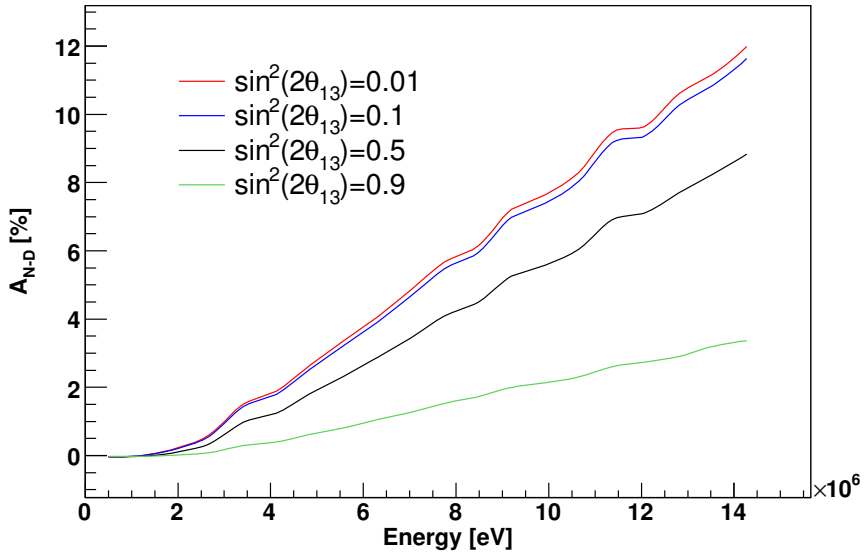

Figure 62: Day-night asymmetry as a function of energy for different values of θ_{13} with $\tan^2(\theta_{12}) = 0.42$ and $\Delta m_{21} = 4 \times 10^{-5} eV^2$, corresponding to Figure (61). A larger θ_{13} is seen to decrease the day-night asymmetry.

compared to their approximation of a constant density and furthermore, from the fact that we set the neutrino energy, whereas they set the neutrino energy based on an electron detected in a CC reaction.

In Figure (64), we have plotted P_{SE} minus the daytime survival probability as a function of $\cos(\theta_{13})$ to better illustrate the effect of θ_{13}, and verify the qualitative behavior of P_{SE} as a function of θ_{13}. We have thus also shown two fitted curves, one corresponding to the eighth order polynomial in equation (119) and the other to a simple term in c_{13}^6, as suggested by [15]. Table (1) shows the relative size of the coefficients for the fit to equation (119) to give an idea of their importance. It is clear that both expressions fit very well in general, and that equation (119) agrees extremely well. We note from Table (1) that the term in c_{13}^8 is not negligible compared to the term in c_{13}^6. The excellent agreement suggests that the first-order decoupling formula for solar neutrinos is very good (as was already shown in section (2.3)) and that the expansions suggested by [47] are also a very good approximation to $P^{\oplus}_{\nu_1 \to \nu_e}$ and $P^{\oplus}_{\nu_3 \to \nu_e}$.

The main conclusions from this section are then that a measurement of the day-night asymmetry is primarily sensitive to Δm_{21} and we have shown that, in principle, it is also sensitive to θ_{13}. Unfortunately, solar neutrino experiments are not likely to be able to claim a non-zero measurement of θ_{13} as the effect is small, due to the particular value of Δm_{21}, and would thus require an extremely

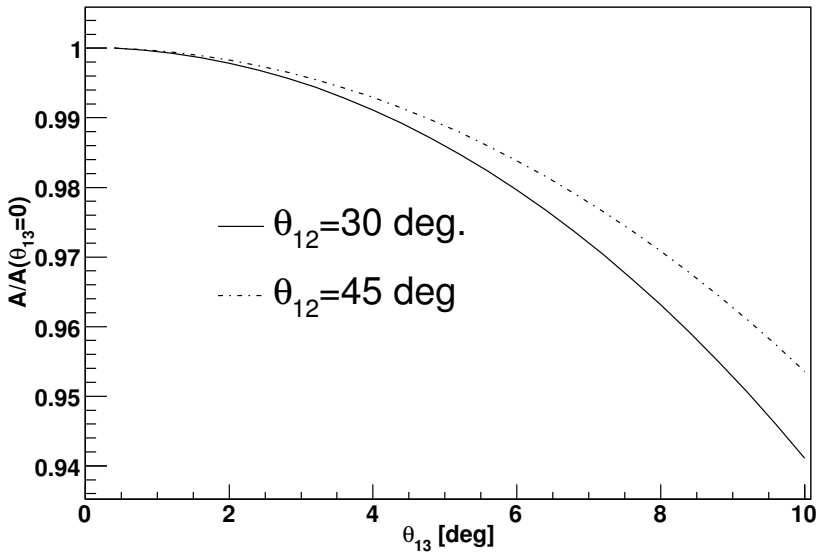

Figure 63: Day-night asymmetry as a function of θ_{13} divided by the asymmetry when $\theta_{13} = 0$ for a neutrino energy of $10MeV$ with $\Delta m_{21} = 7 \times 10^{-5} eV^2$ and two different values of θ_{12}. This figure is to be compared with Figure 4 of [15] and confirms our work as well as their approximation of the Earth as having a constant density.

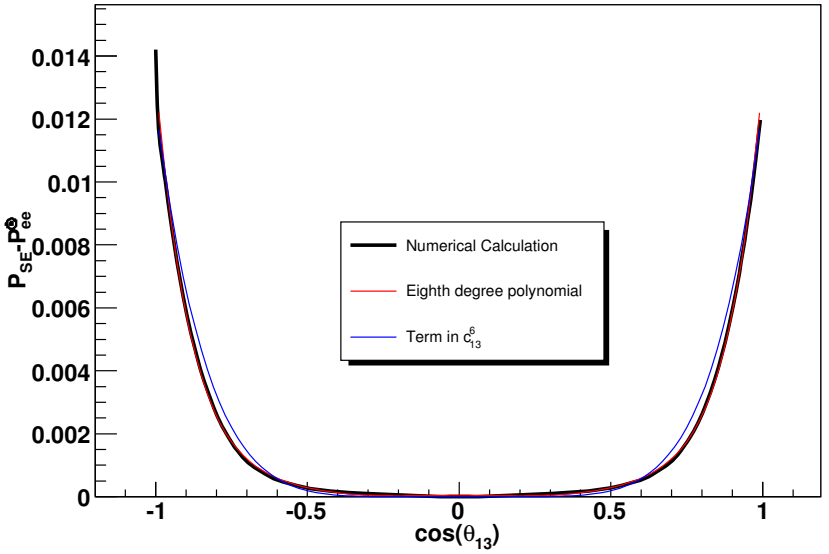

Figure 64: P_{SE} minus daytime survival probability (i.e. $P_{SE} - \bar{P}^{\odot}_{\nu_e \to \nu_e}$) as a function of $\cos(\theta_{13})$ for a $10MeV$ neutrino with $\Delta m_{21} = 4 \times 10^{-5} eV^2$ and $\tan^2(\theta_{12}) = 0.42$. We also show the fit to the eighth order polynomial in equation (119) (see Table (1)) as well as a fit to a term in c_{13}^6. Both fits are very good, and the eighth order polynomial is overall a more accurate description.

A_1	0.0207
A_2	-0.0145
A_3	0.0035
A_4	0.0035
B_1	2.05 $\times 10^{-5}$
B_2	-4.25 $\times 10^{-8}$

Table 1: Fit parameters for the eigth order polynomial in equation (119) for the curve in Figure (64)

accurate measurement.

3 Applications

In the following sections, we examine numerical results obtained using the approximations presented in the Theory section. The calculations were all done using a C++ library written to take advantage of the various approximations and calculate solar neutrino fluxes in the day and at night using the formula for P_{SE}.

3.1 Measuring θ_{13} with Solar Neutrinos

The original motivation of our work was to look at the possibilities of measuring θ_{13}, in particular using the day-night asymmetry, with SNO and solar neutrinos, which we consider in this section. The main difficulty in doing this is that if one wants to measure θ_{13}, then the solar flux will have to be fitted to four parameters: Δm_{21}, θ_{12}, Δm_{31} and θ_{13}. In practice this means that four independent measurements need to be made. We thus make the assumption, in this section, that Δm_{31} can be obtained from atmospheric neutrino measurements and that Δm_{21} can be obtained from reactor neutrino experiments, in particular the KAMLAND collaboration. Their experiment is sensitive to both of the two-flavour mixing parameters, however, they have shown to be more sensitive to Δm_{21} than θ_{12} [9]. We hence assume that the mass-squared differences are fixed from other experiments and that SNO then only needs to make two independent measurements to constrain the two mixing angles that are involved in the electron flavour survival probability. Throughout this section we will use $\Delta m_{21} = 7 \times 10^{-5} eV^2$ (which is slightly below the latest 'solar+KAMLAND' fits ([8], [9])) and $\Delta m_{31} = 1 \times 10^{-3} eV^2$, which is also slightly below the best fit value from [11], although compatible, and as we have seen earlier, has very little impact on solar neutrinos.

SNO obviously has the ability to make more than two different measurements, so we must seek which ones give the best constraints on θ_{13}. The first possibility is to make two measurements of the flux at different energies, to see how the two depend on θ_{13}, and the second possibility is to look at day and night time measurements, since the day-night asymmetry was shown in section (2.5) to also depend on θ_{13}. One can then imagine combining these different sets of measurements. The aim of this section is to show this theoretical dependence without actually fitting the data for the angles, which is beyond the scope of this thesis.

3.1.1 With the Day-Night Asymmetry

We will first consider the possibility of constraining θ_{13} with measurements of the day-night asymmetry. When we started this work, this was a novel idea; however, other authors, in particular

[15], have looked into the same idea and published results while we were still doing research. Our approach is however quite different, although we draw similar conclusions.

We have already seen in section (2.5) that there is not a very large day-night asymmetry with the current experimental values of the mixing parameters. We hence already know that such measurements will have to be made with a high degree of accuracy, and in fact this will necessarily be beyond the capabilities of SNO, which currently measures an asymmetry consistent with zero. Nonetheless, it is still of theoretical interest to consider the possibility that might be of use for the next generation of experiments.

This section will only focus on the day-night asymmetry integrated over the ^8B spectrum. The next section will consider the energy dependence. In order to measure the two mixing angles, we find it convenient to plot the survival probability as a function of these two angles, in order to look at the correlation between the two. We will also focus on a region of parameter space around the experimental values of the mixing angles. We will examine the dependence for $0.3 < \tan^2(\theta_{12}) < 0.7$, which is roughly a 2σ bound from [8], and we will impose $0 < \sin^2\theta_{13} < 0.3$ (see [11]).

Figure (65) shows the survival probability in the day, that is, averaged over the Sun and Sun-Earth distance, but with no matter effect from the Earth, as a function of θ_{12} and θ_{13} integrated over the ^8B spectrum between $3MeV$ and $15MeV$. The calculation was done using the three-flavour adiabatic approximation with the two flavour jump probability and the formula for P_{SE} that was derived in section (2.5). In an experimental situation, one would then measure the survival probability (in SNO, this is related to the CC/NC ratio), and hence the corresponding contour in Figure (65). A very qualitative estimate would then require a measurement of the solar survival probability to within $\sim 3\%$ to pick out a contour.

The second measurement can be done by considering the day-night asymmetry, $\mathcal{A}_{\mathcal{N}-\mathcal{D}}$. Figure (66) shows the average night time survival probability and Figure (67) shows the corresponding day-night asymmetry in the θ_{12}-θ_{13} plane. Again, if one were to use a measurement of the day-night asymmetry to deduce the corresponding contour, this should be done with a precision around $\sim 3\%$. For comparison, the last SNO measurement of the day-night asymmetry [8] is of the order of 100% (consistent with no asymmetry) and there is thus not much hope in using this type of measurement to fit for θ_{13} with current experiments. It is however interesting to note that an accurate measurement of a small day-night asymmetry would be sufficient to claim a non-zero value for θ_{13}, as the correlation with θ_{12} appears to be small.

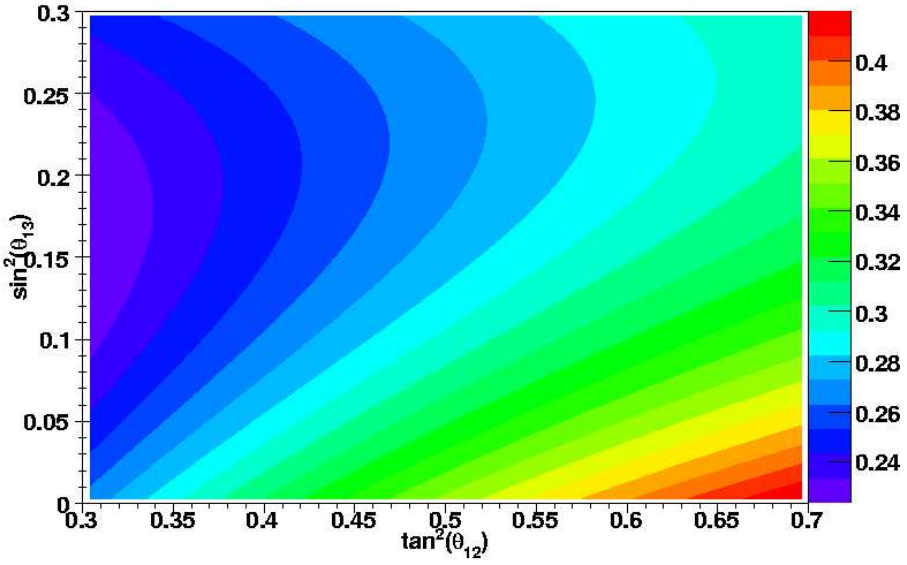

Figure 65: Daytime flux integrated from $3MeV$ to $15MeV$ as a function of $\tan^2(\theta_{12})$ and $\sin^2(\theta_{13})$

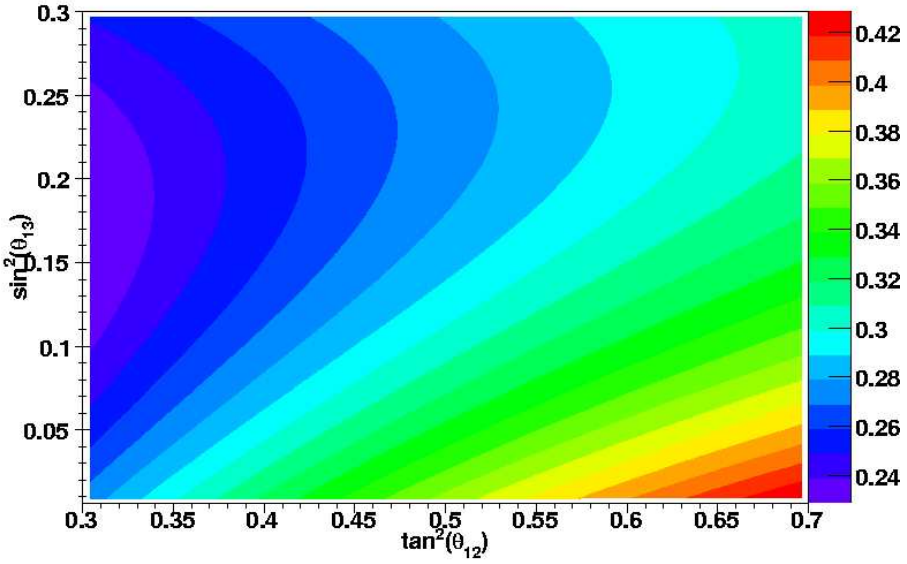

Figure 66: Night time flux integrated from $3MeV$ to $15MeV$ as a function of $\tan^2(\theta_{12})$ and $\sin^2(\theta_{13})$ averaged over the zenith angle exposure function of SNO for Nadir angles between $\frac{\pi}{2}$ and π.

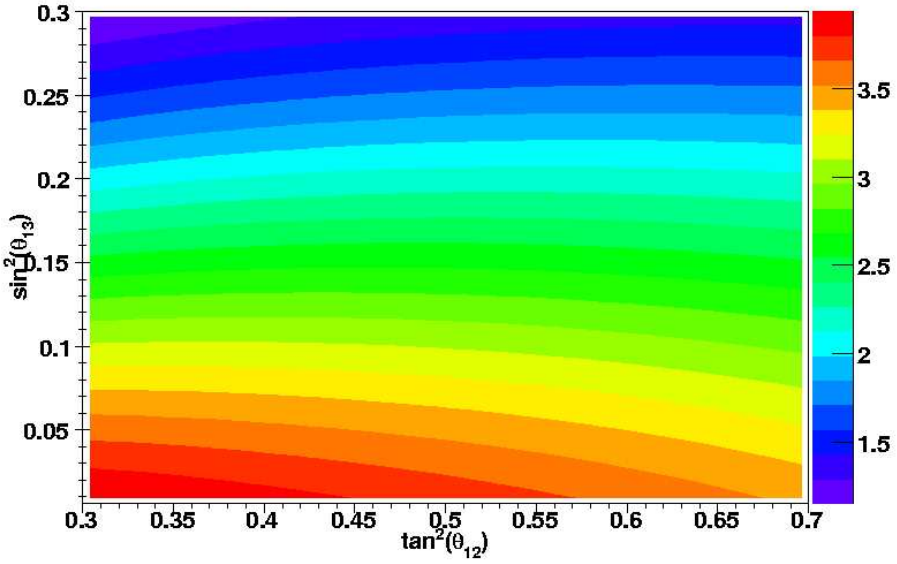

Figure 67: Day-Night asymmetry (in percent) integrated from $3MeV$ to $15MeV$ as a function of $\tan^2(\theta_{12})$ and $\sin^2(\theta_{13})$. The values are calculated using Figures (65) and (66)

3.1.2 With Fluxes at Different Energies

The idea of using the fluxes at different energies appears to have been first proposed by [48] who used the concept to fit and obtain a non-zero value for θ_{13} with results from solar neutrinos, although the measurement is not statistically significant. For completeness, we use our own computer code to illustrate the effect and discuss how it might be used to measure θ_{13}.

In our version of the analysis, we plot the survival probability as a function of θ_{12} and θ_{13} integrated over different ranges of energies. Figure (68) shows the day-time survival probability over two different ranges in energies (1 to $6MeV$ (left), and 6 to $15MeV$ (right)). The corresponding day-night asymmetry is not useful in a measurement at different energies as we have shown in section (2.5) that there is virtually no day-night asymmetry at low energies.

One notes that there is a qualitatively different behaviour at different energies. Future experiments sensitive to low-energy solar neutrinos should be able to make these measurements and help to constrain θ_{13}. In particular, the lower energy range appears to be the best for constraining θ_{13}, as the contours are almost horizontal. It appears that one 5% measurement alone, in this energy range, could be sufficient to claim a non-zero value for θ_{13}. This appears to be a very exciting conclusion as several proposals for low energy solar neutrino experiments are now being seriously considered.

The main conclusions of this section are that, in principle, solar neutrinos can be used to measure

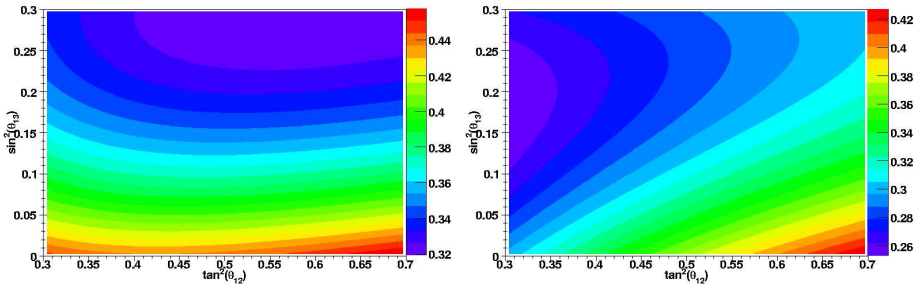

(a) Day time survival probability integrated between 1 and $6MeV$

(b) Day time survival probability integrated between 6 and $15MeV$

Figure 68: Day time flux integrated from $1MeV$ to $6MeV$ (left) and from $6MeV$ to $15MeV$ (right) as a function of θ_{12} and θ_{13}.

θ_{13}. Although we have seen that the day-night asymmetry is much more dependent on θ_{13} than θ_{12}, we have shown that one would require an extremely accurate measurement to determine a non-zero value for θ_{13}. The best hope for measuring θ_{13} with solar neutrinos is then to measure accurately the (day-time) survival probability at lower energies.

3.2 Defining the Night Bin for Underground Detectors

In this section, we examine how the matter above an underground detector affects the flux of neutrinos. We will see that the night bin should be defined for Nadir angles between 0 and $\frac{\pi}{2} + \epsilon$, where ϵ is a small angle making the night bin longer. The difference comes from the detector being underground and thus leaving a non-negligible path through the Earth when the Nadir angle is equal to $\frac{\pi}{2}$ (see Figure (14)).

To illustrate this effect, we consider a detector $2km$ underground, consistent with the SNO location. We use a model that involves propagating neutrinos through the Earth by starting them in a given mass eigenstate mixture which is essentially the same method as presented in section (2.4). Consider neutrinos in the state:

$$|\nu >= k_1|\nu_1 > +k_2|\nu_2 > e^{-i\phi} \tag{120}$$

In Figure (69), we show the survival probability as a function of energy and Nadir angle for neutrinos that started in the state defined by equation (120) and averaged over the phase ϕ. The mixing parameters were chosen as $\tan^2(\theta_{12}) = 0.42$ and $\Delta m_{21} = 7 \times 10^{-5} eV^2$ corresponding to the best-fit two-flavour case. Several features are visible on this plot, the most striking being the vertical line corresponding to the mantle-core interface. One also notes the vacuum oscillations in distance (proportional to $\cos(\eta)$) that are approached when $\eta = \frac{\pi}{2}$ as well as the fact that the Earth has a larger effect at higher energies. One can also see the effect of the LMA spectrum, giving a higher survival probability at lower energies and washing out the effect of the Earth at those energies. The mass eigenstate contents in equation (120) were calculated as a function of energy from the Sun. We have tested this model with the mass eigenstates being constant as a function of Energy and came to the same conclusions.

When this plot was first made, it seemed that the various features were quite large and might be observable with the SNO detector. Since SNO does not have the resolution to distinguish the features that are energy dependent [4], one can integrate Figure (69) over the ^8B spectrum to obtain the dependence on the Nadir angle. Obviously, the detector's resolution of the Nadir angle is excellent, since all neutrino events are tagged in time. Figure (70), shows this energy integrated survival probability as a function of Nadir angle. We note the survival probability having two different average values, corresponding to the night flux (when $\eta < \frac{\pi}{2}$) and day flux (when $\eta > \frac{\pi}{2}$). The difference between these two is then the day-night asymmetry.

[4] SNO has a resolution of about $1MeV$ on electron energy

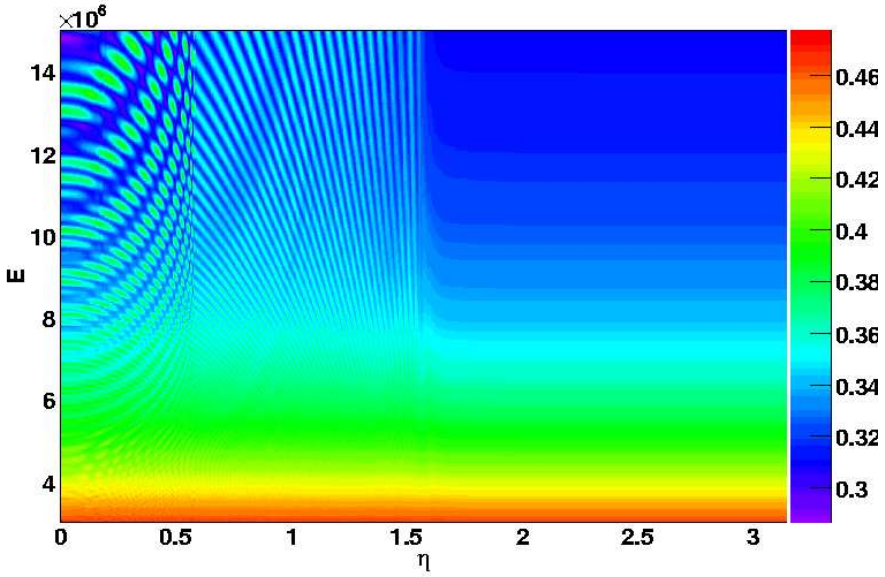

Figure 69: Survival probability through the Earth as a function of Nadir angle (in radians) and energy (in eV) for a detector $2km$ underground and neutrinos that started in the state defined by equation (120) and averaged over the phase. The mixing parameters are set to $\tan^2(\theta_{12}) = 0.42$ and $\Delta m_{21} = 7 \times 10^{-5} eV^2$.

One notes that the average between the day and night fluxes actually changes slightly above $\eta = \frac{\pi}{2}$. This comes from the fact that at $\eta = \frac{\pi}{2}$, the path length through the Earth is still about $160km$ and there is still a chance for the coherence acquired at the boundary with the Earth to have a (small) effect since the vacuum oscillation length for 10 MeV neutrinos is about $350km$ when $\Delta m_{21} = 7 \times 10^{-5} eV^2$. However, it is noted that with the current experimental values of the mixing parameters, the effect of the Earth is quite small, as seen in previous sections.

Finally, we can use Figure (70) to extract values for the day-night asymmetry, depending on the size of the night bin. The values for the day (D) and night (N) time fluxes, as well as the day-night asymmetry, A_{N-D}, are shown in table (2), for the usual bin size and when one uses a non-zero value for epsilon (given in degrees):

ϵ	A_{N-D} (%)
0	2.29
13	1.99

Table 2: Day-night asymmetry for two different sizes of the night bin (ϵ given in degrees). Results were obtained by integrating Figure (69) with the zenith angle exposure function for SNO, and the ^8B spectrum between $5MeV$ and $15MeV$.

First, we note that in either case, the asymmetry is very small and would require a measurment

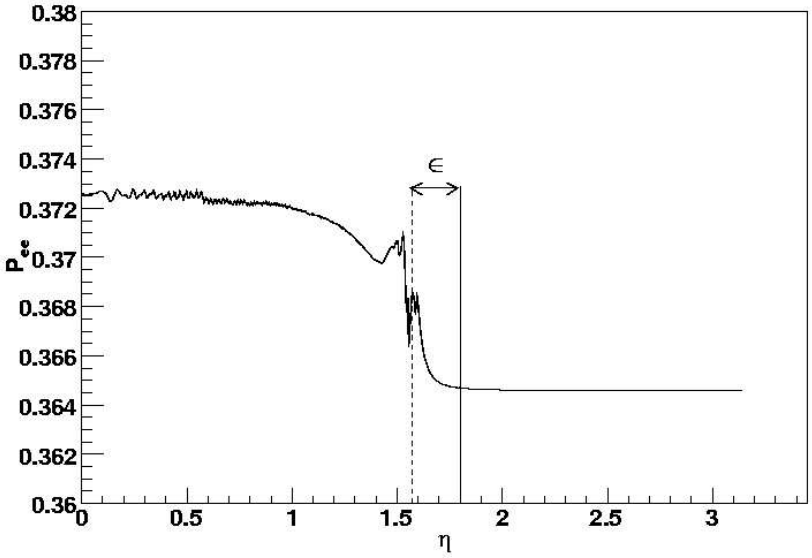

Figure 70: Same as Figure (69) but integrated over the ^8B spectrum between 3 and 15 MeV, as a function of Nadir angle (in radians). The dotted line corresponds to $\eta = \frac{\pi}{2}$, and ϵ is the extra amount the night bin should be extended. In this plot, ϵ is approximately 13 degrees.

with the corresponding accuracy. Second, there is a difference between the two values, with a relative difference of about 13% of the value when the night bin extends to $\eta = \frac{\pi}{2} + \epsilon$. The surprising conclusion is that the asymmetry is actually smaller for the case with ϵ not equal to zero, since this case 'weighs in' values of the survival probability that are lower than the average night value.

The conclusion of this section is that, in order to be rigorous, one should extend the length of the night bin, if one wants the day-night asymmetry to be a measurement of the effect of the Earth on solar neutrinos. Regrettably, this makes the day-night asymmetry even smaller and harder to measure conclusively.

4 Summary and Conclusions

In this thesis, we have provided an extensive overview of the oscillation calculations for solar neutrinos. We started by introducing the theoretical framework for neutrino calculations in section (2.1) and then applied them to the propagation of neutrinos through arbitrary media in section (2.2). We showed that the numerical propagation of neutrinos is not affected by discontinuous density boundaries as long as one imposes the condition that the flavour content be continuous through the interface. Various approximations were also introduced in section (2.2) and in particular, it was shown that the adiabatic approximation is very accurate for media with smoothly varying density profiles.

In section (2.3), we examined the propagation of neutrinos in the Sun, in light of the approximations that were introduced in section (2.2). We also presented our own numerical algorithms for the propagation of solar neutrinos and showed that the step size is best chosen by an algorithm that uses the wavelength in matter before the MSW resonance and then switches to exponentially increasing steps in the parts of the Sun where the oscillations are close to the vacuum regime. We concluded this section by recommending that the fastest and most accurate method of propagating solar neutrinos is a combination of the three-flavour adiabatic approximation used with a two-flavour jump probability. This is consistent with the idea that the third mass eigenstate is effectively decoupled from the first two.

Section (2.4) examined the propagation of neutrinos in the Earth. The case of an incoherent beam arriving at the Earth from vacuum was considered and it was shown that the interface with the Earth reintroduces coherence in the beam. It was seen that this was the result of one of the mass eigenstates being regenerated at a particular point in space. We also examined the influence of the Earth on the survival probabilities as a function of the mixing parameters and showed that the Earth has a small effect with the current best-fit values of the mixing parameters.

In section (2.5), we presented our most significant contribution, when we examined the survival probability for solar neutrinos when they traverse the Earth. We introduced a three-flavour formula that allows one to calculate the survival probability separately in the Sun and in the Earth and then combine these to obtain the final result. In addition to providing a computationally efficient formalism, we also showed how the day-night asymmetry behaves as a function of θ_{13}, in a manner consistent with the results found by others in the literature. We concluded by showing that the day-night asymmetry is most sensitive to Δm_{21}. We also showed that the asymmetry depended on θ_{13} more than on θ_{12}.

We presented two examples of applications of our theoretical findings. We first examined how a solar neutrino experiment could measure θ_{13} in section (3.1). It was shown that the day-night asymmetry provided a useful tool for constraining θ_{13} in theory, but that the required precision was unrealistic for current experiments. We concluded section (3.1) by showing that a low-energy measurement of the day solar survival probability would provide the best constraint for θ_{13}. Finally, in section (3.2) we considered the effect of modeling a solar neutrino detector underground, as is the case for the Sudbury Neutrino Observatory. We showed that a rigorous definition of the day-night asymmetry required extending the night bin to account for the matter effect on Earth-skimming neutrinos, as the path length through the Earth is comparable to the oscillation length in that case.

References

[1] J. N. Bahcall and P. I. Krastev. Does the sun appear brighter at night in neutrinos? *Phys. Rev.*, C56:2839, 1997.

[2] The SNO Collaboration. The sudbury neutrino observatory. *Nuclear Instruments and Methods in Physics Research*, A449:172, 2000.

[3] B. Pontecorvo. Inverse beta processes and nonconservation of lepton charge. *Sov. Phys. JETP*, 7:172, 1958.

[4] M. Gell-Mann and A. Pais. Behavior of neutral particles under charge conjugation. *Phys. Rev.*, 97:1387, 1955.

[5] The Super-Kamiokande Collaboration. Measurement of the flux and zenith-angle distribution of upward through-going muons in kamiokande ii+iii. *Phys. Rev. Lett.*, 81:2016, 1998.

[6] The SNO Collaboration. Direct evidence for neutrino flavor tranformation from neutral-current interactions in the sudbury neutrino observatory. *Phys. Rev. Lett.*, 89:011301, 2002.

[7] R. Jr. Davis, D. S. Harmer, and K. C. Hoffman. Search for neutrinos from the sun. *Phys. Rev. Lett.*, 20:1205–1209, 1968.

[8] The SNO Collaboration. Electron energy spectra, fluxes, and day-night asymmetries of b-8 solar neutrinos from the 391-day salt phase sno. *Phys. Rev. C*, 72:055502, 2005.

[9] The KamLAND collaboration. Measurement of neutrino oscillation with kamland: Evidence of spectral distortion. *Phys. Rev. Lett.*, 94:081801, 2005.

[10] The Super-Kamiokande Collaboration. Evidence for an oscillatory signature in atmospheric neutrino oscillations. *Phys. Rev. Lett.*, 93:101801, 2004.

[11] M. Maltoni, T. Schwetz, M. A. Tortola, and J. W. F. Valle. Status of three-neutrino oscillations after the sno-salt data. *Phys. Rev.*, D68:113010, 2003.

[12] T. K. Kuo and J. T. Pantaleone. Three neutrino oscillations and the solar neutrino experiments. *Phys. Rev.*, D35:3432, 1987.

[13] S. T. Petcov. Exact analytic description of two-neutrino oscillations in matter with exponentially varying density. *Phys. Lett.*, B200:373, 1988.

[14] S. J. Parke. Nonadiabatic level crossing in resonant neutrino oscillations. *Phys. Rev. Lett.*, 57:1275, 1986.

[15] M. Blennow, T. Ohlsson, and H. Snellman. Day-night effect in solar-neutrino oscillations with three flavors. *Phys. Rev.*, D69:073006, 2004.

[16] J. S. Kim and K. Lee. The earth regeneration effect of solar neutrinos: A numerical treatment with three active neutrino flavors. *Comput. Phys. Commun.*, 135:176, 2001.

[17] V. N. Gribov and B. Pontecorvo. Neutrino astronomy and lepton charge. *Phys. Lett.*, B28:493, 1969.

[18] S. M. Bilenky and B. Pontecorvo. Quark-lepton analogy and neutrino oscillations. *Phys. Lett.*, B61:248, 1976.

[19] S. M. Bilenky and B. Pontecorvo. Again on neutrino oscillations. *Nuovo Cim. Lett.*, 17:569, 1976.

[20] S. M. Bilenky and B. Pontecorvo. The lepton-quark analogy and muonic charge. *Yad. Fiz.*, 24:603, 1976.

[21] ALEPH, DELPHI, L3, and OPAL The LEP Collaboration. Electroweak parameters of the z0 resonance and the standard model: the lep collaborations. *Phys. Lett.*, B276:247, 1992.

[22] The SNO Collaboration. Measurement of the total active ^8b solar neutrino flux at the sudbury neutrino observatory with enhanced neutral current sensitivity. *Phys. Rev. Lett.*, 92:181301, 2004.

[23] C. Weinheimer, B. Degen, A. Bleile, J. Bonn, L. Bornschein, 0. Kazachenko, A. Kovalik, and E.W. Otten. High precision measurement of the tritium beta spectrum near its endpoint and upper limit on the neutrino mass. *Phys. Lett.*, B460:219–226, 1999.

[24] Z. Maki, M. Nakagawa, and S. Sakata. Remarks on the unified model of elementary particles. *Prog. Theor. Phys.*, 28:870, 1962.

[25] L. Wolfenstein. Neutrino oscillations in matter. *Phys. Rev.*, D17:2369, 1978.

[26] S.P. Mikheyev and A. Yu. Yu. Smirnov. *Yad. Fiz.*, 42:1441, 1985.

[27] H. A. Bethe. Possible explanation of the solar-neutrino puzzle. *Phys. Rev. Lett.*, 56:1305, 1986.

[28] J. Linder. Derivation of neutrino matter potentials induced by earth. *hep-ph/0504264*, 2005.

[29] T. K. Kuo and J. T. Pantaleone. Neutrino oscillations in matter. *Rev. Mod. Phys.*, 61:937, 1989.

[30] D. J. Griffiths. *Introduction To Quantum Mechanics*. Prentice Hall, Inc., 1995.

[31] C. Zener. Non adiabatic crossing of energy levels. *Proc. R. Soc. A*, 137:696, 1932.

[32] W. C. Haxton. Adiabatic conversion of solar neutrinos. *Phys. Rev. Lett.*, 57:1271, 1986.

[33] S. Toshev. Nonadiabatic neutrino transitions in matter with linearly varying density. *Phys. Lett.*, B198:551, 1987.

[34] C. S. Lim, K. Ogure, and H. Tsujimoto. How precisely can we reduce the three-flavor neutrino oscillation to the two-flavor one only from delta(m(12)**2)/delta(m(13)**2) ¡ approx. 1/15? *Phys. Rev.*, D67:033007, 2003.

[35] G. L. Fogli, E. Lisi, and D. Montanino. Matter-enhanced three-flavor oscillations and the solar neutrino problem. *Phys. Rev.*, D54:2048–2062, 1996.

[36] J. N. Bahcall, M. H. Pinsonneault, and S. Basu. Solar models: Current epoch and time dependences, neutrinos, and helioseismological properties. *Astrophys. J.*, 555:990, 2001.

[37] J. N. Bahcall, A. M. Serenelli, and S. Basu. New solar opacities, abundances, helioseismology, and neutrino fluxes. *Astrophys. J.*, 621:L85, 2005.

[38] The K2K Collaboration. Evidence for muon neutrino oscillation in an accelerator-based experiment. *Phys. Rev. Lett.*, 94:081802, 2005.

[39] J. M. Dziewonski and D. L. Anderson. Preliminary reference earth model. *Physics of the Earth and Planetary Interiors*, 25:297, 1981.

[40] S. T. Petcov. Diffractive-like (or parametric-resonance-like?) enhancement of the earth (day-night) effect for solar neutrinos crossing the earth core. *Phys. Lett.*, B434:321, 1998.

[41] E. K. Akhmedov. Remarks on parametric resonance of neutrino oscillations in the earth. *hep-ph/9903302*, 1999.

[42] A. H. Guth, L. Randall, and M. Serna. Day-night and energy variations for maximal neutrino mixing angles. *JHEP*, 08:018, 1999.

[43] A. J. Baltz and J. Weneser. Effect of transmission through the earth on neutrino oscillations. *Phys. Rev.*, D35:528, 1987.

[44] A. J. Baltz and J. Weneser. Matter oscillations: Neutrino transformation in the sun and regeneration in the earth. *Phys. Rev.*, D37:3364, 1988.

[45] E. K. Akhmedov, R. Johansson, M. Lindner, T. Ohlsson, and T. Schwetz. Series expansions for three-flavor neutrino oscillation probabilities in matter. *JHEP*, 04:078, 2004.

[46] S. P. Mikheev and A. Yu. Smirnov. Resonance oscillations of neutrinos in matter. *Sov. Phys. Usp.*, 30:759–790, 1987.

[47] A. N. Ioannisian, N. A. Kazarian, A. Y. Smirnov, and D. Wyler. A precise analytical description of the earth matter effect on oscillations of low energy neutrinos. *Phys. Rev.*, D71:033006, 2005.

[48] S. Goswami and A. Y. Smirnov. Solar neutrinos and 1-3 leptonic mixing. *Phys. Rev.*, D72:053011, 2005.